SCIENCE ▪ PASSION ▪ TECHNOLOGY

SAXS and WAXS principles

Heinz Amenitsch
TU-Graz & Austrian SAXS beamine, ELETTRA

Elettra Sincrotrone Trieste

Layout

PART I: SAXS and WAXS principles

-Introduction to the Theory (“Graz School”)

-From Experiments to Real Space

-Bio-SAXS (“Hamburg School”)

PART II: SAXS applications in life science and material science using synchrotron

-Examples: -Chemistry
-Hierarchical Materials

-Grazing Incidence SAXS (“no school”)
-Biomembranes
-*In situ* Chemistry

amenitsch@tugraz.at &
amenitsch@elettra.trieste.it

Soft Condensed Matter (© P. Schurtenberger)

Soft Matter - „complex fluids“ world between fluid and solid

Polymers

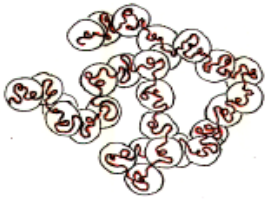

Length- and Timescales Contrasts

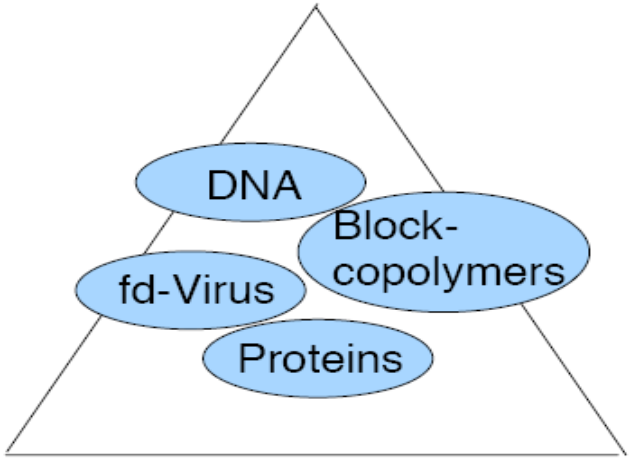

Colloids

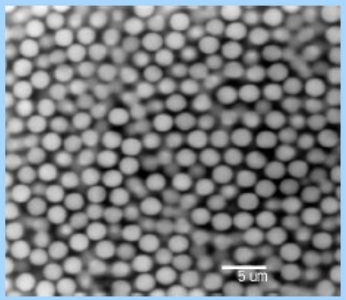

Surfactants

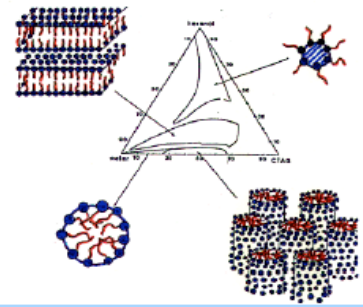

Equilibrium and Non-Equilibrium States

Characteristic length and time scales

(© P. Schurtenberger)

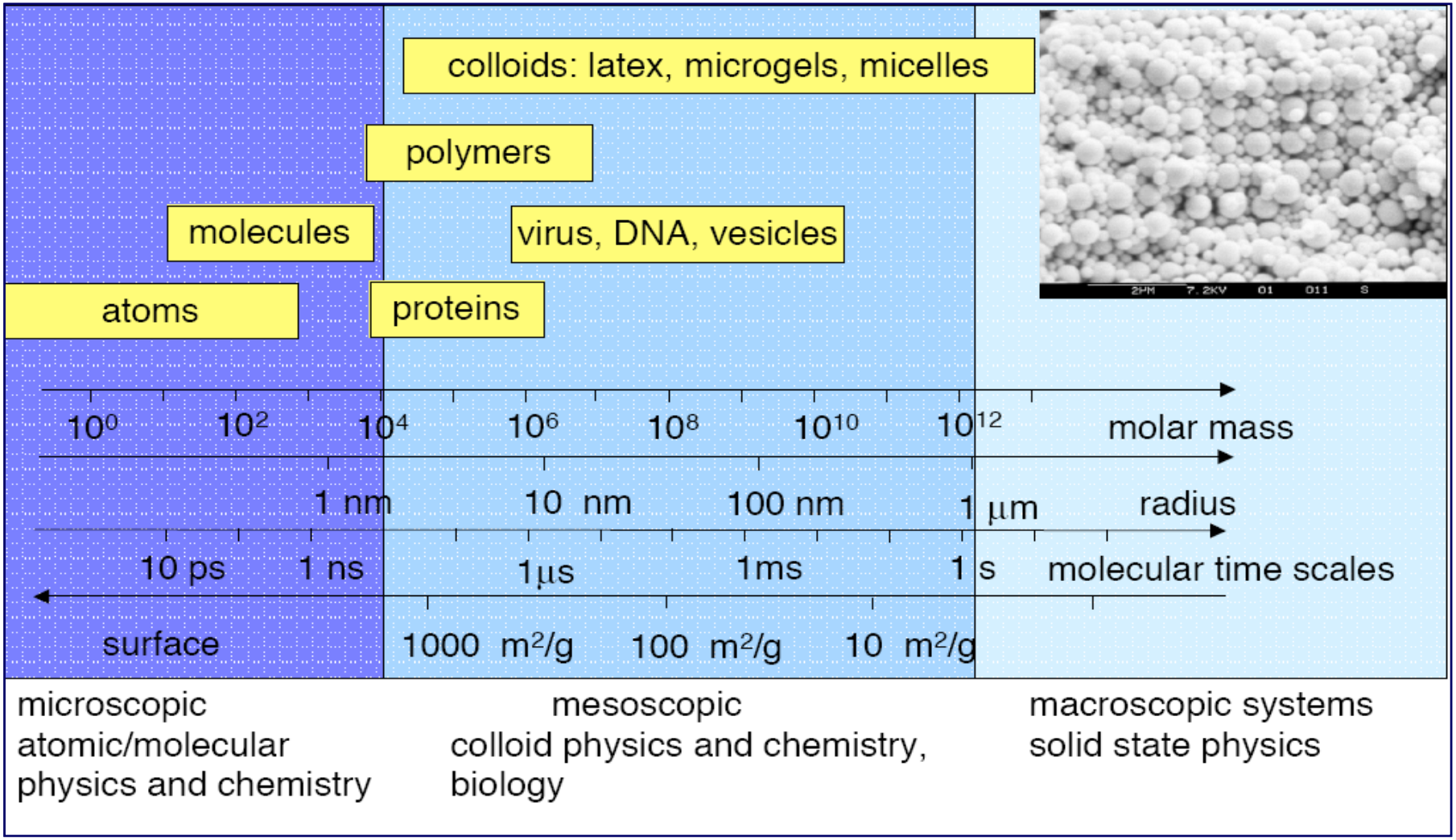

amenitsch@tugraz.at &
amenitsch@elettra.trieste.it

Research topics

ZnS NPs growth in a liquid jet

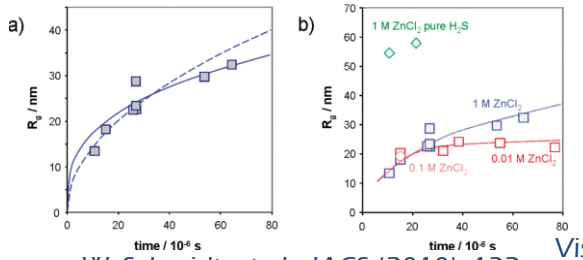

W. Schmidt, et al., JACS (2010), 132, 6822-6826

CdS nucleation and growth

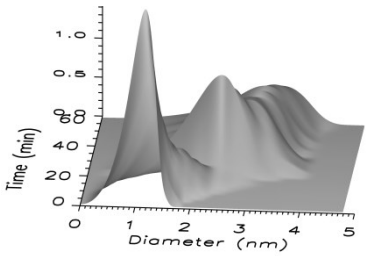

Viswanatha,R. *et al. J. Phys. Chem. Lett.* 1, 304 (2010)

Formation of mesoporous & crystalline materials

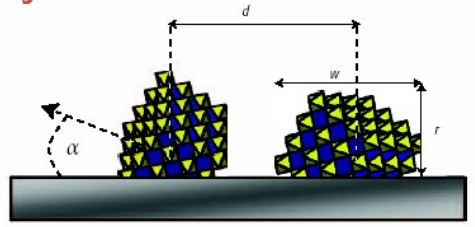

Grosso, D. et.al. *Nature Materials* 2004, *3*, 787-792.

Proteins

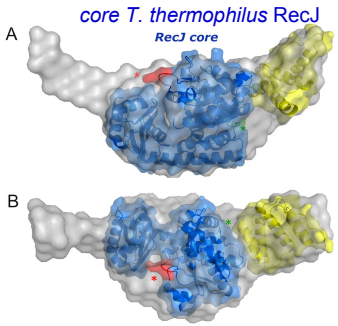

helical domain of the acyl-CoA

Krastanova I. et al. J. Biol. Chem. (2012)

Nanosystems

Biomechanics human arteries

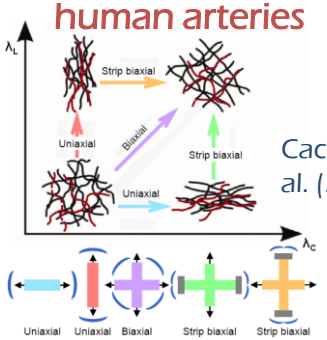

Cacho-Nerin, F., et al. (2015)

Biomembranes & drug delivery systems

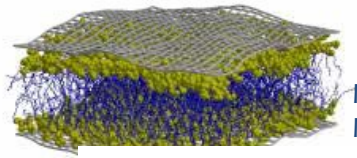

R. Böckmann, University of Zürich.

Rappolt M, Pabst G, Mariani et al.

Mesostructured SiO_2 produced by aerosol reaction

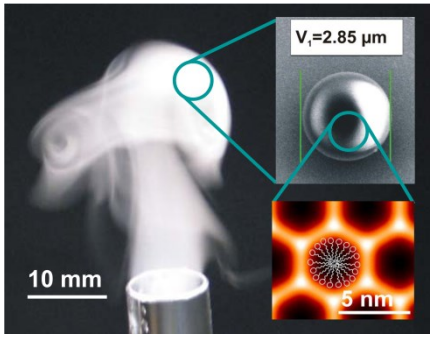

I.Shyjumon, et al., Rev.Scient.Instr., 79 (4), 043905 (2008), Langmuir (2011)

amenitsch@tugraz.at &
amenitsch@elettra.trieste.it

SAXS and WAXS

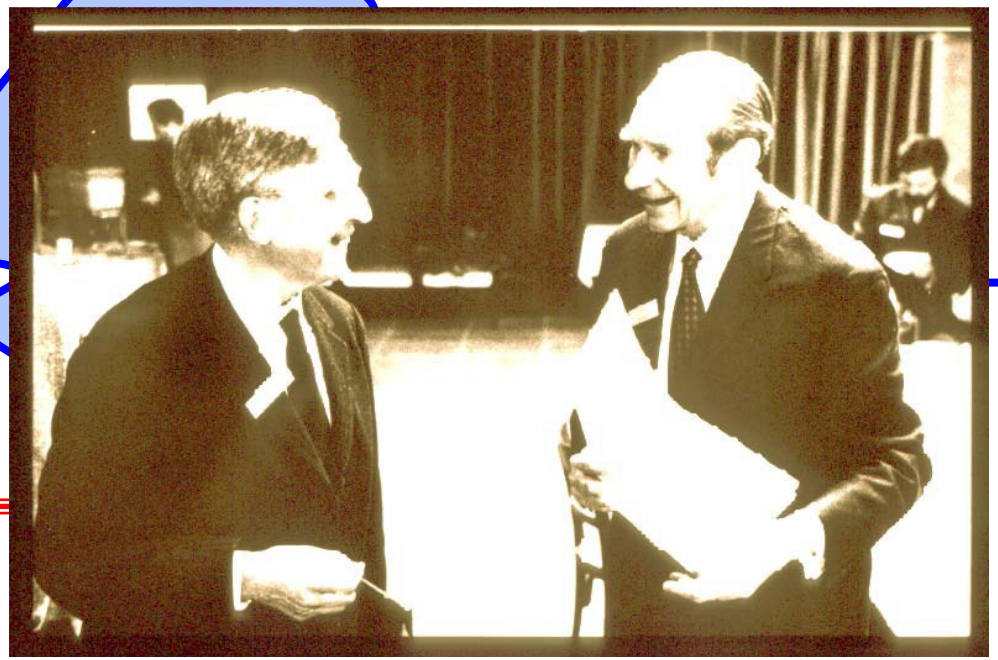

DETECTOR

Beam Stop

X-rays

SAXS

Andre Guinier Otto Kratky

The pioneers of Small Angle Scattering

WAXS

amenitsch@tugraz.at &
amenitsch@elettra.trieste.it

SAXS and WAXS

Small – Angle : Supramolecular Envelope

Bragg's law:

$$\sin \theta/2 = \lambda / 2d$$

small θ large d

For CuK_α 0.154 nm (8 keV)

20 deg	0.5 nm
0.9 deg	10 nm
0.09 deg	100 nm

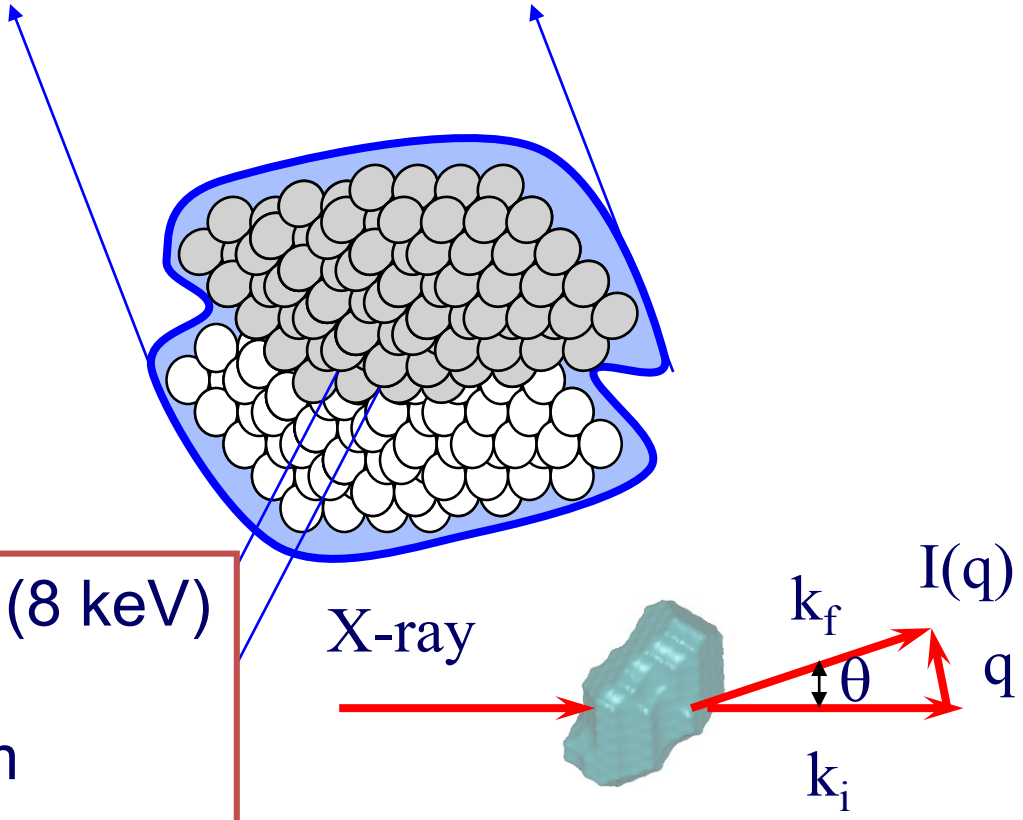

Molecular Lattice

The Scattered Field $E_s(q)$

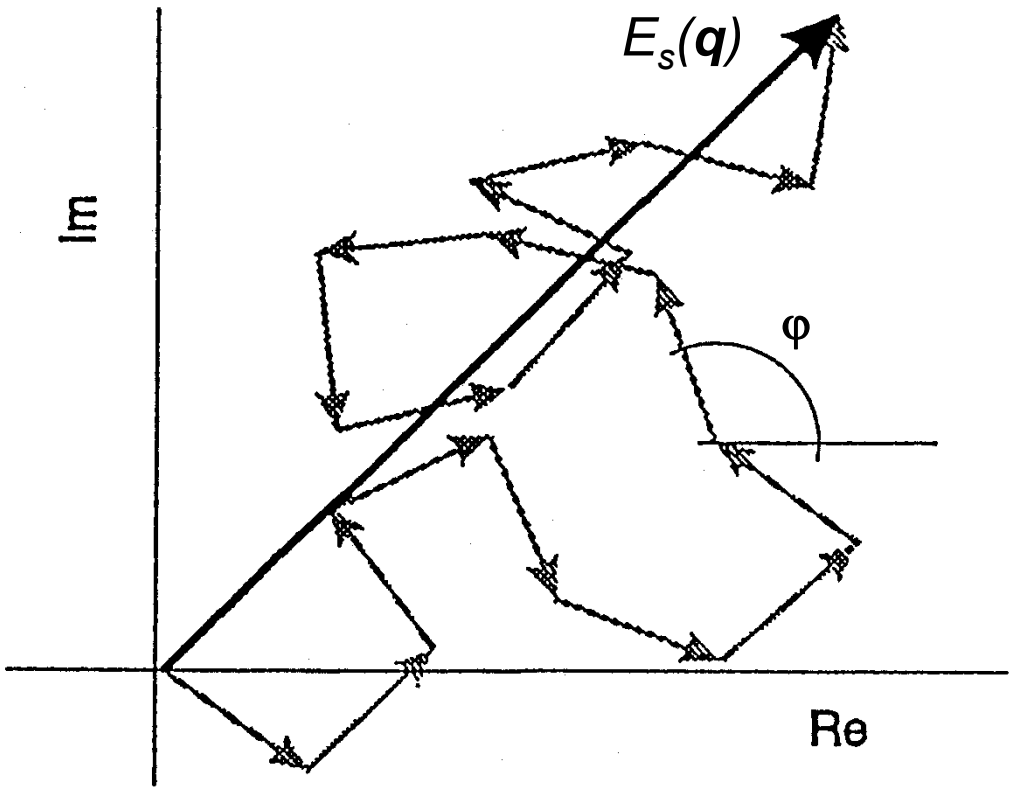

The scattering amplitudes of all coherently scattered waves have to be added according to their amplitude and relative phase $e^{i\varphi}$.

The phase difference depends on the relative location of the scattering centers.

amenitsch@tugraz.at &
amenitsch@elettra.trieste.it

The Phase Difference φ and the Scattering Vector q

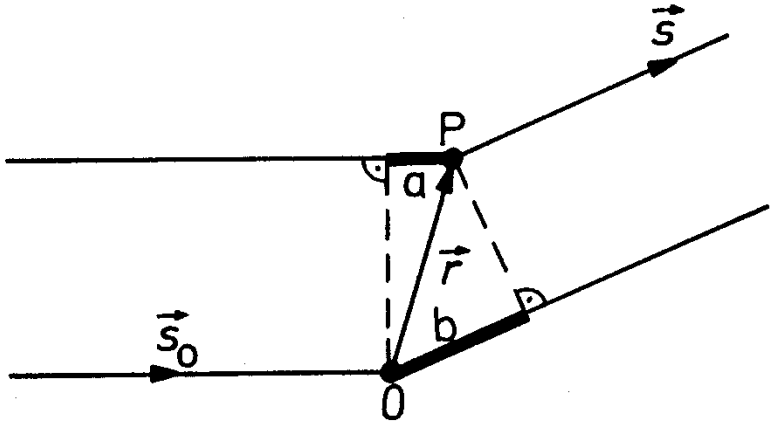

$$a = \vec{r} \cdot \vec{s}_0$$
$$b = \vec{r} \cdot \vec{s}$$

The path length difference is given by the length difference between the two paths a and b:

$$a - b = rs_0 - rs = -r(s-s_0)$$

The phase difference φ is given by the wave number $(2\pi/\lambda)$ times the path length difference:

$$\varphi = -(2\pi/\lambda)r(s-s_0)$$

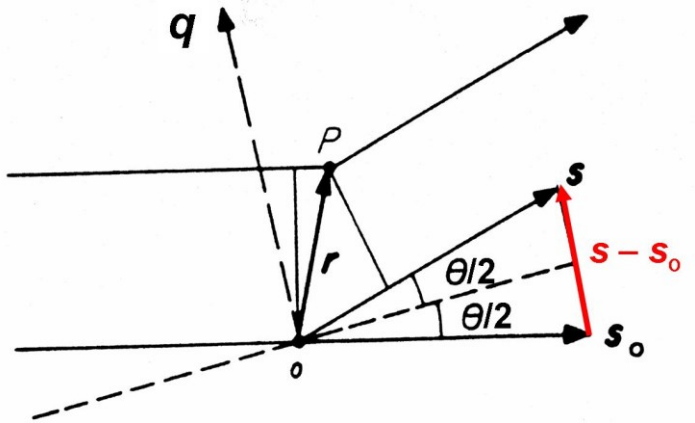

Now we introduce the scattering vector $\boldsymbol{q}$:

$$\boldsymbol{q} = (2\pi/\lambda)(s-s_0) \rightarrow \varphi = -qr$$

Its magnitude is:

$$q = 4\pi/\lambda \sin \theta/2$$

amenitsch@tugraz.at & amenitsch@elettra.trieste.it

The Scattered Field $E_s(\mathbf{q})$

In order to find the total scattered field we have to integrate over the whole illuminated scattering volume *V*

$$E_s(\mathbf{q}) = const \int_V \rho(\mathbf{r})\, e^{-i\mathbf{qr}}\, d\mathbf{r}$$

We can now express the density $\rho(\mathbf{r})$ by its mean $\bar{\rho}$ and its fluctuations $\Delta\rho(\mathbf{r})$:

$$\rho(\mathbf{r}) = \bar{\rho} + \Delta\rho(\mathbf{r})$$

The Fourier integral is linear, so we can rewrite the above equation:

$$E_s(\mathbf{q}) = const\left[\int_V \bar{\rho}\cdot e^{-i\mathbf{qr}}\, d\mathbf{r} + \int_V \Delta\rho(\mathbf{r})\, e^{-i\mathbf{qr}}\, d\mathbf{r}\right]$$

Taking into account the large dimension of the scattering volume we get:

$$E_s(\mathbf{q}) = const \int_V \Delta\rho(\mathbf{r})\, e^{-i\mathbf{qr}}\, d\mathbf{r}$$

amenitsch@tugraz.at & amenitsch@elettra.trieste.it

From Scattering Amplitudes to Scattering Intensities

For monodisperse dilute systems we can write:

$$I_s(q) = N < |E_1(\mathbf{q})|^2 > = N I_1(q)$$

We have introduced the single particle scattering amplitude $E_1(\mathbf{q})$ which is the scattered field resulting from integration over the particle volume only.

$$E_1(\mathbf{q}) = \int_V \Delta\rho(\mathbf{r})\, e^{-i\mathbf{qr}}\, d\mathbf{r}$$

$$|E_1(\mathbf{q})|^2 = E_1(\mathbf{q}) \cdot E_1^*(\mathbf{q}) = \int_V \int \Delta\rho(\mathbf{r}_1)\, \Delta\rho(\mathbf{r}_2)\, e^{-i\mathbf{q}(\mathbf{r}_1 - \mathbf{r}_2)}\, d\mathbf{r}_1\, d\mathbf{r}_2$$

We put $\mathbf{r}_1 - \mathbf{r}_2 = \mathbf{r}$ and use $\mathbf{r}_2 = \mathbf{r}_1 - \mathbf{r}$ and introduce the *convolution square* of the density fluctuations:

$$\gamma(\mathbf{r}) \equiv \Delta\beta^2(\mathbf{r}) = \int_V \Delta\rho(\mathbf{r}_1)\, \Delta\rho(\mathbf{r}_1 - \mathbf{r})\, d\mathbf{r}_1$$

amenitsch@tugraz.at & amenitsch@elettra.trieste.it

SAXS and WAXS

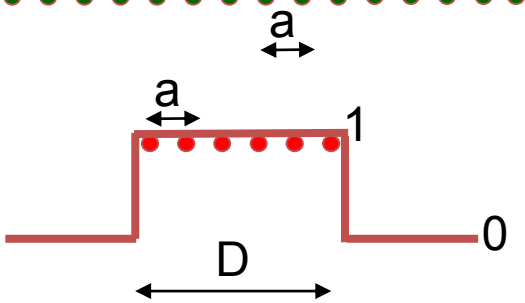

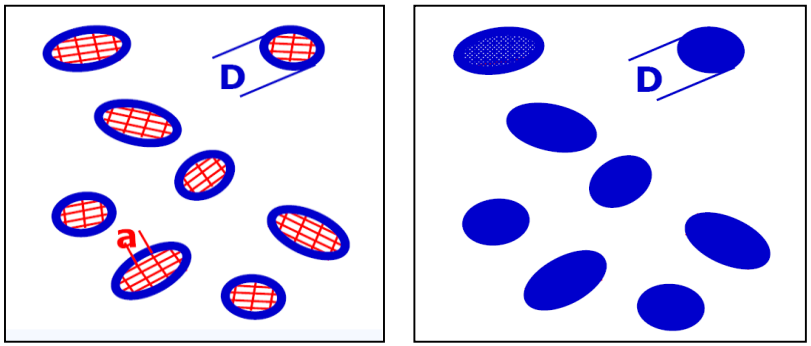

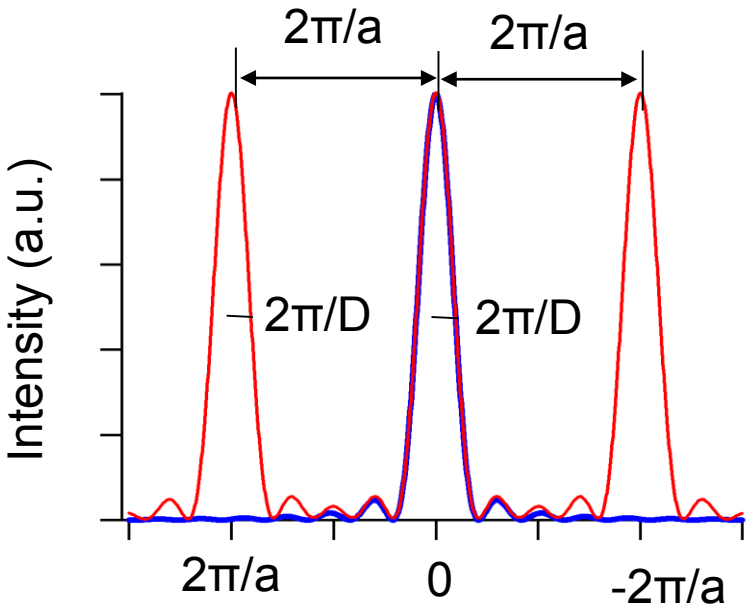

$$q = \frac{4\pi}{\lambda} \cdot \sin(\theta/2)$$

SAXS:
peak width (+ shape) → particle size

WAXS:
positions → lattice (type, spacings, strain)
width + shape → particle size
+ lattice strain fluctuations

amenitsch@tugraz.at &
amenitsch@elettra.trieste.it

The *Convolution Square* of the Density Fluctuations $\gamma(\mathbf{r})$ and $\gamma(r)$:

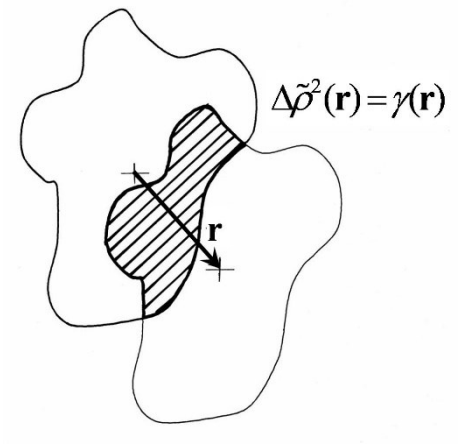

The function *γ(**r**)* is calculated by shifting the "ghost" particle a vector ***r*** and integrating the overlapping volume.

This function is also called *spatial autocorrelation function (ACF)*.

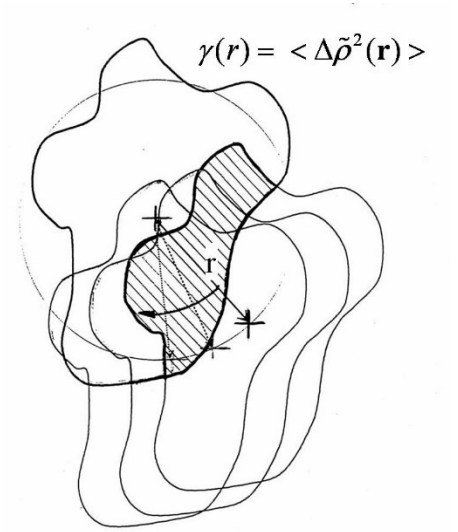

The spatially averaged convolution square γ(r) results from the same process, the ghost is shifted by a distance $r = |\mathbf{r}|$, but we have to average over all possible directions in space.

$$\gamma(r) = \beta_0^2(r) - V(\bar{\rho})^2 = <\Delta\beta_0^2(\mathbf{r})> = <\int_V \Delta\rho(\mathbf{r}_1)\,\Delta\rho(\mathbf{r}_1 - \mathbf{r})\,d\mathbf{r}_1>$$

amenitsch@tugraz.at & amenitsch@elettra.trieste.it

RDG: Spatially Averaged Intensity *I(q)*

The spatially averaged intensity *I(q)* is given by:

$$I(q) = <|E_1(\mathbf{q})|^2> = <\int_V \Delta\beta_0^2(\mathbf{r})\, e^{-i\mathbf{qr}}\, d\mathbf{r}>$$

$$= 4\pi \int_0^\infty \gamma(r)\, r^2\, \frac{\sin qr}{qr}\, dr$$

by introducing the *pair distance distribution function* (PDDF) *p(r)* with

$$p(r) = \gamma(r) \cdot r^2 = \Delta\beta_0^2(r) \cdot r^2$$

we finally get

$$I(q) = 4\pi \int_0^\infty p(r)\, \frac{\sin(qr)}{qr}\, dr$$

amenitsch@tugraz.at & amenitsch@elettra.trieste.it

The Scattering Problem and the Inverse Scattering Problem

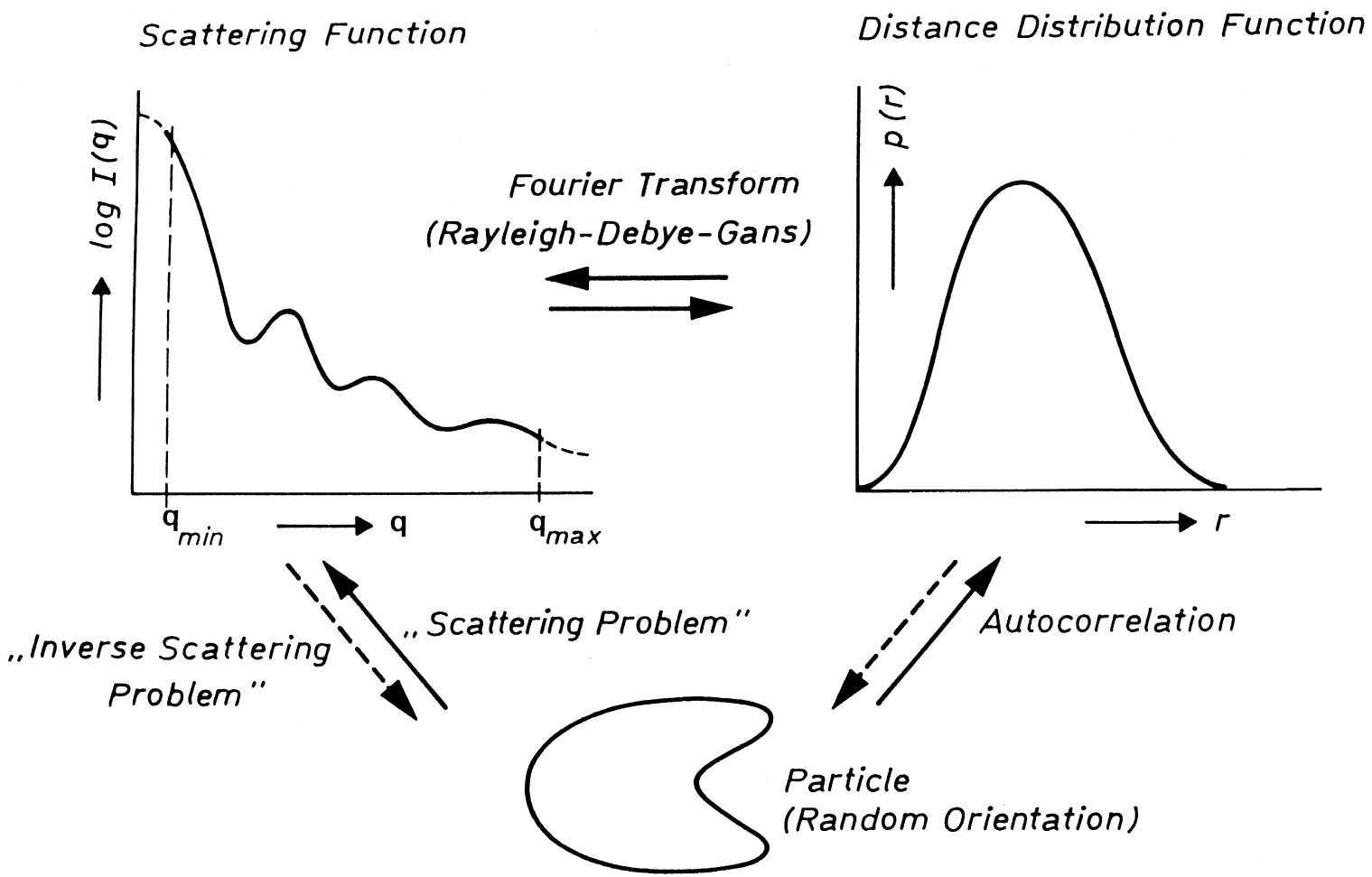

amenitsch@tugraz.at &
amenitsch@elettra.trieste.it

Definition of the *Pair Distance Distribution Function* (PDDF) *p(r)*

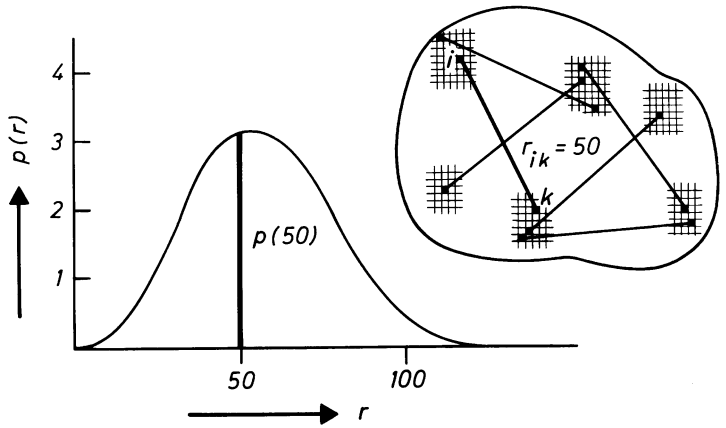

We can relate the meaning of a distance histogram to the PDDF *p(r)* if the particles are homogeneous. The height of *p(r)* is proportional to the number of distances that can be found inside the particle within the interval *r* and *r+dr*

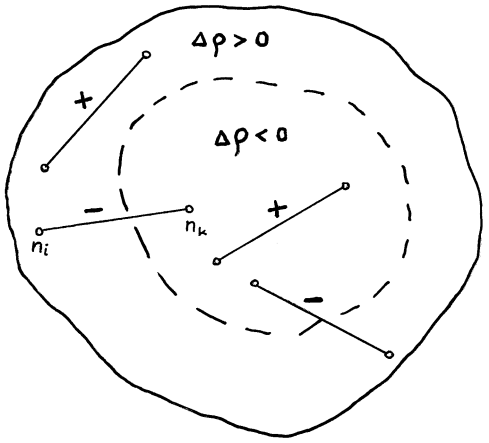

The *p(r)* function of inhomogeneous particles is proportional to the product of the difference scattering lengths $n_i n_k$ [$n_i = \Delta\rho(\mathbf{r}_i)dV(\mathbf{r}_i)$] of two volume elements *i* and *k* with a center-to-center distance between *r* and *r+dr* and we sum over all pairs with this distance.

amenitsch@tugraz.at &
amenitsch@elettra.trieste.it

Inverse Problem in Scattering – Artists View*

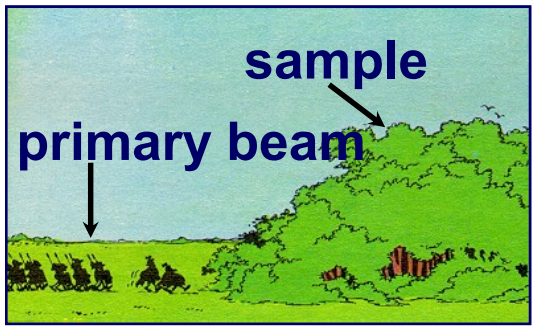

design of the experiment

result in q-space

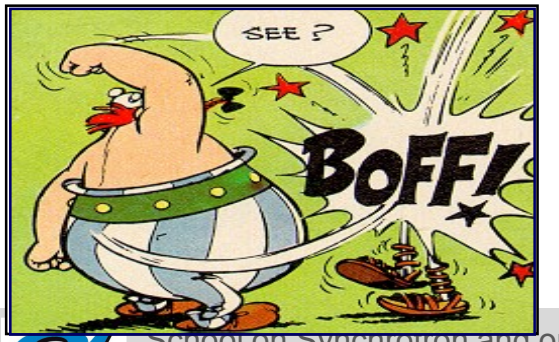

?

structure of the scattering particle

*** "Asterix in Belgium"**

associated by Anna Stradner & Gerhard Fritz

amenitsch@tugraz.at &
amenitsch@elettra.trieste.it

RDG: The Particle Form Factor

$$I_s(q) = NI_1(q) = NI_1(0)P(q)$$

$I_1(0) = V^2 \Delta\rho^2$ intensity of single particle at q = 0

$P(q)$ particle form factor, where

$$P(q) = \frac{I_1(q)}{I_1(q \to 0)}$$

The normalized form factor *P(q)* contains information about size and structure of the particle.

Form factor of a homogeneous sphere:

$$P(q) = \left[\frac{3(\sin qR - qR\cos qR)}{(qR)^3} \right]^2$$

amenitsch@tugraz.at &
amenitsch@elettra.trieste.it

The Particle Form Factor

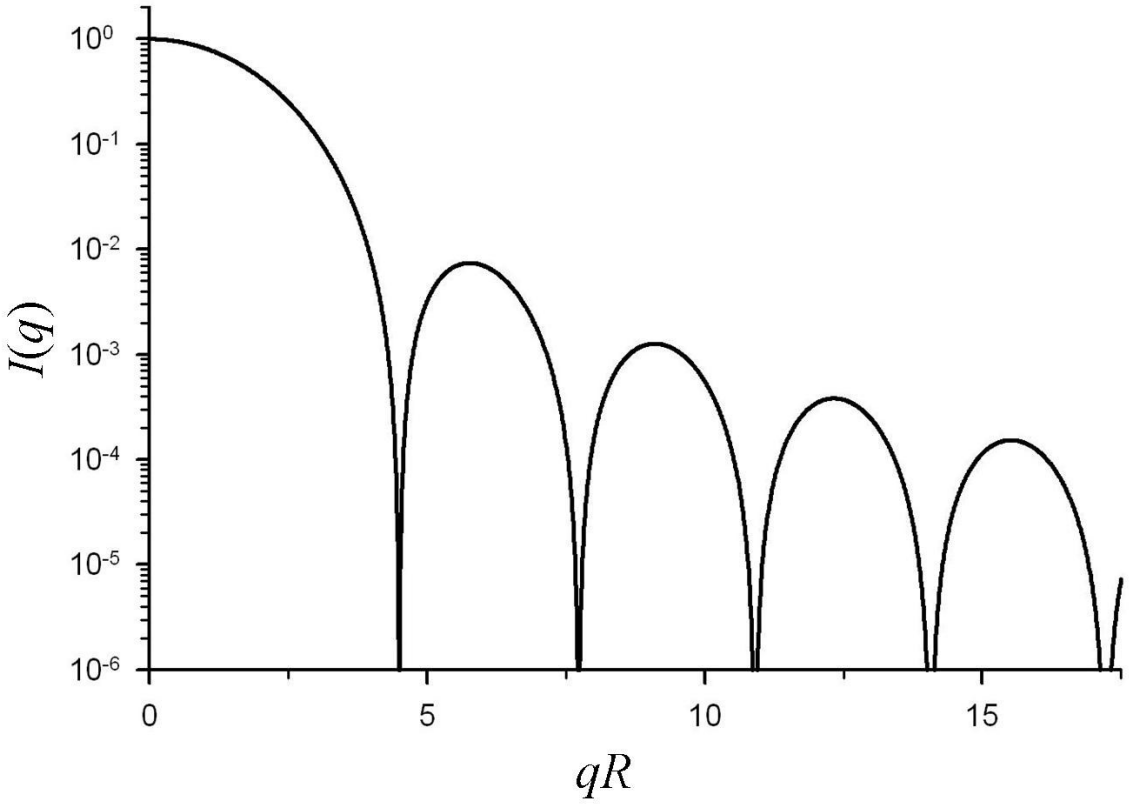

The function has minima for tan(qR) = qR, or qR = 4.49, 7.73, …

amenitsch@tugraz.at &
amenitsch@elettra.trieste.it

Different Shapes of Homogeneous Particles

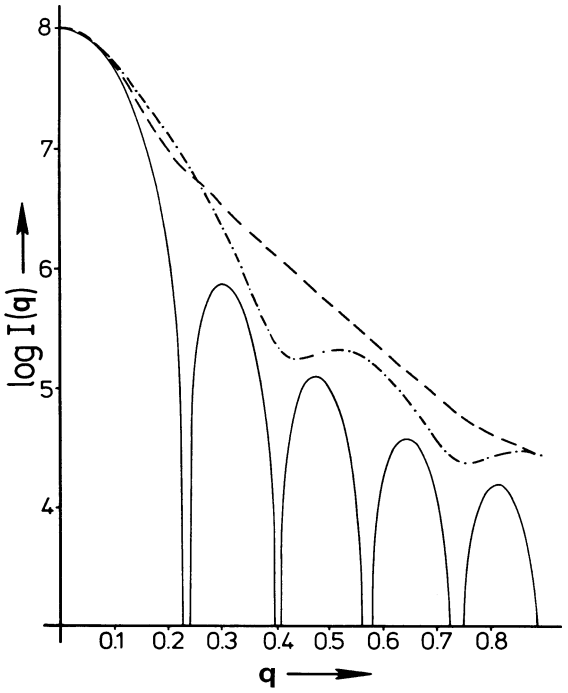

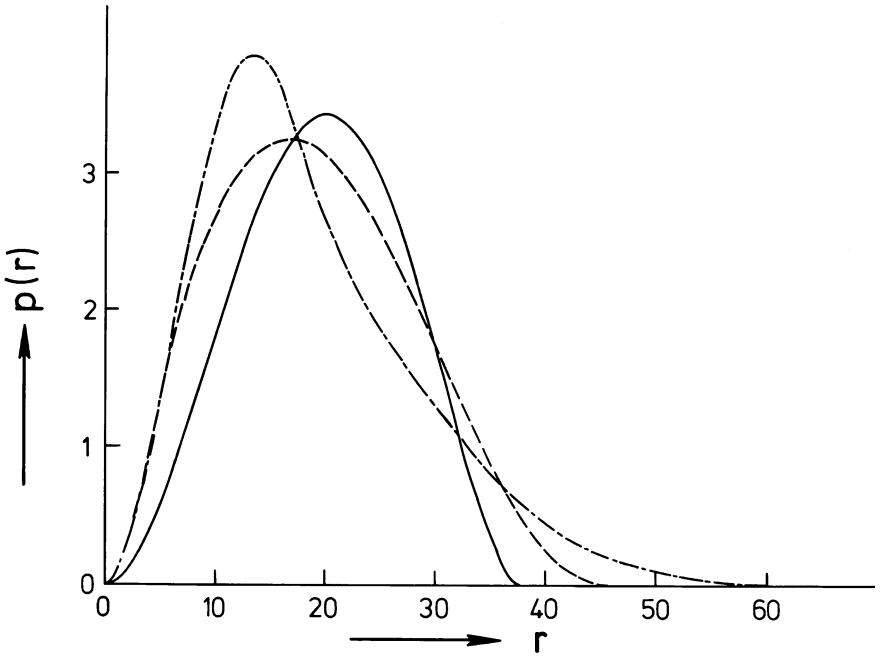

Comparison of a sphere (full line) an oblate ellipsoid (dashed line) and a prolate ellipsoid with the same volume.

amenitsch@tugraz.at &
amenitsch@elettra.trieste.it

Rod-like Particles

Let us regard a rod of length *L* and of cross-section A_c = The cross-section A_c (with maximum dimension d) should be small in comparison to the length of the whole particle L (d<<L). For $q > 1/L$ we can write

$$I(q) = \frac{L\pi}{q} \cdot I_c(q)$$

The cross-section scattering function $I_c(q)$ is related to the cross-section distance distribution $p_c(r)$ by

$$I_c(q) = 2\pi \int_0^\infty p_c(r) J_0(qr)\, dr$$

where

$$p_c(r) = \gamma_c(r) \cdot r = 2\pi r \int_{Ac} \Delta\rho_c(r') \Delta\rho_c(r'+r)\, dr$$

amenitsch@tugraz.at & amenitsch@elettra.trieste.it

Scattering Function for a Long, Rod-like Particle Schematic Representation

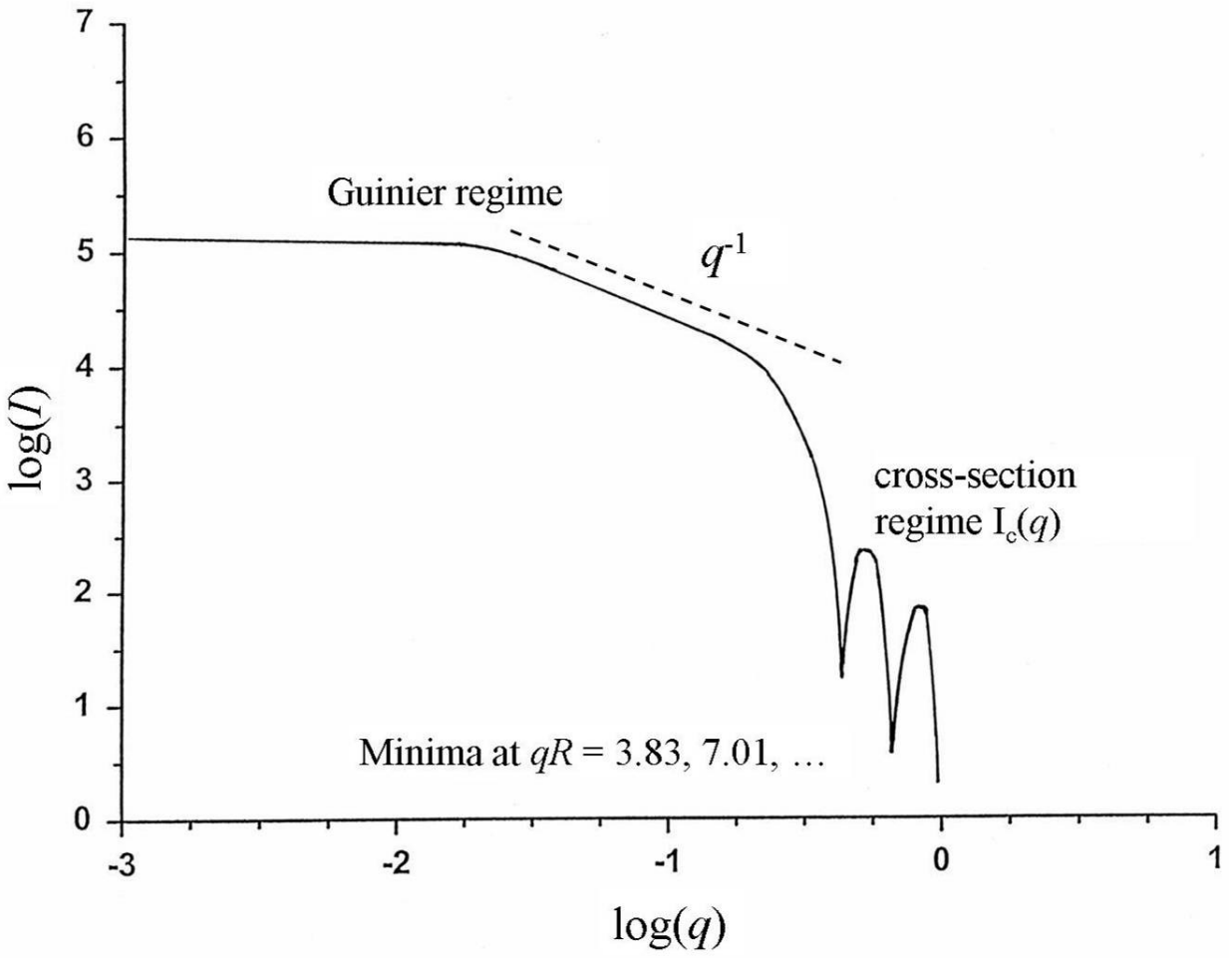

The different regimes can be visualized is a *log(I)* vs. *log(q)* plot of the scattering curve:

The Guinier regime, the q^{-1} regime and the cross-section regime.

amenitsch@tugraz.at & amenitsch@elettra.trieste.it

PDDF's for Rod-like Particles

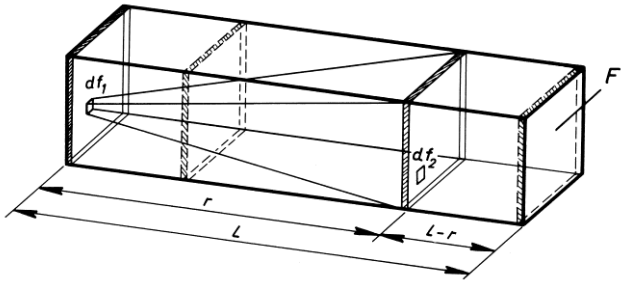

$$p(r) = \frac{2}{4\pi} \int_r^L \int_A \int_A \Delta\rho^2 df_1\, df_2\, dx = \frac{1}{2\pi} \Delta\rho^2 A_c^2 (L - r),$$

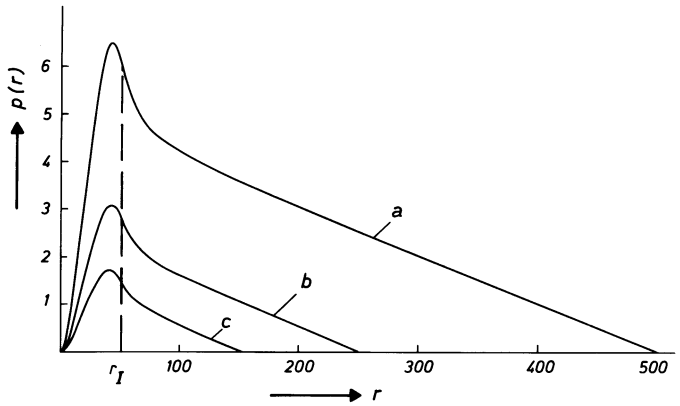

PDDF from homogeneous prisms with edge lengths of: (a) 50:50:500, (b) 50:50:250 and (c) 50:50:150

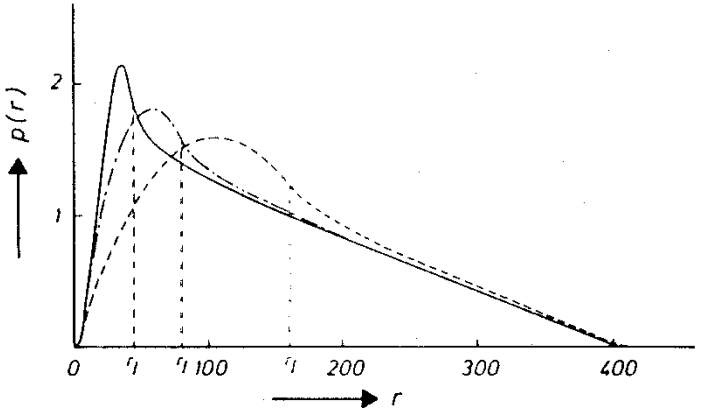

PDDF for three parallel epipeds with constant length L (400 Å) and constant cross-section area A_c but varying length of the edges: 40:40, -≺-≺- 80:20 and ----- 160:10.

amenitsch@tugraz.at &
amenitsch@elettra.trieste.it

Let us now consider a flat particle, with a finite and constant thickness D_t, being extremely large in the two other dimensions with an area A. In full analogy to the case of the rod we can separate the scattering amplitude into a *planar factor* $2\pi Aq^{-2}$ and a *thickness-factor* $I_t(q)$, i.e. the total intensity is given by

$$I(q) = I_{plane} \cdot I_t(q) = \frac{2\pi A}{q^2} \cdot I_t(q).$$

The thickness-factor is related to the thickness distance distribution $p_t(r)$ by

$$I_t(q) = 2\int_0^\infty p_t(r)\cos(qr)\,dr$$

where

$$p_t(r) = \gamma_t(r) = 2\int_0^\infty \Delta\rho_t(r')\,\Delta\rho(r'+r)\,dr.$$

amenitsch@tugraz.at & amenitsch@elettra.trieste.it

Scattering Function for a Flat, Lamellar Particle. Schematic Representation

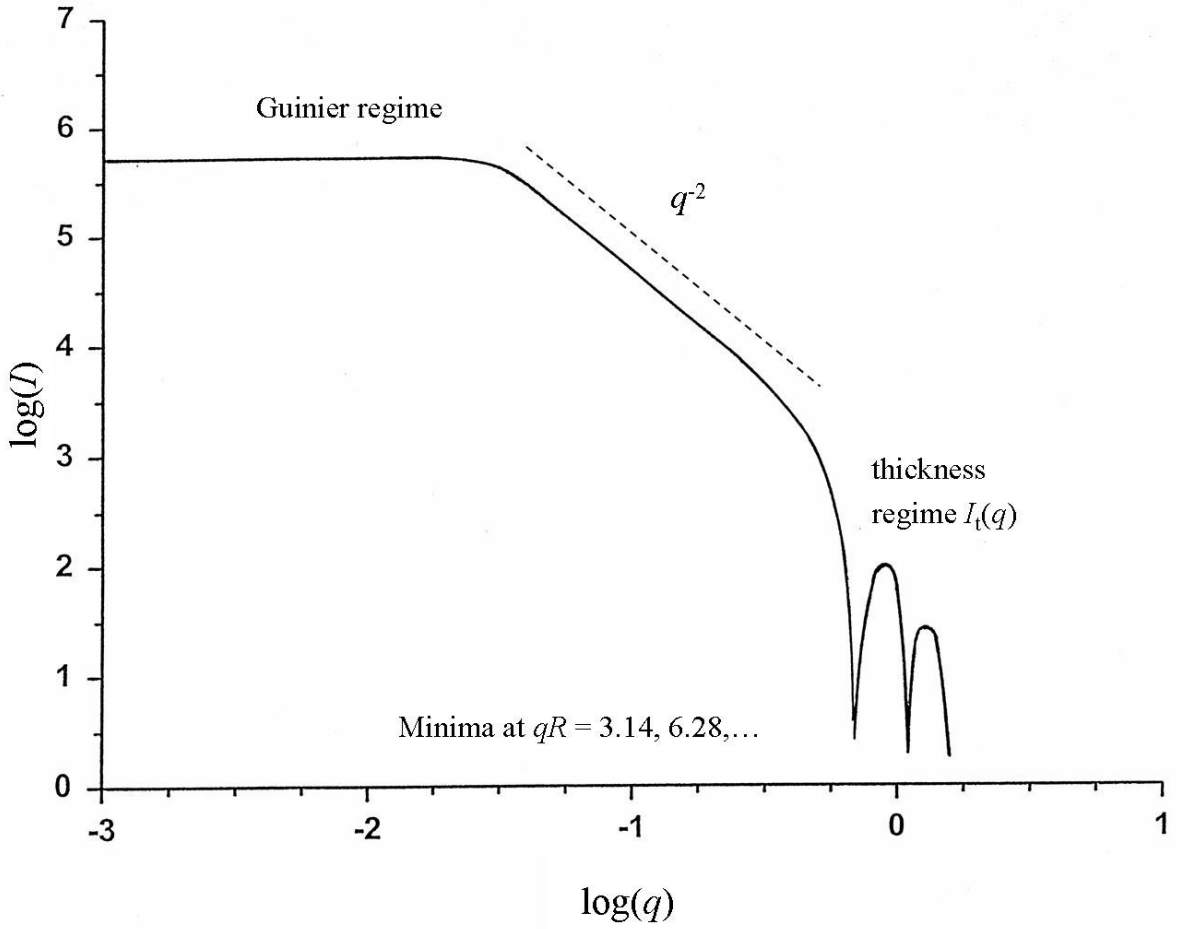

The different regimes can be visualized is a *log(I)* vs. *log(q)* plot of the scattering curve:

The Guinier regime, the q^{-2} regime and the thickness regime.

amenitsch@tugraz.at &
amenitsch@elettra.trieste.it

PDDF‘s for Flat Particles

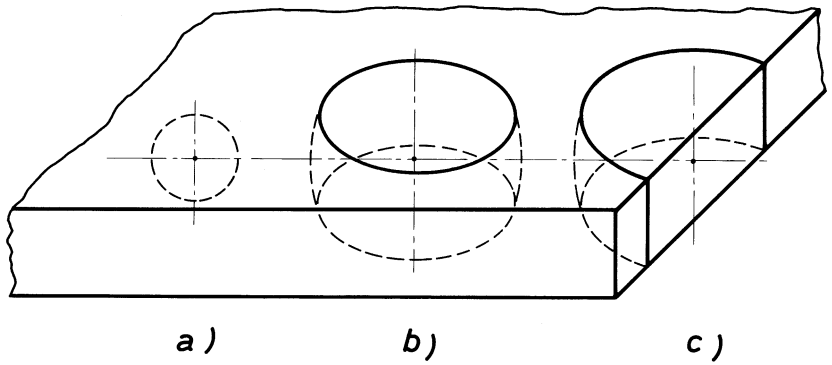

Sketch for the qualitative discussion of the PDDF of a flat particle

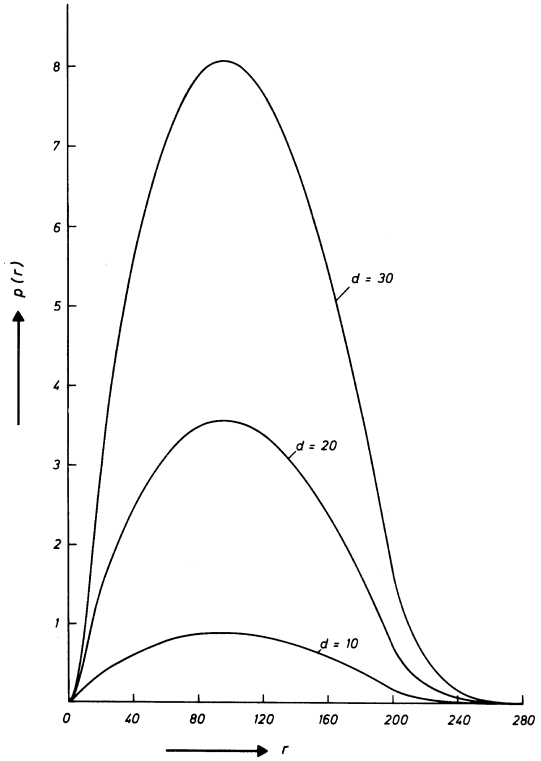

PDDFs of lamellar particles with the same basal plane (200 x 200Å) and different thickness D_t: (a) D_t = 10Å, (b) D_t = 20Å and (c) D_t = 30Å.

amenitsch@tugraz.at &
amenitsch@elettra.trieste.it

Inhomogeneous Particles: Spheres and Cylinders with Radial Inhomogeneity

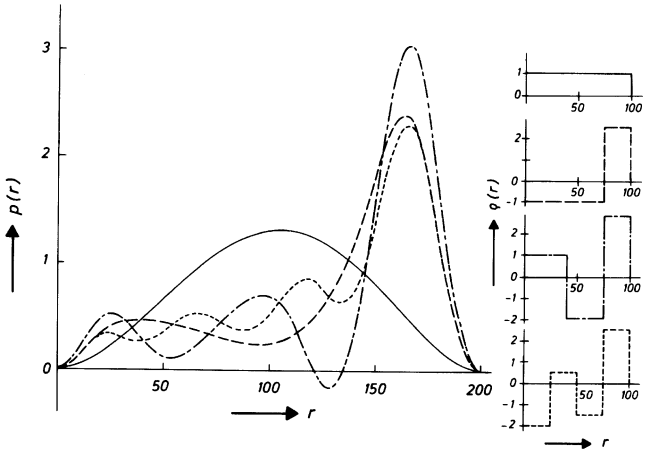

Spherical multilayer models with constant outer diameter of 200 Å. PDDFs in the left part, density profiles in the right part of the figure.

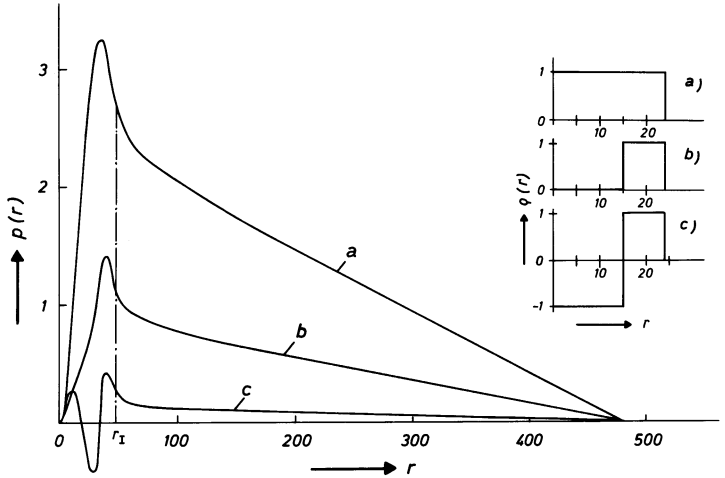

Circular cylinders with a constant length of 480 Å and an outer diameter D_c of 48 Å. (a) Homogeneous cylinder, (b) hollow cylinder, (c) inhomogeneous cylinder. The PDDFs are shown on the left, the corresponding radial density distributions $\rho(r)$ on the right.

amenitsch@tugraz.at & amenitsch@elettra.trieste.it

Aggregates - Dimers

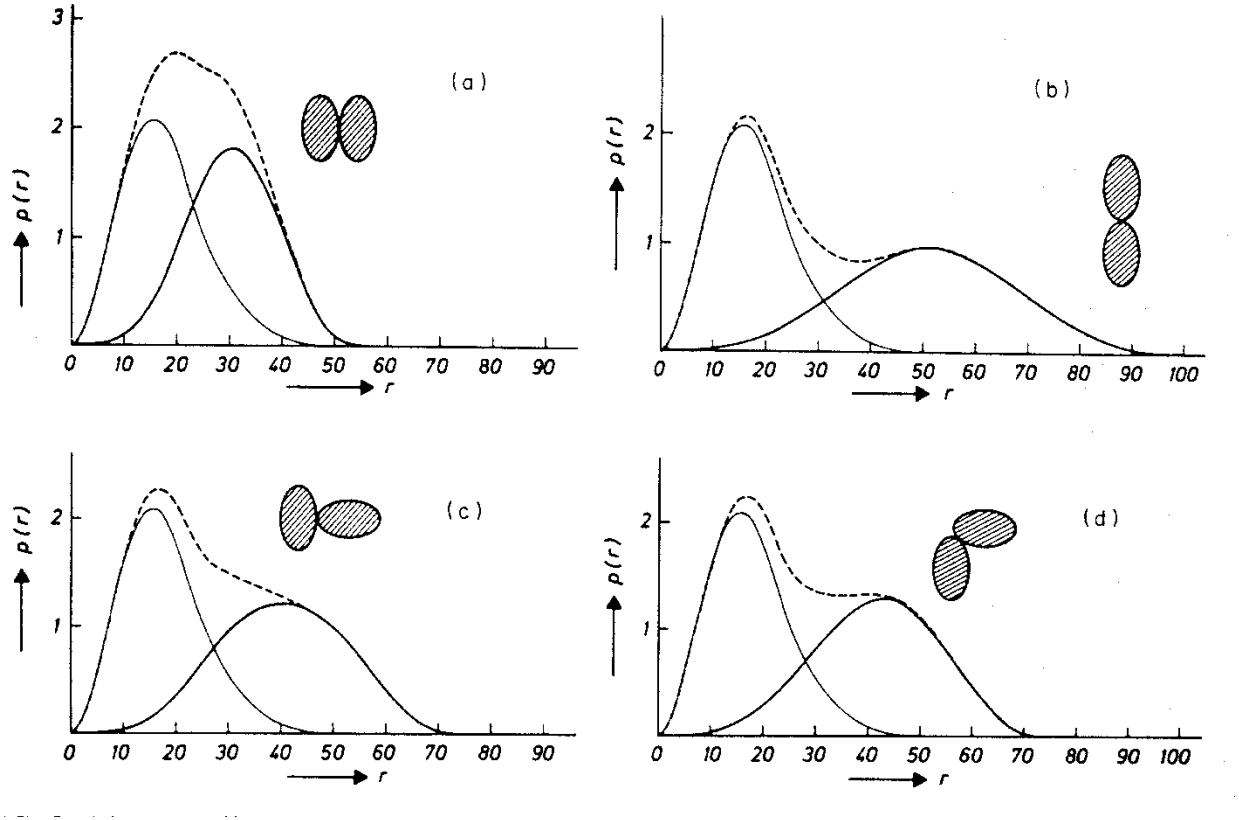

PDDFs from dimer models built from prolate ellipsoids. Monomers (full line), dimers (broken line), and difference between dimers and monomers (thick full line).

amenitsch@tugraz.at &
amenitsch@elettra.trieste.it

Polydisperse Systems

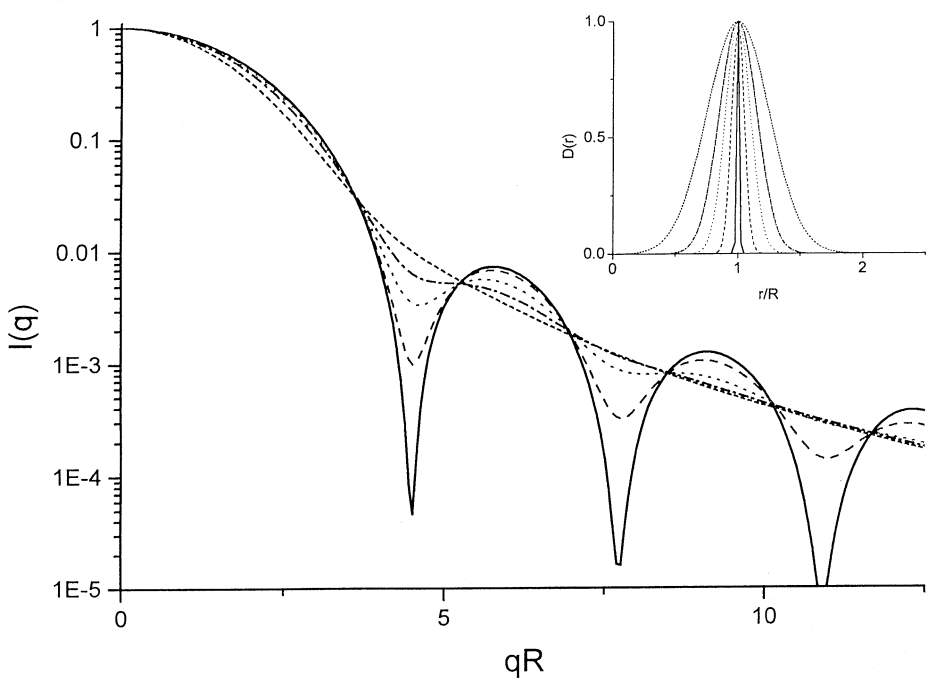

Intensity Distribution

$$I(q) = c_i \int_0^\infty D_i(R) \cdot P_0(q,R)\, dR$$

Volume or Mass Distribution

$$I(q) = c_v \int_0^\infty D_v(R) \cdot R^3 \cdot P_0(q,R)\, dR$$

Number Distribution

$$I(q) = c_n \int_0^\infty D_n(R)\, R^6 \cdot P_0(q,R)\, dR$$

Scattering curves of Gaussian size distributions of spheres with varying width (see inset).

amenitsch@tugraz.at &
amenitsch@elettra.trieste.it

Radius of Gyration

The radius of gyration is one of the most important parameters in the field of small-angle scattering. In full analogy to the radius of intertia in mechanics it is defined as

$$R_g^2 = \frac{\int \Delta\rho\,(r_1)\, r_i^2\, dV_i}{\int \Delta\rho\,(r_i)\, dV_i}$$

According to the momentum theorem of Fourier transformation the second moment of a function in one space is related to the second derivative (curvature) of its Fourier transform at the origin. This relation is the basis of the so-called *Guinier approximation* for the description of *I(q)* for low *q* derived from a series expansion:

$$I(q) = I(0)\, e^{-\frac{q^2 Rg^2}{3}}$$

We can also use another relation for the estimation of the radius of gyration:

$$R_g^2 = \frac{\int p\,(r)\, r^2\, dr}{2\int p\,(r)\, dr}$$

amenitsch@tugraz.at & amenitsch@elettra.trieste.it

Radius of Gyration - Guinier Plot

From the previous equation it is clear that we can calculate the radius of gyration from the PDDF once it is known. Otherwise we can use the Guinier approximation to determine R_g directly from the scattering data with a so-called *Guinier-plot*.

Plotting *ln (I(q)) vs* q^2 we get a straight line with a slope proportional to R_g^2.

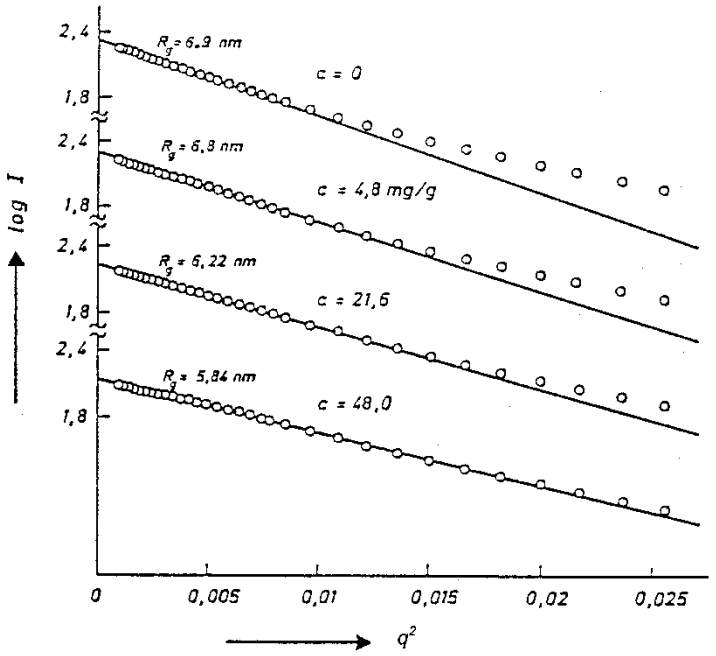

Example for a Guinier plot from scattering data of a protein solution with varying concentration, including an extrapolation to zero concentration.

amenitsch@tugraz.at & amenitsch@elettra.trieste.it

Radius of Gyration of the Cross-Section

For rod-like particles we can also define a radius of gyration of the cross-section which can be calculated from $p_c(r)$ by

$$R_c^2 = \frac{\int p_c(r)\, r^2\, dr}{2\int p_c(r)\, dr}$$

or it can be estimated in reciprocal space form

$$I_c(q) = I_c(0)\, e^{-\frac{q^2 R_c^2}{2}}$$

by a so-called cross section Guinier plot *[log(I(q)q) vs. q^2].*

amenitsch@tugraz.at & amenitsch@elettra.trieste.it

Radius of Gyration of the Thickness Function

For lamellar particles we can also define a radius of gyration of the thickness function which can be calculated from $p_t(r)$ by

$$R_t^2 = \frac{\int p_t(r)\, r^2\, dr}{2\int p_t(r)\, dr}$$

or it can be estimated in reciprocal space form

$$I_t(q) = I_t(0)\, e^{-q^2 R_t^2}$$

by a so-called thickness Guinier plot *[log(I(q)q²) vs. q²].*

amenitsch@tugraz.at & amenitsch@elettra.trieste.it

Porod Limit - Porod Plot - Fractals

We proceed now to the discussion of the **final slope** of the scattering curve at high *q*-values, we may expect this to depend mainly on the fine structure of the particle.

$$I(q)_{q\to\infty} = (\Delta\rho)^2 \cdot \frac{2\pi}{q^4} \cdot S$$

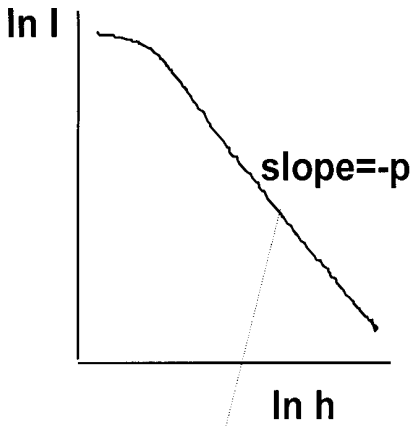

For mass fractals,where
$1 < D < 3$, and $M \propto R^D$
it holds, that
$p = D$

For **surface** fractals, where
$2 < D_s < 3$
it holds, that
$p = 6 - D_s$

Contrast Variation: Index Match

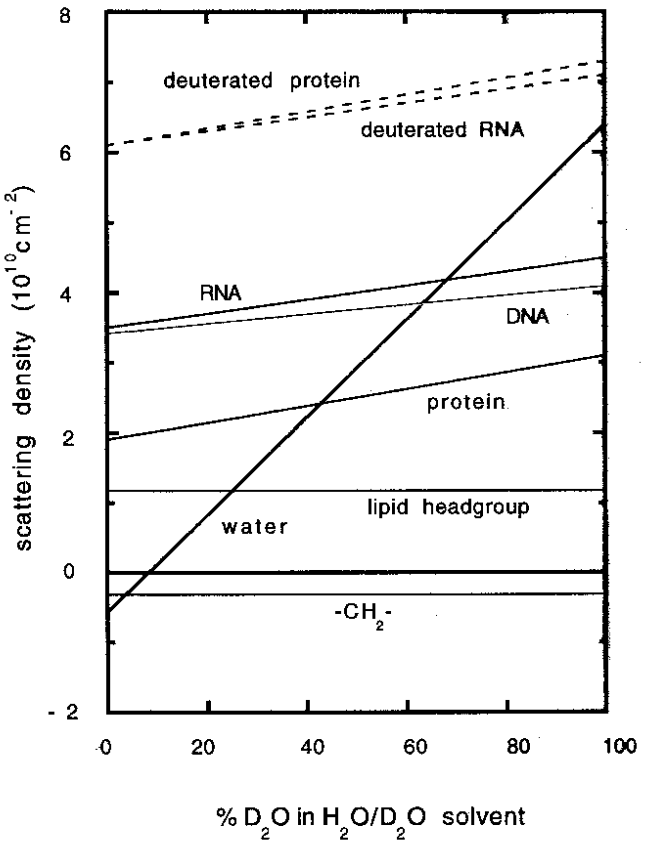

A mixture of H2O and D2O allows to match different regions in a sample.

When the monster came, Lola, like the peppered moth and the arctic hare, remained motionless and undetected, Harold, of course, was immediately devoured!

Autrans'94 R. May (found in „Los Alamos Science")

amenitsch@tugraz.at &
amenitsch@elettra.trieste.it

Contrast Variation in SAXS by Anomalous Scattering

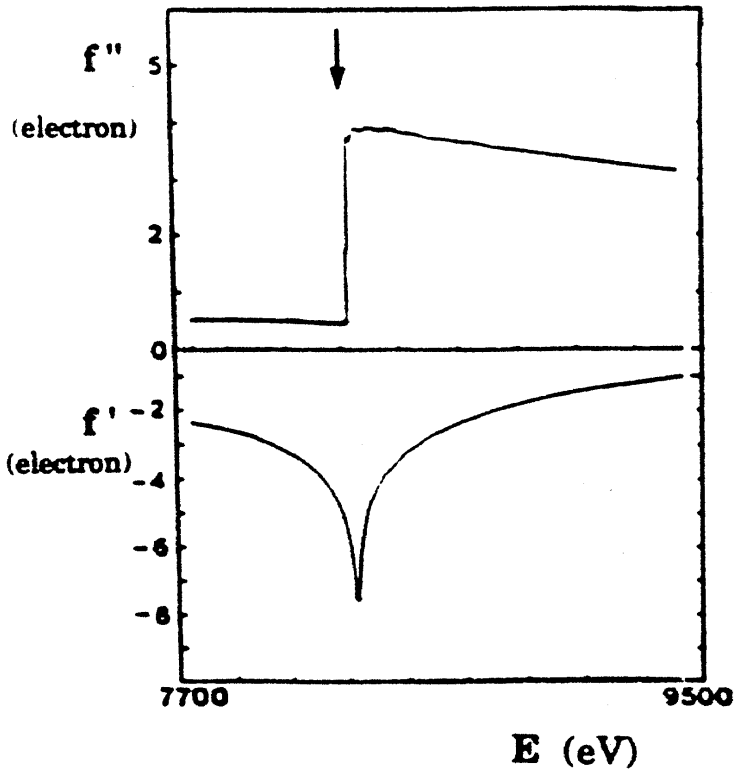

Typical energy dependence of f' and f'' near the absorption edge of an element. Shown here is the nickel *K* edge at 8333 eV.

This method, also known as *resonant small angle scattering* uses another possibility for the variation of the contrast. Near the inner shell absorption edge, the coherent scattering length or atomic scattering factor of an atom is a function of the energy *E* of the X-ray photon:

$$f(E) = Z + f'(E) + if''$$

Energy variation is only possible with the "white" X-ray beam of a synchrotron. The main problem for applications in chemistry is the fact that the edges for *C, H, N* and *O* are outside the useful energy window at very low energies. In solution experiments this effect might be useful for heavy counter ions (Br^+) in micellar systems.

amenitsch@tugraz.at &
amenitsch@elettra.trieste.it

The Scattering Problem and the Inverse Scattering Problem

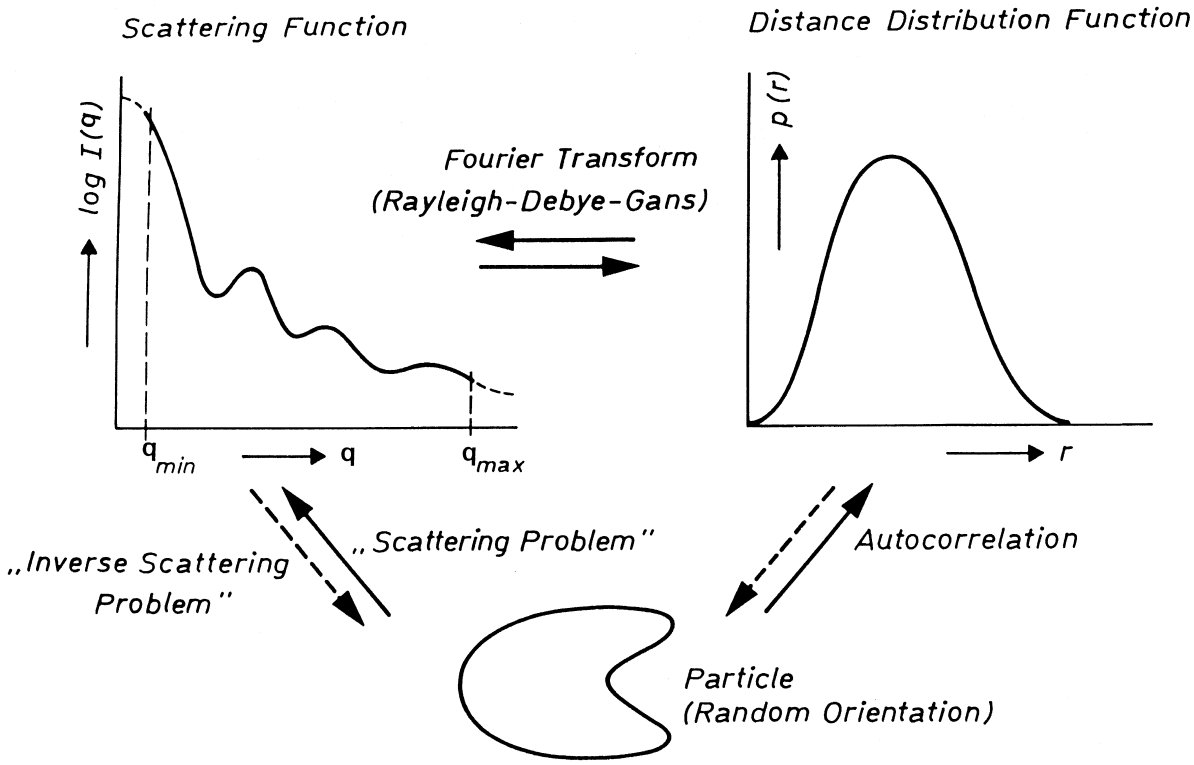

For the solution of the inverse Problem it is essential to be able to calculate the PDDF form the experimental scattering curve with minimum termination effect.

amenitsch@tugraz.at &
amenitsch@elettra.trieste.it

From experimental data to the PDDF

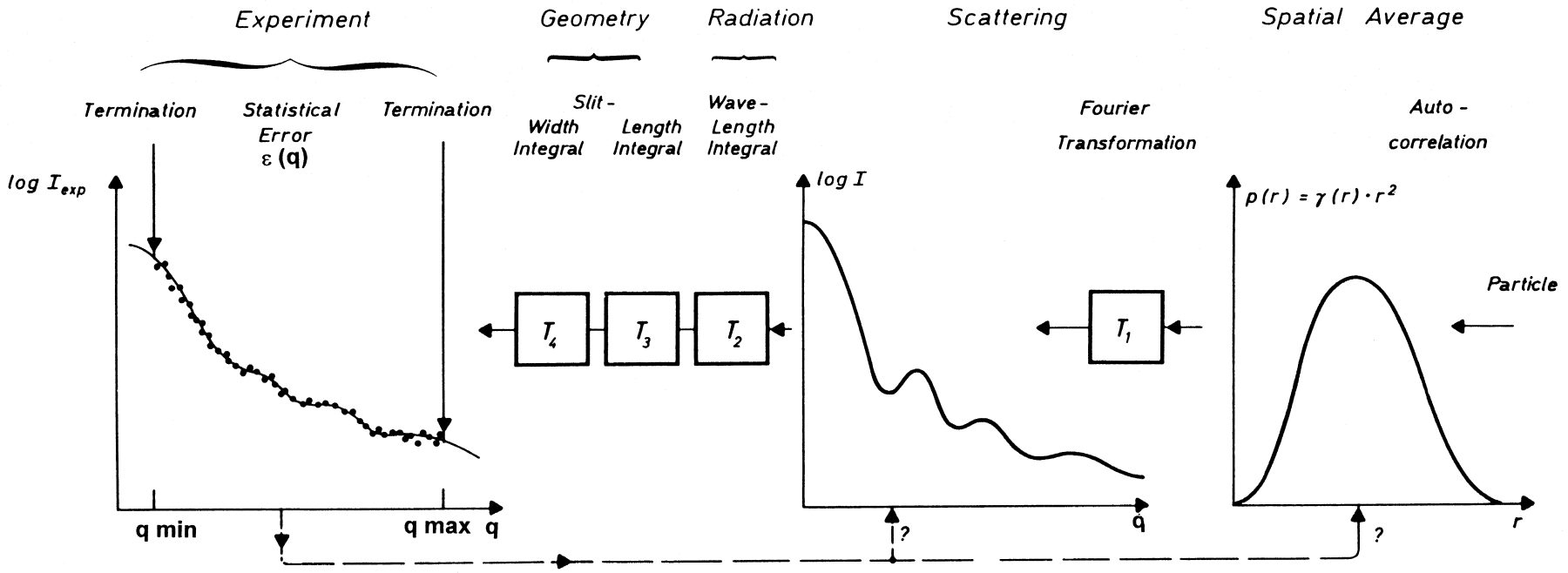

All Transformations T1 to T4 are linear and are mathematically well defined, this does not hold for their inverse transformations.

amenitsch@tugraz.at &
amenitsch@elettra.trieste.it

The Principles of the Indirect Fourier Transformation

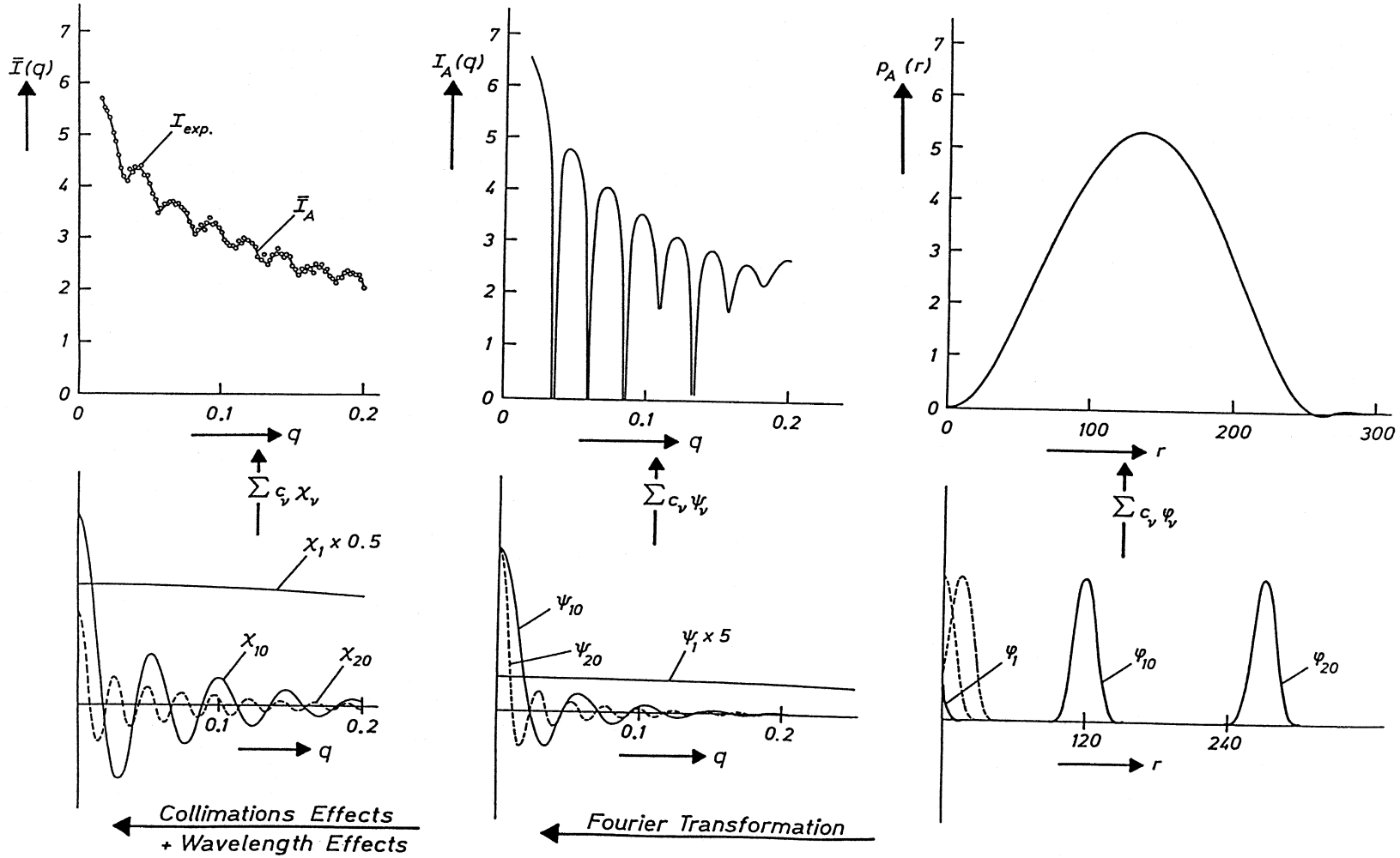

amenitsch@tugraz.at &
amenitsch@elettra.trieste.it

Other IFT Applications - Equations

Summary of the different transforms T_1 used in *IFT*:

Arbitrary shape:

$$I(q) = 4\pi \int_0^\infty p(r) \frac{\sin(qr)}{qr} dr$$

Cylindrical Symmetry:

$$I(q) = \frac{2\pi^2 L}{q} \int_0^\infty p_c(r) J_0(qr) dr$$

Lamellar Symmetry:

$$I_{plane}(q) = \frac{4\pi A}{q^2} \int_0^\infty p_t(r) \cos(qr) dr$$

The structure is the same for all equations, just the kernels of the integrals differ!

amenitsch@tugraz.at & amenitsch@elettra.trieste.it

Deconvolution of the PDDF – The *Magic Square*

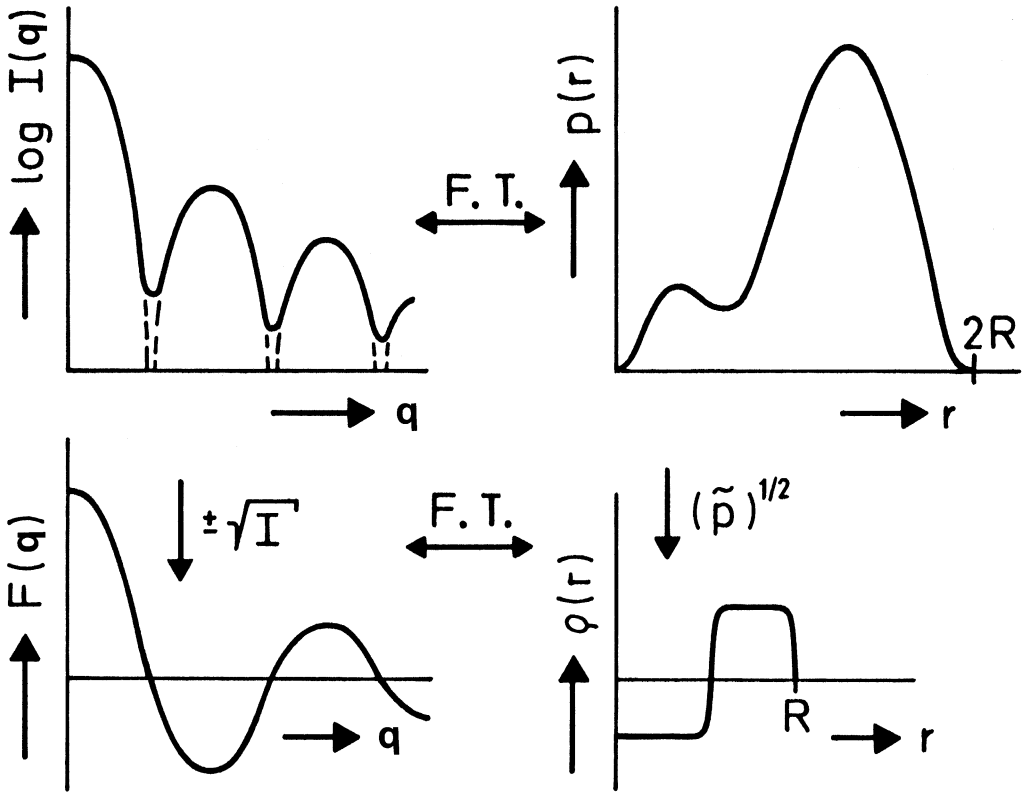

The *Magic square* of small-angle scattering: The correlations between the radial density $\Delta\rho(r)$ and the PDDF $p(r)$ and their Fourier transforms, the scattering amplitude $F(q)$ and scattering intensity $I(q)$ under the assumption of spherical symmetry.

amenitsch@tugraz.at &
amenitsch@elettra.trieste.it

Deconvolution of the PDDF – Principles I

Here we are facing a similar situation as in the *IFT* method: for a given density distribution $\rho(r)$ we can calculate the exact $p(r)$-function for all three cases (spherical, cylindrical and lamellar symmetry) by a convolution square operation but we do not have a useful description of the inverse problem, the so-called convolution square root.

As an additional problem we have to keep in mind the fact, that the convolution square operation is a **nonlinear transformation** which will not allow an inversion by the solution of a simple linear least squares technique like in the case of the indirect Fourier transformation.

We start again with a series expansion of the radial density function $\rho(r)$ in the usual way:

$$\bar{\rho}(r) = \sum_{i=1}^{N} c_i \, \varphi_i(r)$$

amenitsch@tugraz.at & amenitsch@elettra.trieste.it

Deconvolution of the PDDF – Principles II

The approximation for the density profile corresponds to an approximation to the PDDF:

$$\bar{p}(r) = \sum_{i=1}^{N} V_{ii}(r)\, c_i^2 + 2 \sum_{i>k} V_{ik}(r)\, c_i\, c_k$$

The overlap integrals $V_{ik}(r)$ describe the overlapping of the *i-th* with the *k-th* step or shell where one function has been shifted an arbitrary distance *r*. These overlap or convolution integrals are very simple for the planar case (one-dimensional convolution of two step function leads simply to a triangle) but are a bit more complicated for the cylindrical and spherical case:

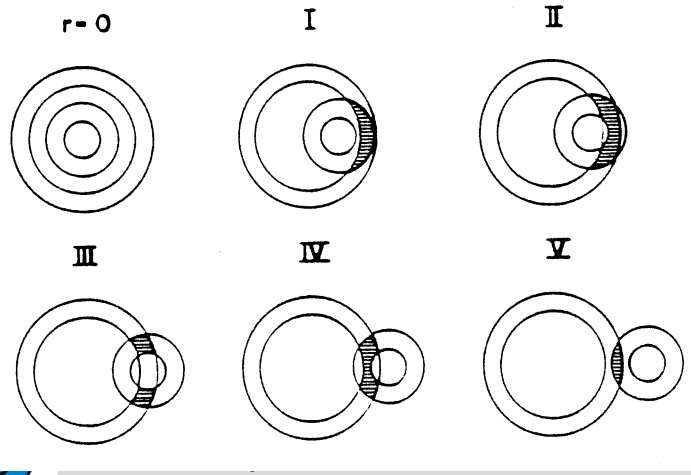

Illustration of the five sub-regions for the calculation of the overlap integrals $V_{ik}(r)$.

amenitsch@tugraz.at &
amenitsch@elettra.trieste.it

Deconvolution of the PDDF – Iterative Solution

The above equation for the PDDF is nonlinear in its coefficients c_i. The corresponding least squares problem has to be linearized by a series expansion where higher order terms are omitted.

Such linearized systems must be solved iteratively. In addition one needs starting values $c_i^{(0)}$ for the first iteration. Here we set all coefficients equal to a constant.

We then calculate the difference function

$$\Delta p(r) = p(r) - \bar{p}^{(o)}(r)$$

which would be zero only if we would know the exact coefficients c_i.

Now we calculate correction terms Δc_i in order to minimize $\Delta p(r)$ in a least square sense.

$$\sum_{i=1}^{N} V_{ii}(r)\left[\left(c_i + \Delta c_i\right)^2\right] + 2\sum_{i>k} V_{ik}(r)\left[\left(c_i + \Delta c_i\right)\left(c_k + \Delta c_k\right) - c_i c_k\right] = \Delta p(r)$$

amenitsch@tugraz.at & amenitsch@elettra.trieste.it

Deconvolution of the PDDF – Iterative Solution II

We linearize this equation by omitting the second order terms Δc_i^2 and $\Delta c_i \Delta c_k$ and we get

$$2\sum_{k=1}^{N}\sum_{i=1}^{N} c_i \, V_{ik}\left(r_j\right) \Delta c_k = \Delta p\left(r_j\right)$$

for $j = 1,2,3,\ldots M$ and $M > N$. These equations can be written in matrix notation

$$A_{jk}\Delta c_k = \Delta p_j \quad \text{or} \quad \mathbf{A}\Delta\mathbf{c}^{(0)} = \Delta\mathbf{p}^{(0)}$$

where the matrix elements A_{jk} are given by

$$A_{jk} = 2\sum_{i=1}^{N} c_i \, V_{ik}\left(r_j\right)$$

This system is solved with a weighted least squares condition considering the standard deviations of the function $\Delta p(r)$ and we get the correction terms $\Delta\mathbf{c}$.

amenitsch@tugraz.at & amenitsch@elettra.trieste.it

Deconvolution of the PDDF – Iterative Solution III

They allow the calculation of improved coefficients $c_i^{(1)}$:

$$c_i^{(1)} = c_i^{(0)} + \Delta c_i$$

and with these coefficients we start the next iteration, get further improvements and if this iterative procedure converges we have solved the problem.

This problem is, however, again an *ill-posed problem* so that we have to add again a stabilization criterion and we have to solve the nonlinear problem by iteration for every *Lagrange multiplier*.

Many applications performed in the meantime have shown that the deconvolution technique works well in combination with the indirect transformation method, also in cases where the conditions of symmetry are not perfectly fulfilled.

amenitsch@tugraz.at & amenitsch@elettra.trieste.it

SAXS 2.0: Theoretical Background

Assumption of monodisperse globular particles:

$$I(q) = n.P(q).S(q)$$

n ... Particle density
q ... Scattering vector
I(q) ... Scattering Intensity
P(q) ... Form Factor $P(q) \leftrightarrow p(r)$
S(q) ... Structure Factor $[S(q) - 1] \leftrightarrow [g(r) - 1]$
Interaction Potential: Hard Spheres Potential
Closure relation: Percus-Yevick-Approximation (analyt. Solution)
Kinning & Thomas, *Macromolecules* (1984), **17**

amenitsch@tugraz.at & amenitsch@elettra.trieste.it

Fourier Transformation

$$I(q) = n.P(q).S(q)$$

Form Factor $P(q)$ ↔ Pair Distance Distribution Function $p(r)$

$$P(q) = 4\pi \int_0^\infty [\blacksquare] \frac{\sin(qr)}{qr} dr$$

Structure Factor $[S(q) - 1]$ ↔ Total Correlation Function $[g(r) - 1]\ r^2$

$$S(q) - 1 = 4\pi [\blacksquare] \int_0^\infty [\blacksquare] \frac{\sin(qr)}{qr} dr$$

Due to the nearly identical structure of these equations it is obvious that it is not a trivial task to split the scattering intensity into these factors by mathematical means

GIFT (=General Indirect Fourier Transformation)

amenitsch@tugraz.at & amenitsch@elettra.trieste.it

Particle Form Factor P(q) - Artists View©

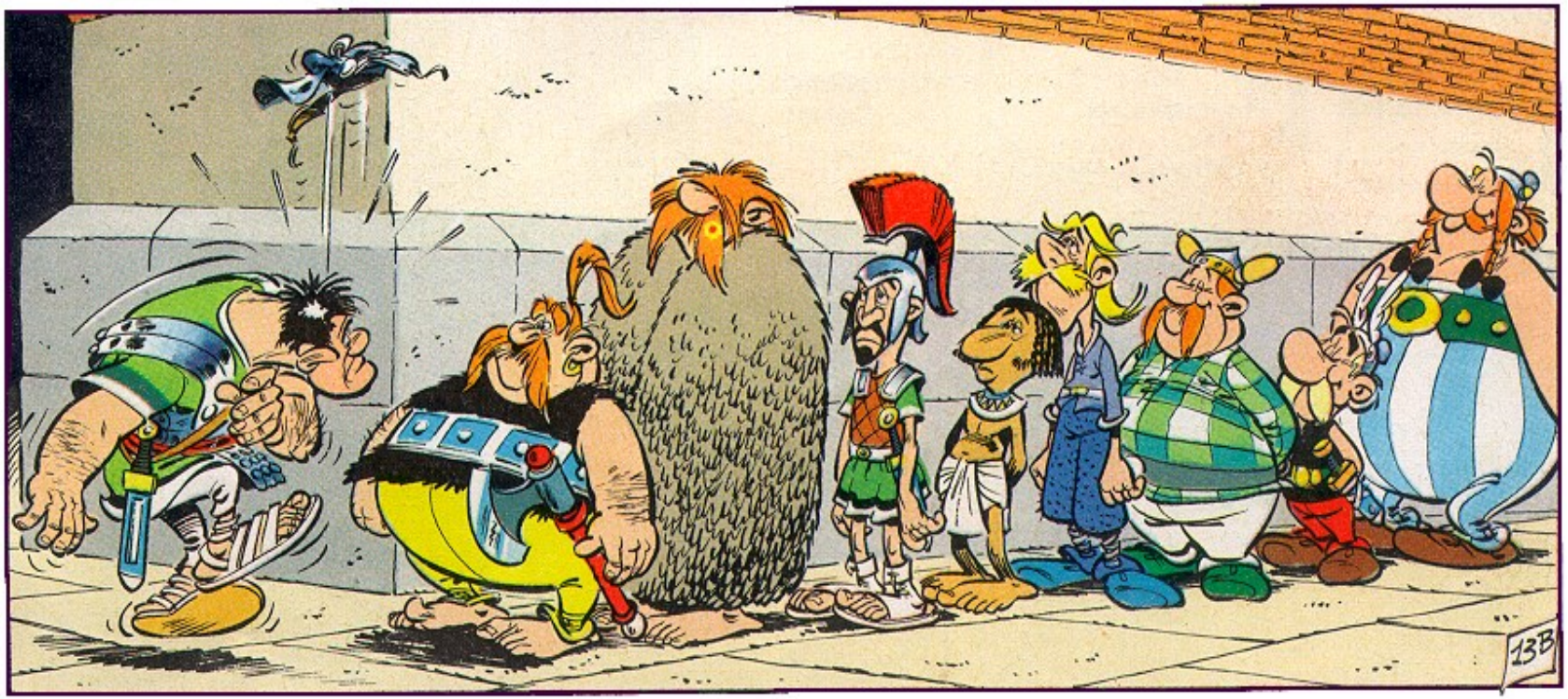

©**Asterix Legionnaire,** associated by Judith Brunner-Popela

amenitsch@tugraz.at &
amenitsch@elettra.trieste.it

Structure factor S(q) - Artists View©

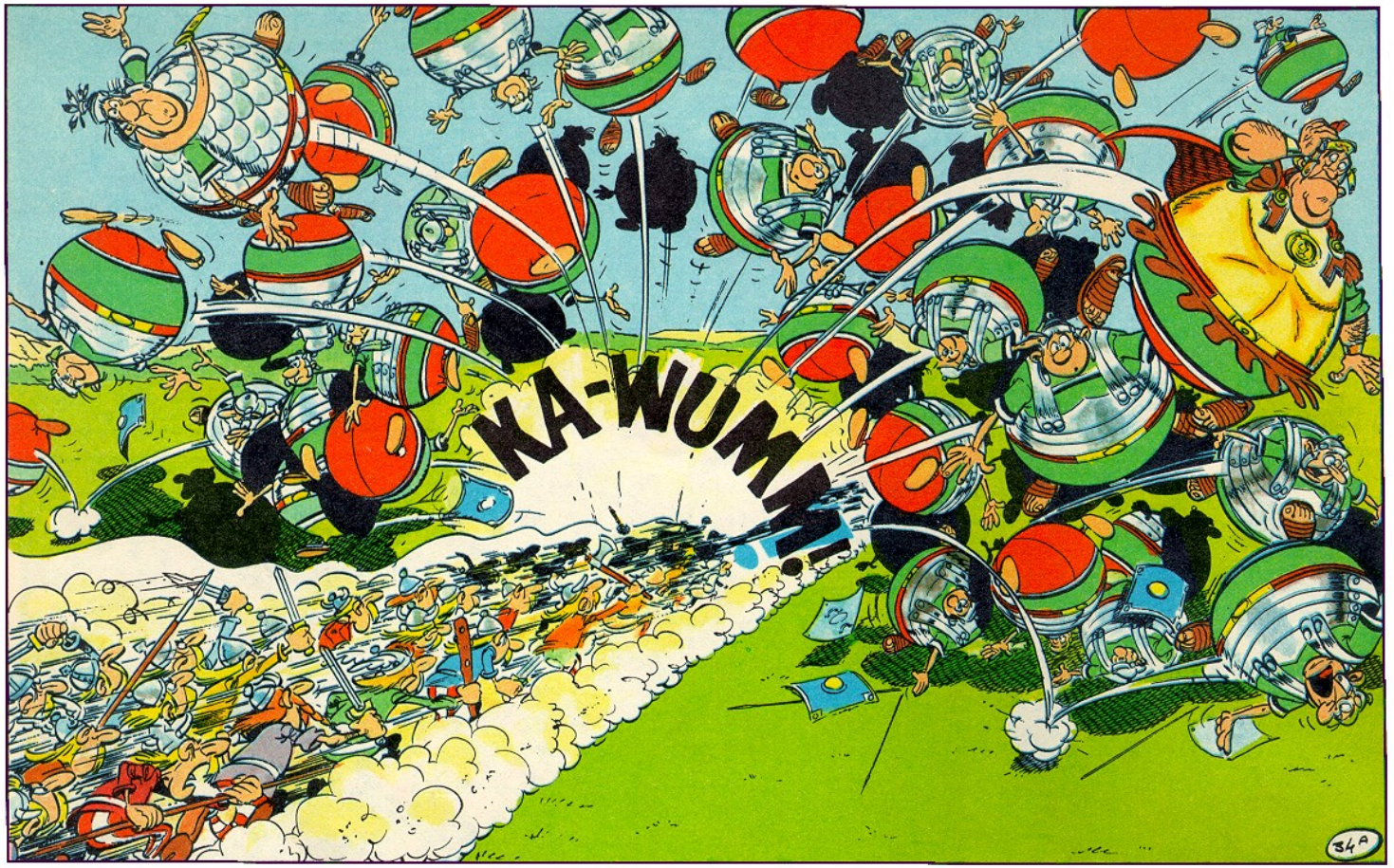

© **Le Grand Fossé** associated by Judith Brunner-Popela

amenitsch@tugraz.at &
amenitsch@elettra.trieste.it

D.Svergun Hamburg Group

General principle of SAS modelling

1D scattering data ***(or multiple data sets)***

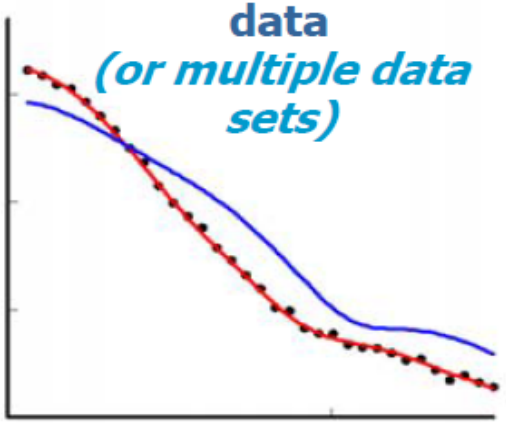

Trial-and-error

3D search model

$\boldsymbol{X} = \{X\} = \{X_1 \ldots X_M\}$

M parameters

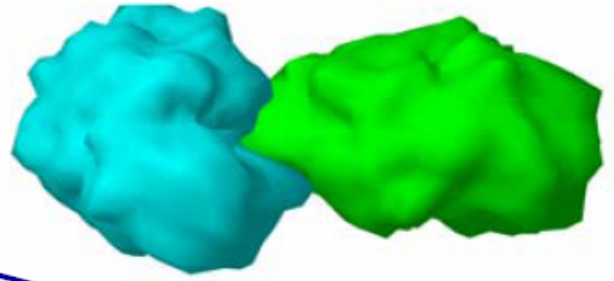

discrepancy: $\chi^2 = \frac{1}{N-1}\sum_j \left[\frac{I_{\exp}(s_j) - cI(s_j)}{\sigma(s_j)}\right]^2$

Non-linear search

Additional information is ALWAYS required to resolve or reduce ambiguity of interpretation at given resolution

amenitsch@tugraz.at & amenitsch@elettra.trieste.it

Constraints and Restraints

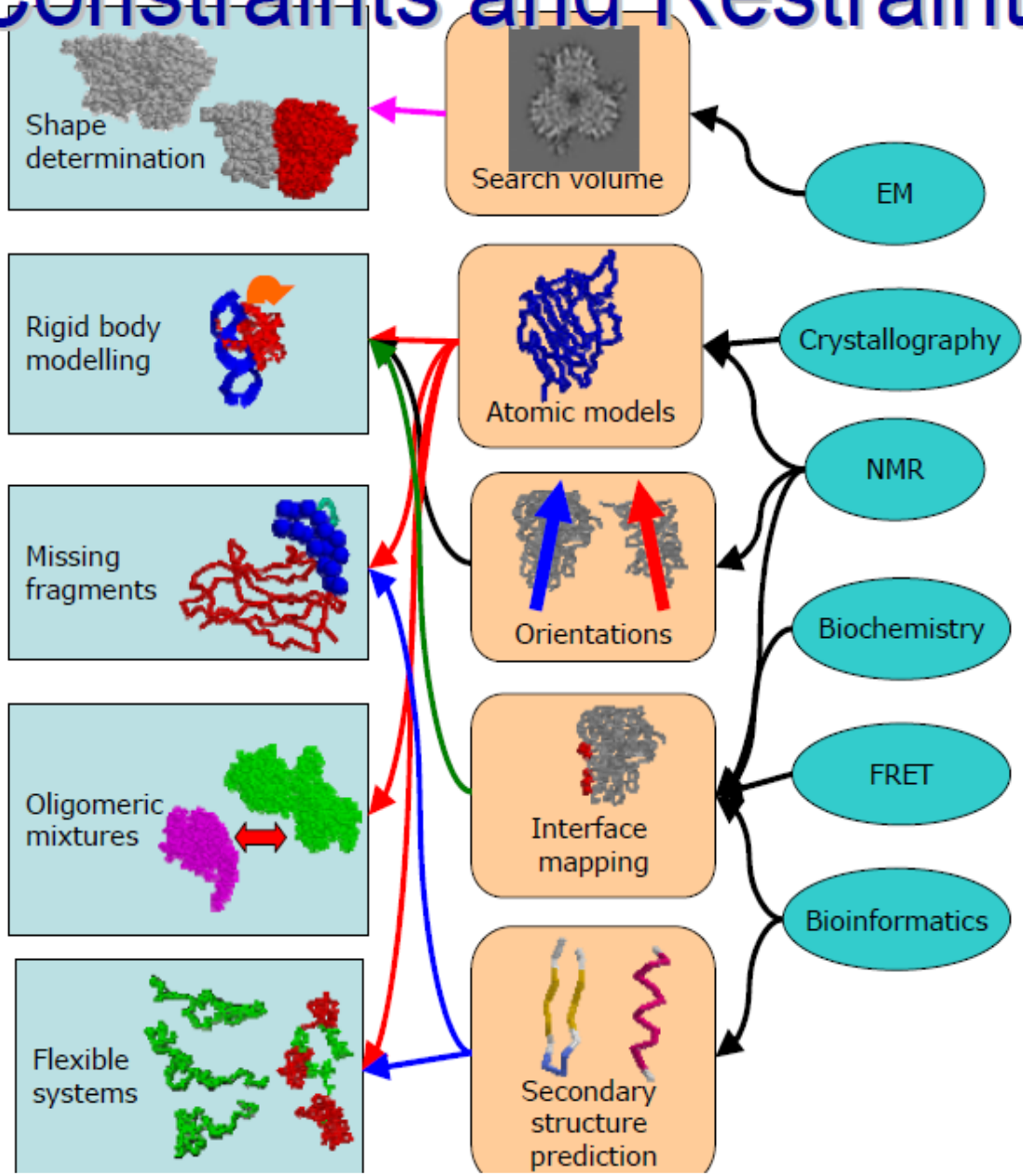

amenitsch@tugraz.at &
amenitsch@elettra.trieste.it

Target function

- To reduce the ambiguity of data analysis

$$E(\{X\}) = \chi^2[(I(s), I_{\exp}(s)] + \sum_i \alpha_i P_i$$

  is minimized

- Penalties describe model-based restraints and/or introduce the available additional information from other methods: MX, NMR, EM etc)

- If the number of free parameters is small, a brute force (grid) search may be applied, otherwise a Monte-Carlo based technique (e.g. simulated annealing) is employed to perform the minimization of *E({X})*

amenitsch@tugraz.at & amenitsch@elettra.trieste.it

Ab initio shape determination

A sphere of radius D_{max} is filled by densely packed beads of radius $r_0 << D_{max}$

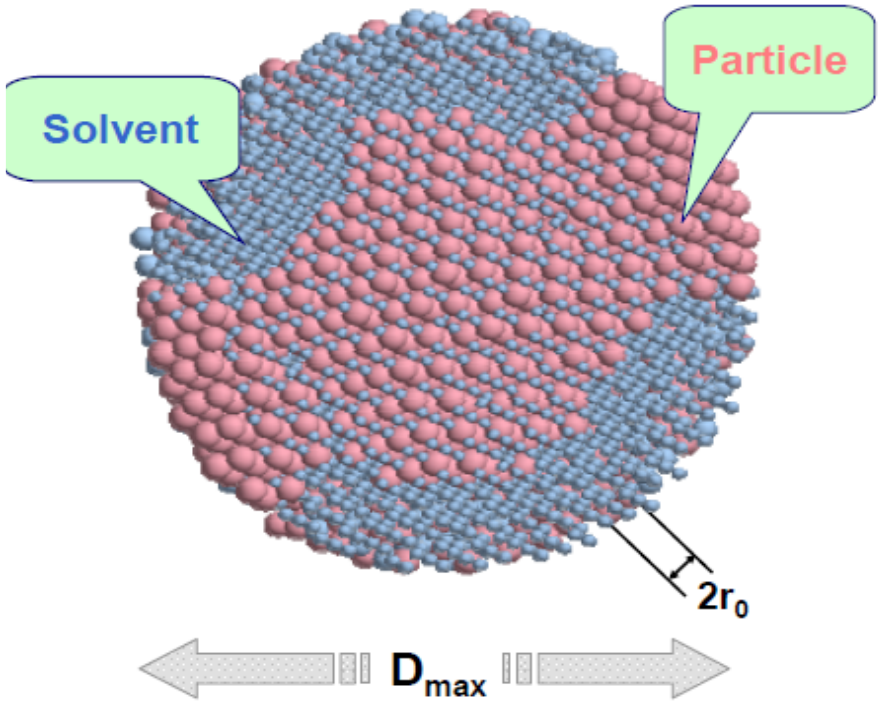

Vector of model parameters:

Position (j) = X_j = { 1 if particle / 0 if solvent

(phase assignments)

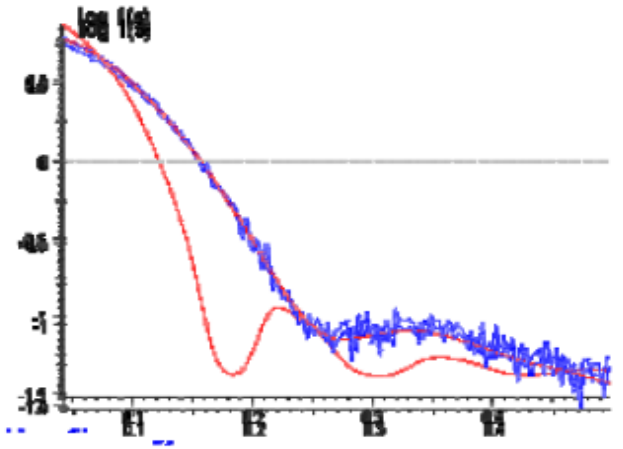

Svergun, D.I. (1999) *Biophys. J.* 76, 2879-2886

amenitsch@tugraz.at & amenitsch@elettra.trieste.it

Bead Modelling: DAMMIN

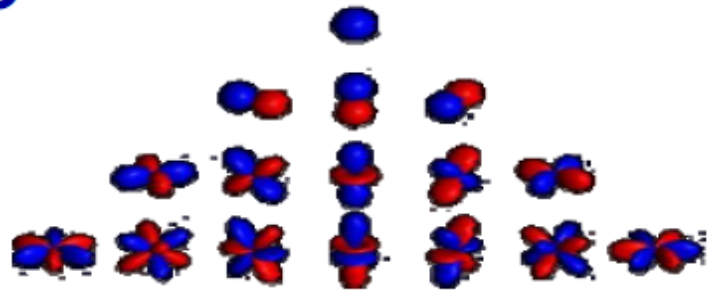

- Scattering intensity is computed using spherical harmonics

$$A_{lm}^{(k)}(s) = i^l \sqrt{2/\pi}\, f(s) \sum_{j=1}^{N_k} j_l(sr_j)\, Y_{lm}^*(\omega_j)$$

$$I(s) = 2\pi^2 \sum_{l=0}^{\infty} \sum_{m=-l}^{l} \left\{ \sum_{k=1}^{K} \left[\Delta\rho_k A_{lm}^{(k)}(s)\right]^2 + 2 \sum_{n>k} \Delta\rho_k A_{lm}^{(k)}(s) \Delta\rho_n \left[A_{lm}^{(n)}(s)\right]^* \right\}$$

- Penalty terms ensure compactness and connectivity

compact

loose

disconnected

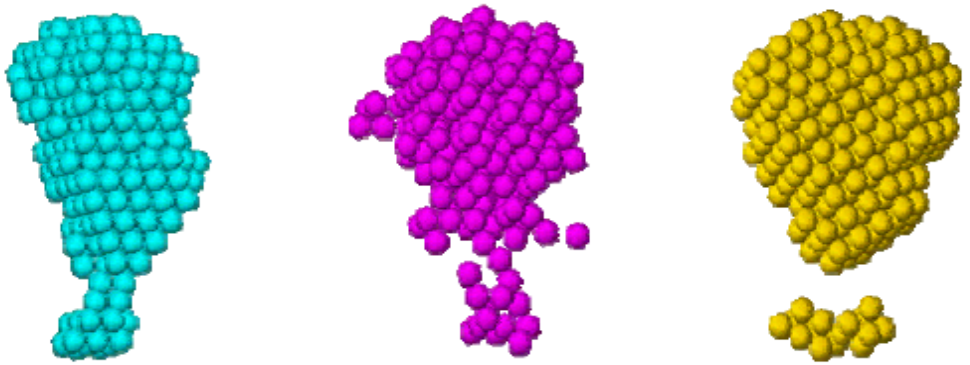

Svergun, D.I. (1999) *Biophys. J.* 76, 2879-2886

amenitsch@tugraz.at & amenitsch@elettra.trieste.it

Scattering on human CDC45 Protein

CDC45 protein conserved in all eukaryotes
initiation of DNA replication
progression of the replication fork

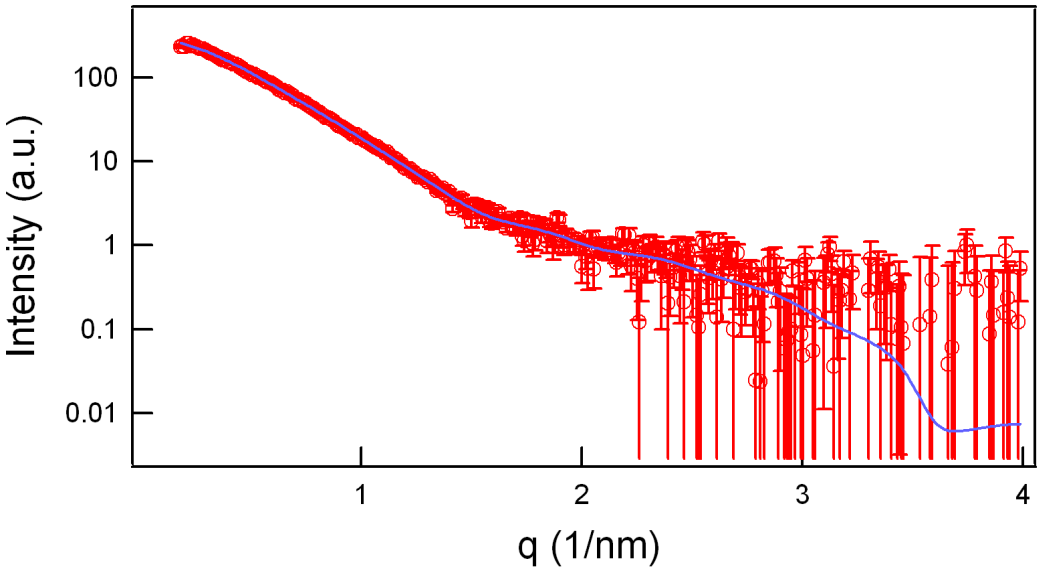

hCDC45, 1.85 mg/ml, 40µl, 30 s

Kastranova I, Onesti S et al.,J.Biol.Chem. (2012)

core T. thermophilus RecJ

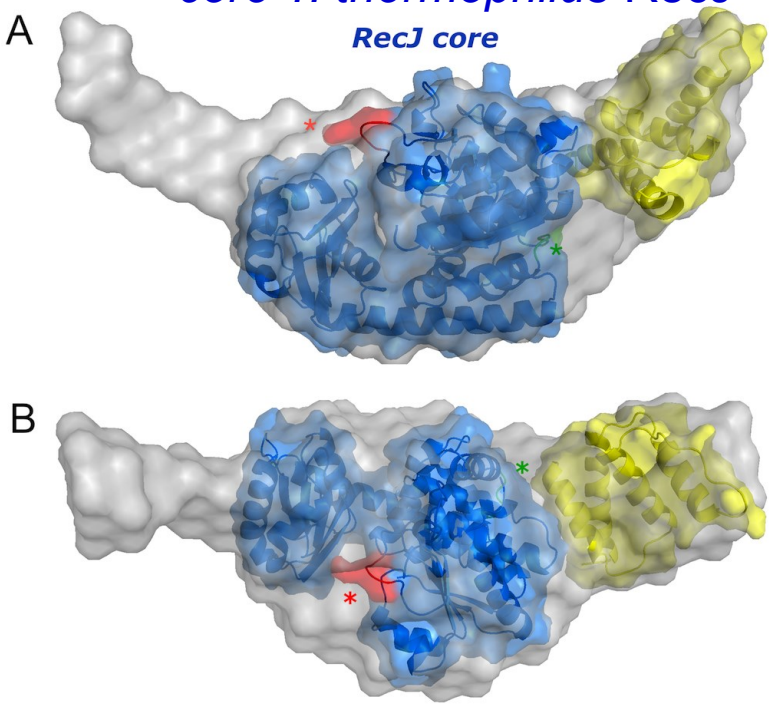

helical domain of the acyl-CoA

amenitsch@tugraz.at &
amenitsch@elettra.trieste.it

Multiphase bead modelling

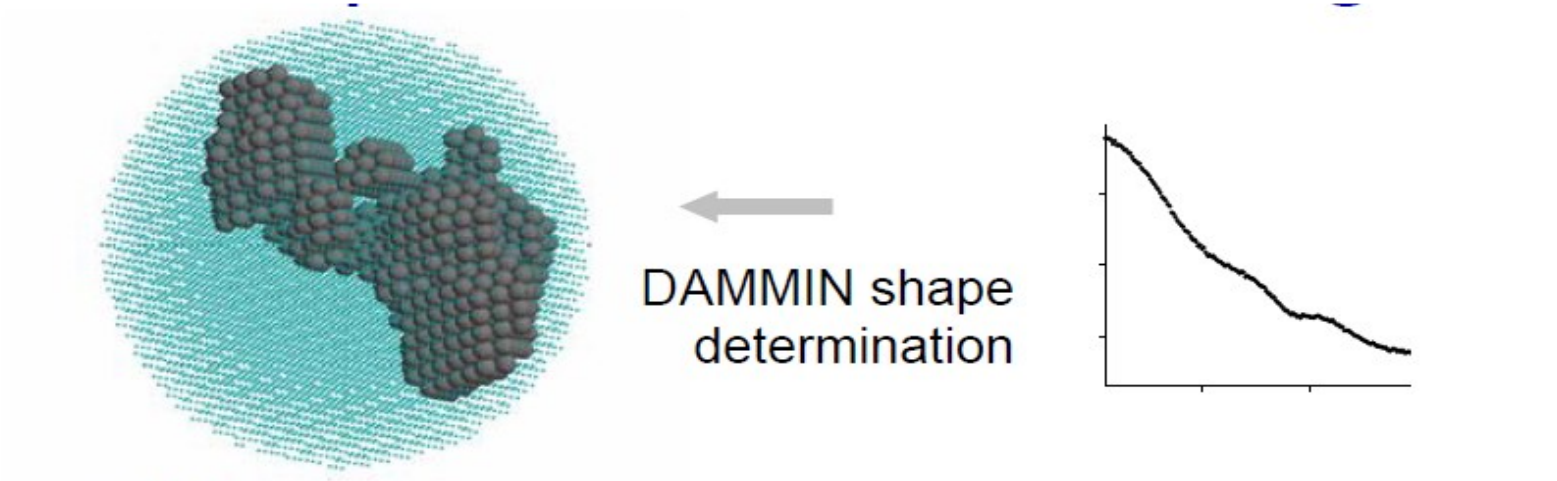

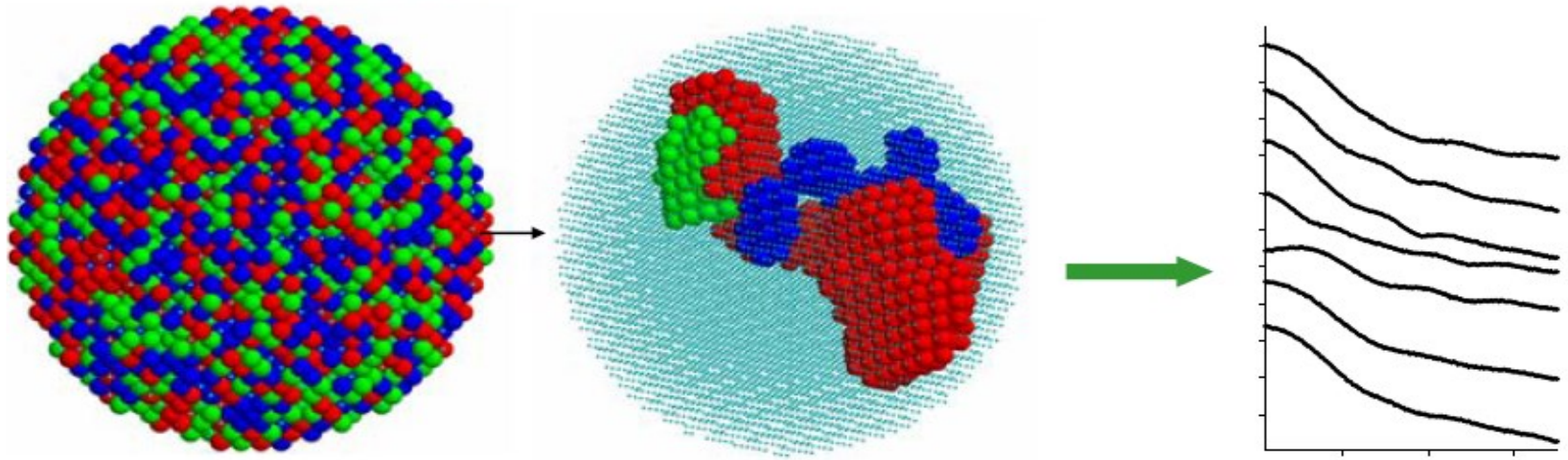

- One can differentiate between distinct parts of the particle
- Several curves are fitted assuming the same arrangement of the parts in different samples

amenitsch@tugraz.at &
amenitsch@elettra.trieste.it

How to compute SAS from atomic model

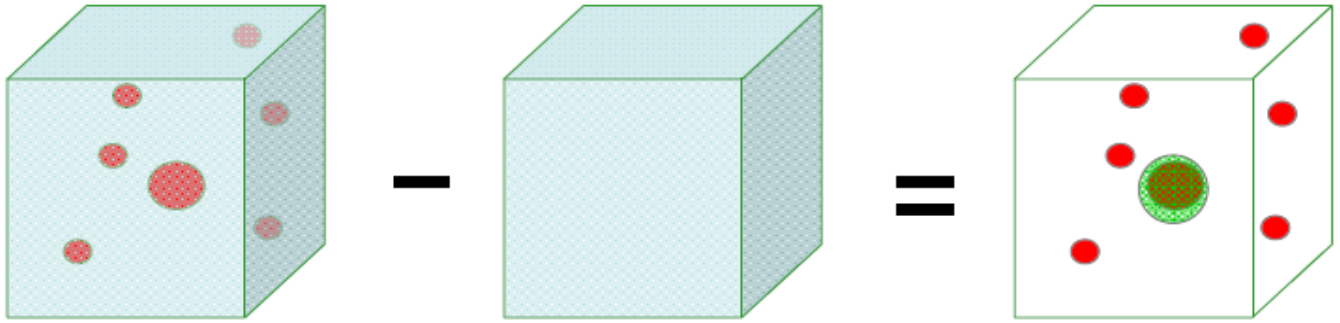

$I_{solution}(s)$ $I_{solvent}(s)$ $I_{particle}(s)$

- To obtain scattering from the particles, solvent scattering must be subtracted to yield effective density distribution $\Delta\rho = \langle\rho(\mathbf{r}) - \rho_s\rangle$, where ρ_s is the scattering density of the solvent
- Further, the bound solvent density may differ from that of the bulk

amenitsch@tugraz.at & amenitsch@elettra.trieste.it

Scattering from a macromolecule in solution

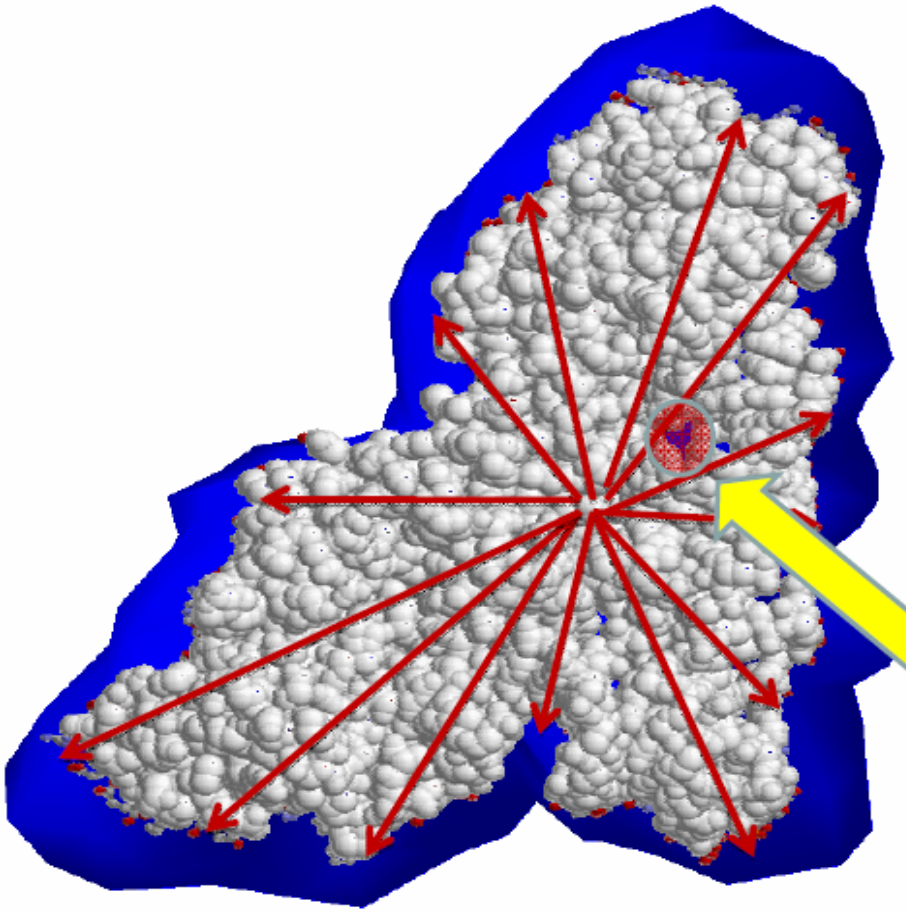

Atomic scattering

- Excluded volume

+ Shell scattering
Envelope function **F(ω)**

Internal cavities

amenitsch@tugraz.at &
amenitsch@elettra.trieste.it

Scattering from a macromolecule in solution

$$I(s) = \left\langle |A(s)|^2 \right\rangle_\Omega = \left\langle |A_a(s) - \rho_s E(s) + \delta\rho_b B(s)|^2 \right\rangle_\Omega$$

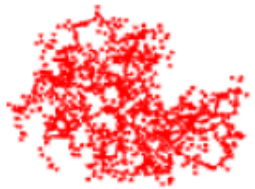

- $A_a(s)$: atomic scattering in vacuum (total scattering length / number of e^-)

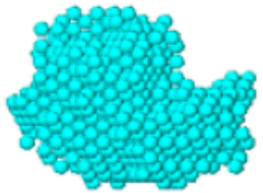

- $E(s)$: scattering from the excluded volume (normalized)

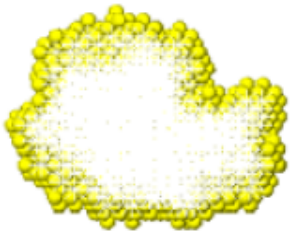

- $B(s)$: scattering from the hydration shell (normalized)

CRYSOL (X-rays): Svergun et al. (1995). *J. Appl. Cryst.* **28**, 768
CRYSON (neutrons): Svergun et al. (1998) *P.N.A.S. USA*, **95**, 2267

amenitsch@tugraz.at & amenitsch@elettra.trieste.it

Scattering components (lysozyme)

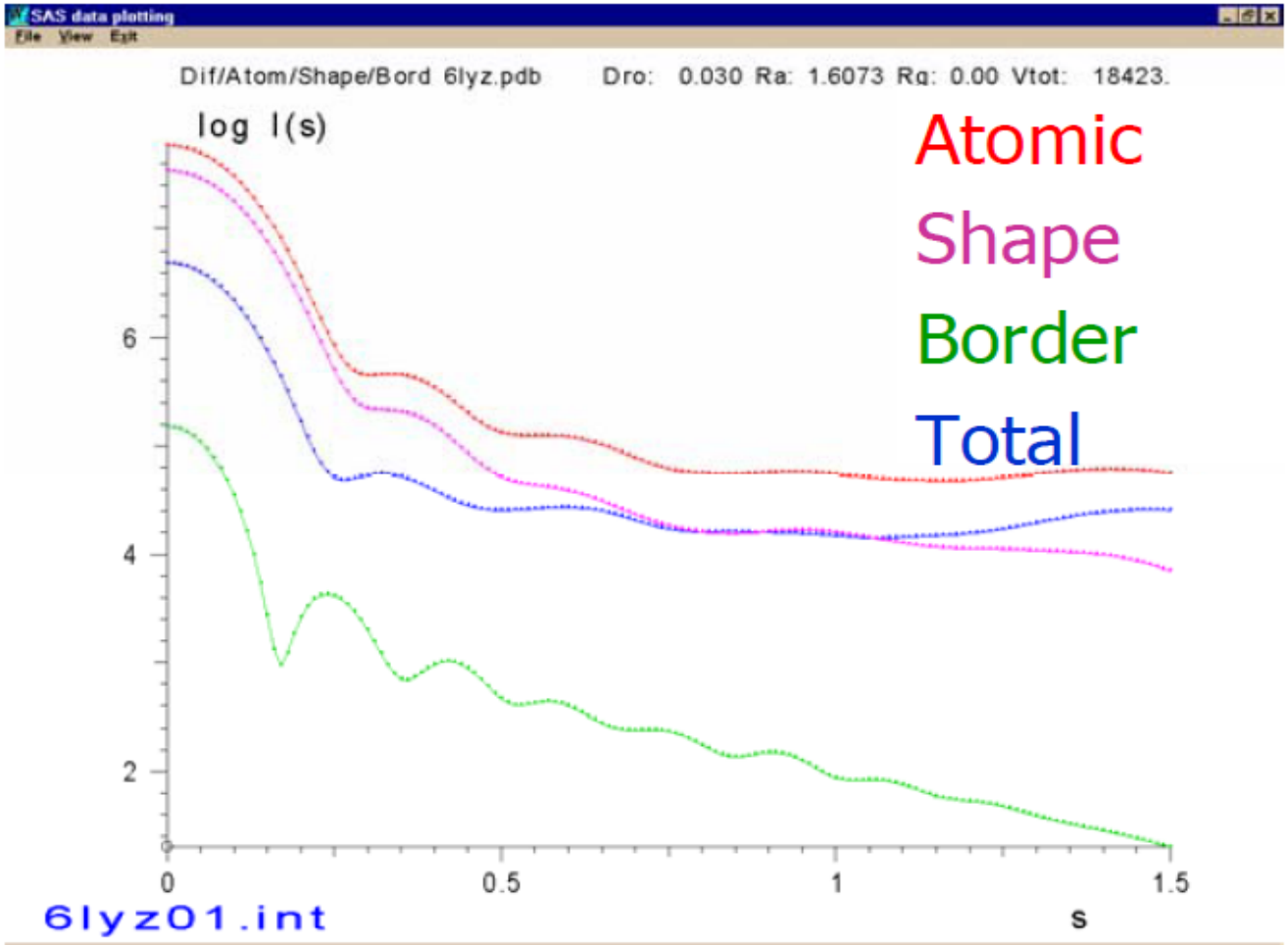

amenitsch@tugraz.at &
amenitsch@elettra.trieste.it

amenitsch@tugraz.at &
amenitsch@elettra.trieste.it

SCIENCE ▪ PASSION ▪ TECHNOLOGY

SAXS applications in life science and material science using synchrotron

Heinz Amenitsch
TU-Graz & Austrian SAXS beamine, ELETTRA

Elettra Sincrotrone Trieste

Anorganische CHEMIE

Sample Environment

Temperature
-195 ° C to 1100 ° C
20 ° C / 2 ms

IR-Laser

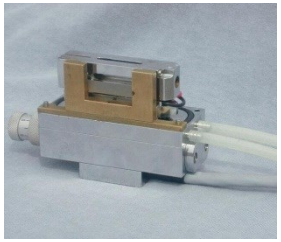

Peltier Moduls /
Oxford Cryostream

Pressure
0 - 3 Kbar
3000 bar/ 10 ms

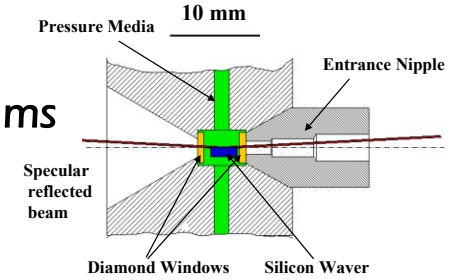

Hydrostatic HP-Cell

Liquids, Solids, Powders, Films, Gas-phase

Heat capacity
-40 to 150° C
1° C /min

DSC Microcalix

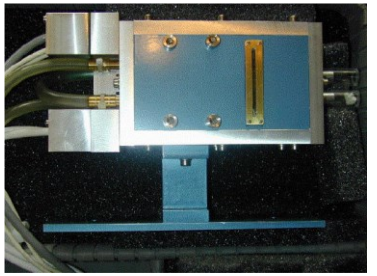

Chemical Potential
50 ms /70 µs

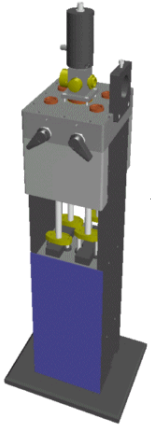

Biologic SFM-4

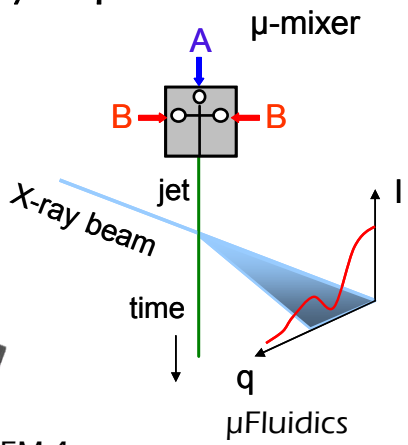

µFluidics

Single Particle Experiments

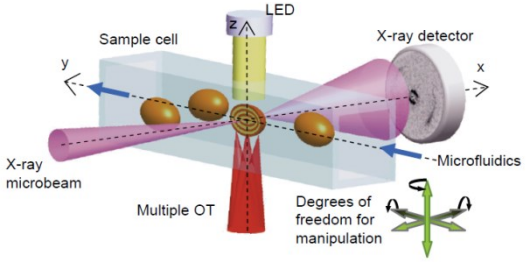

Mechanical Parameters
Force, Extension
Biaxial device
20 µs, s
physiological conditions

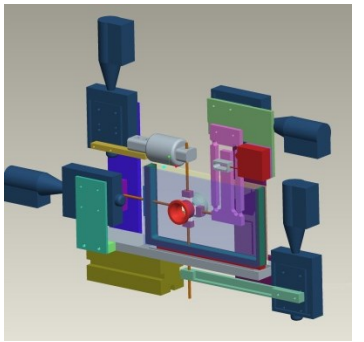

Simultaneous characterization: IR-Spectroscopy, UV-vis

amenitsch@tugraz.at &
amenitsch@elettra.trieste.it

F.Toma, et al., Nature Chemistry, (2010), 10.1038/NCHEM.761

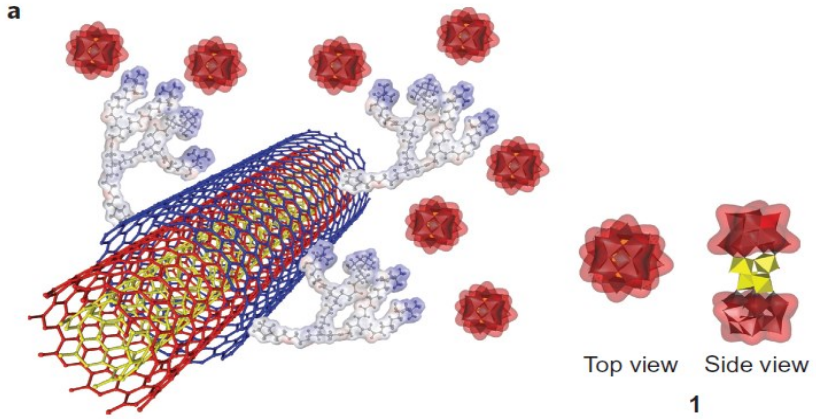

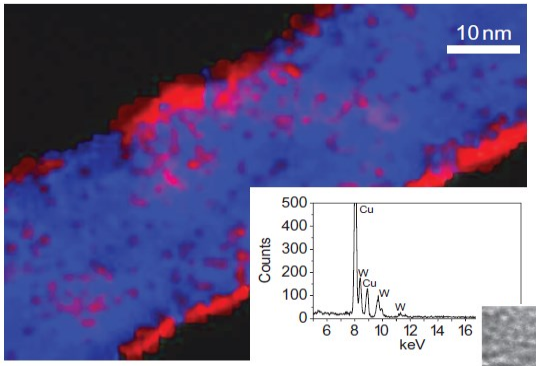

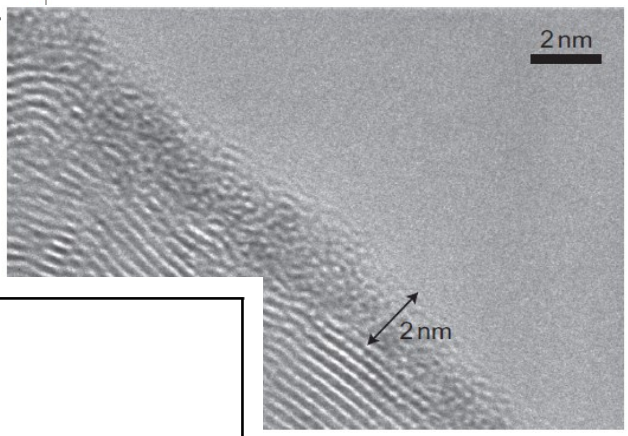

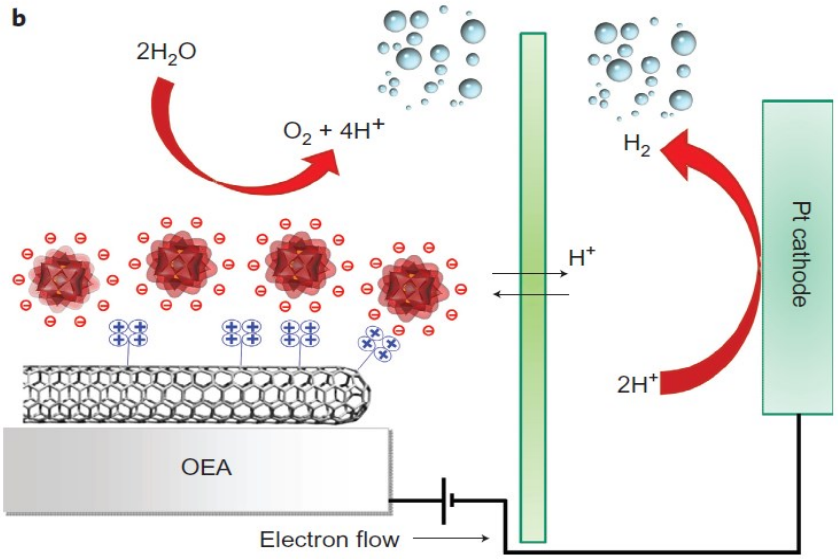

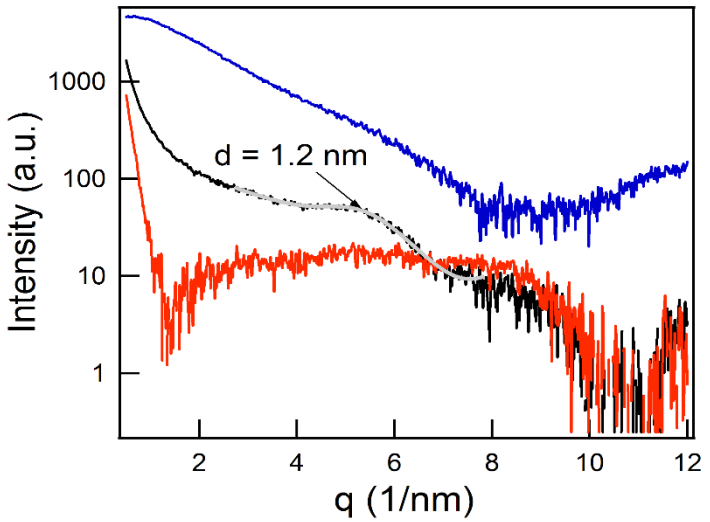

amenitsch@tugraz.at &
amenitsch@elettra.trieste.it

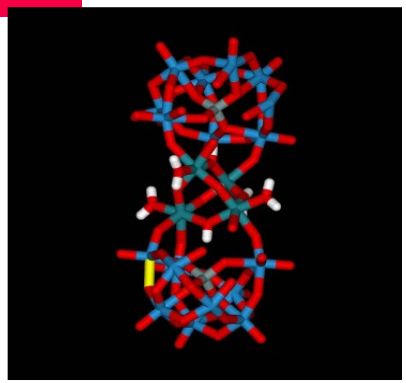

Ru4POM

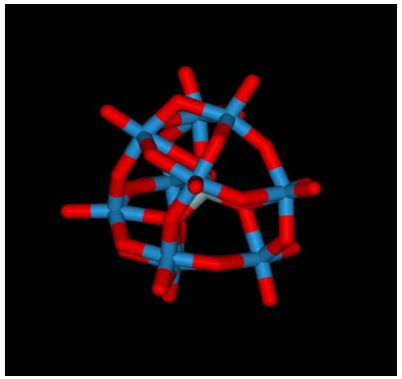

Precursor $SiW_{10}O_{36}$

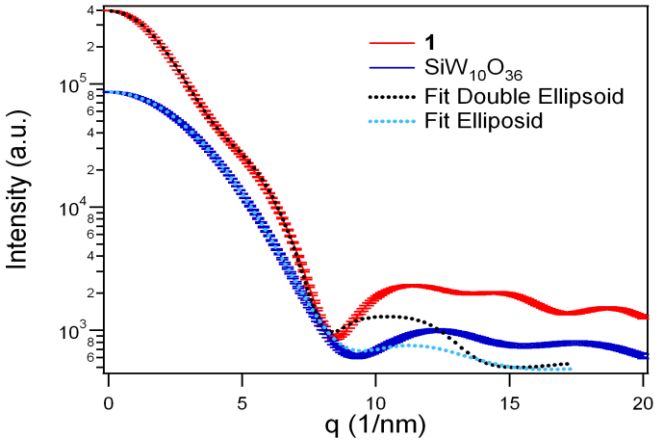

Simulation Crysol ATSAS D.Svergun

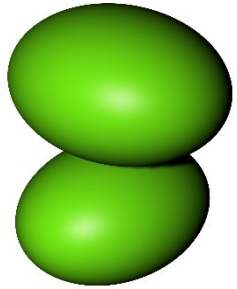

Double ellipsoid model

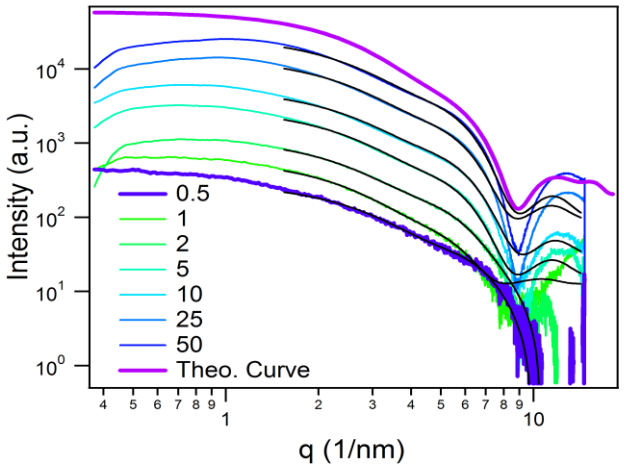

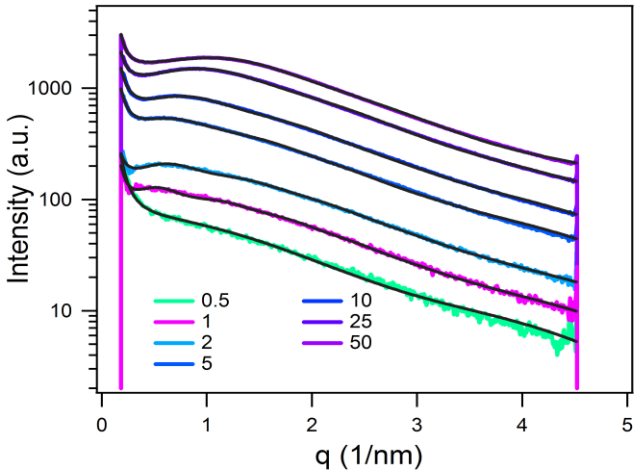

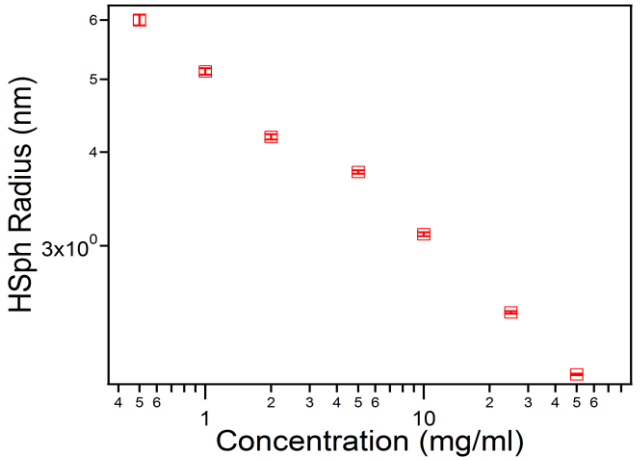

amenitsch@tugraz.at &
amenitsch@elettra.trieste.it

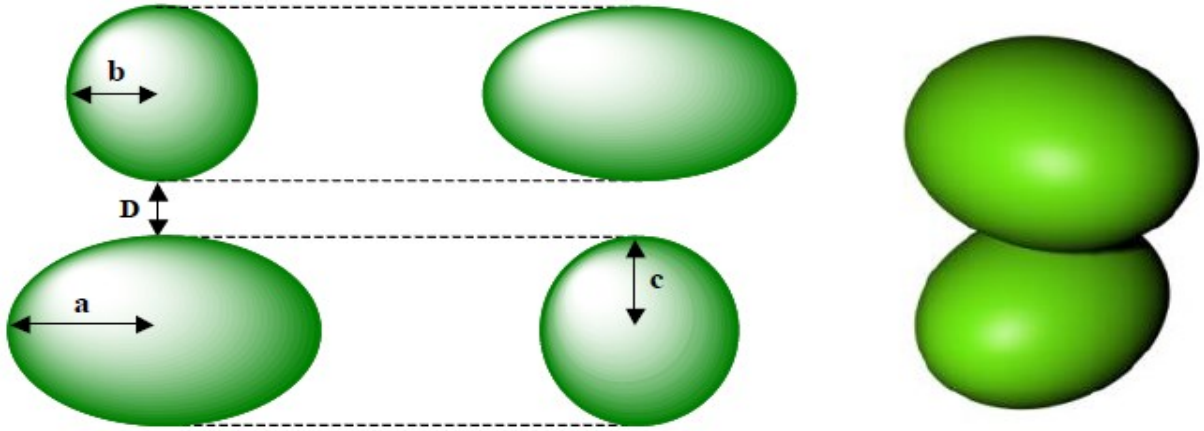

Front view Side view 3D model

$$I_{scat} = I_0 \cdot \frac{1}{\pi} \int_0^{\pi} d\beta \int_0^{\pi/2} d\alpha \cdot \sin(\alpha) \cdot \frac{1}{4} \cdot F_{2ellip}(q,a,b,c,D,\alpha,\beta)^2 \qquad (1)$$

$$F_{2ellip}(q,a,b,c,R,\alpha,\beta)^2 = \left(F_{ellip}(R_1,q) + F_{ellip}(R_2,q)\right)^2 \cdot \cos\left(q \cdot (D/2+c) \cdot \cos(\alpha)\right)^2 +$$

$$+ \left(F_{ellip}(R_1,q) - F_{ellip}(R_2,q)\right)^2 \cdot \sin\left(q \cdot (D/2+c) \cdot \cos(\alpha)\right)^2$$

$$F_{ellip}(R,q) = 3 \cdot \frac{\sin(q \cdot R) - q \cdot R \cdot \cos(q \cdot R)}{(q \cdot R)^3}$$

$$R_1 = \sqrt{\left(a^2 \cdot \sin(\beta)^2 + b^2 \cdot \cos(\beta)^2\right) \cdot \sin(\alpha)^2 + c^2 \cdot \cos(\alpha)^2}$$

$$R_2 = \sqrt{\left(b^2 \cdot \sin(\beta)^2 + a^2 \cdot \cos(\beta)^2\right) \cdot \sin(\alpha)^2 + c^2 \cdot \cos(\alpha)^2}$$

amenitsch@tugraz.at & amenitsch@elettra.trieste.it

Amphiphilic designer-peptides

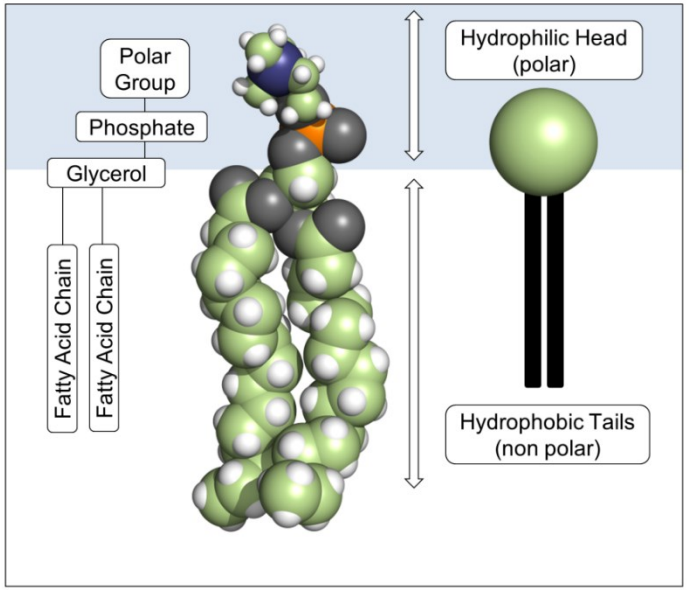

a phospholipid

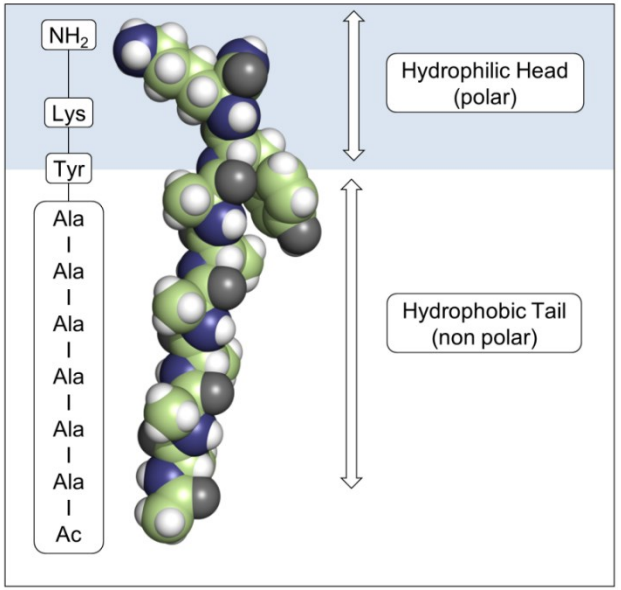

an amphiphilic designer-peptide

a6yk

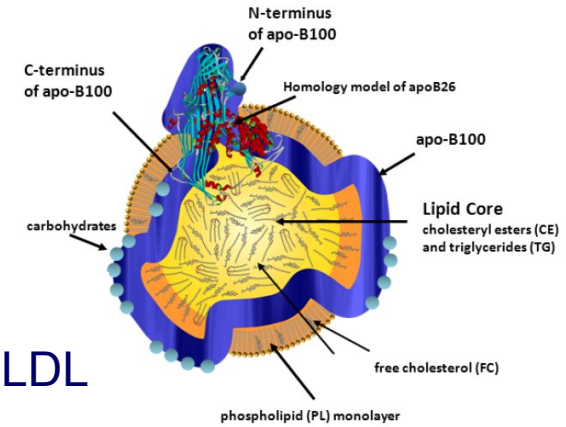

LDL

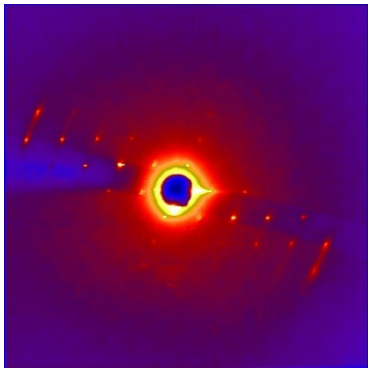

Gazit, E. *Chem. Soc. ReV.* **2007**
Cherny, I.; et al., *Angew. Chem., Int. Ed.* **2008**

amenitsch@tugraz.at &
amenitsch@elettra.trieste.it

Self-assembly

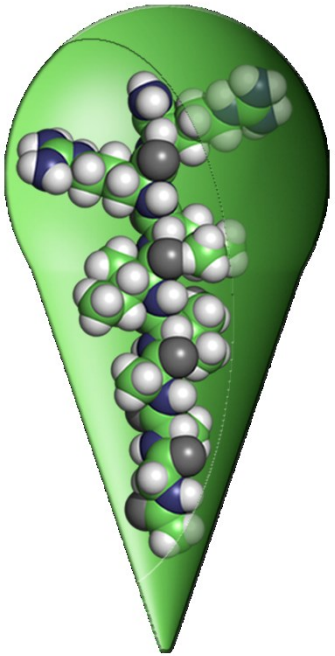

Spherical Micelles

Vesicles

Bilayers

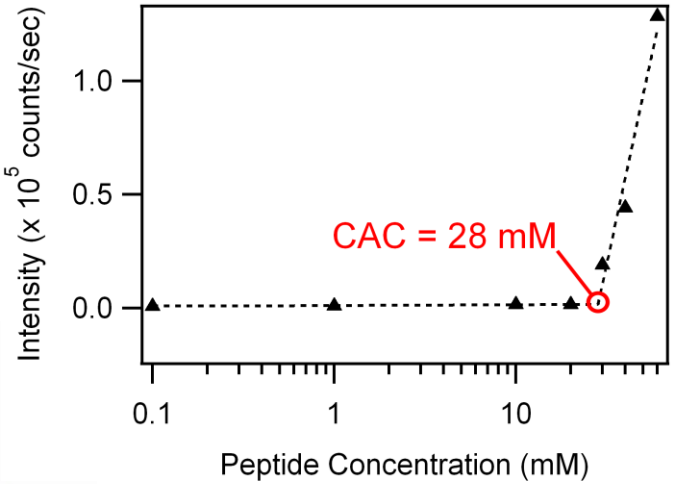

Self-Assembly

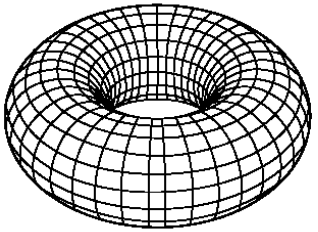

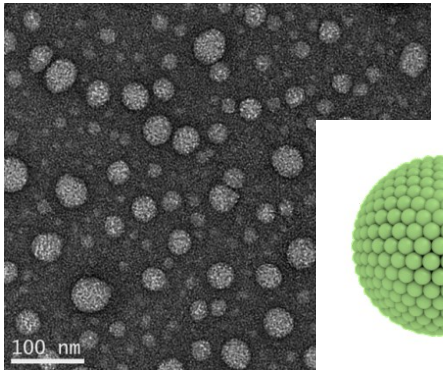

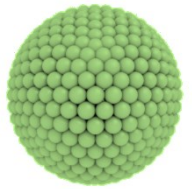

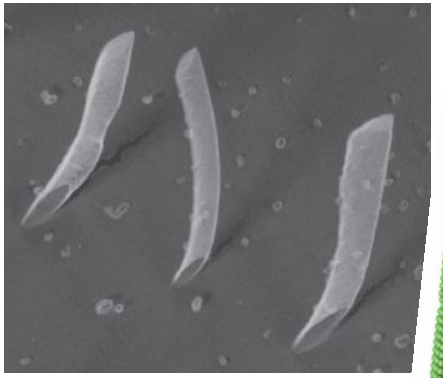

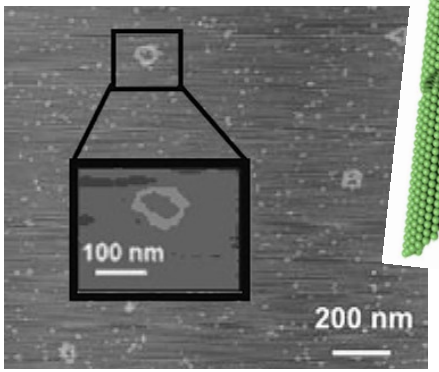

amenitsch@tugraz.at &
amenitsch@elettra.trieste.it

It‘s a double helix!

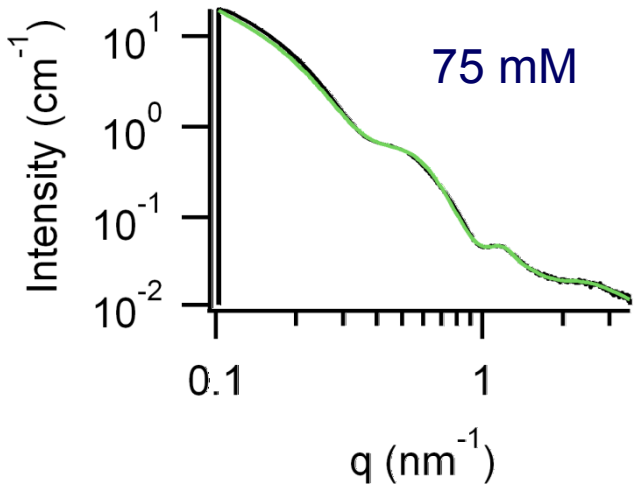

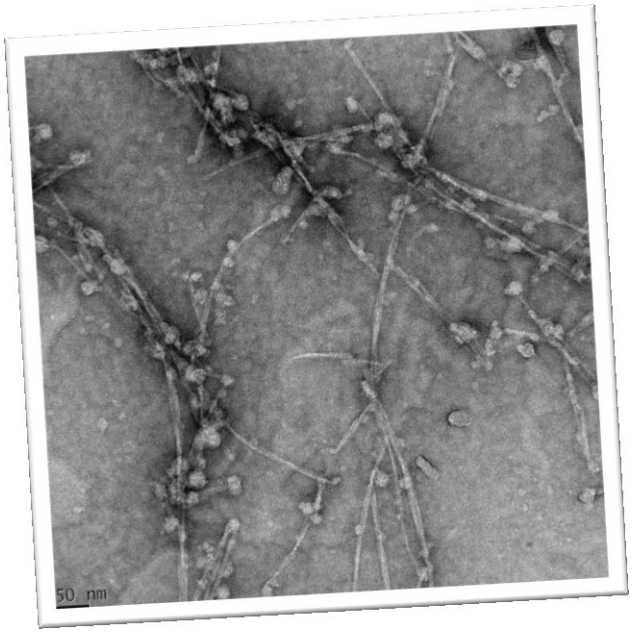

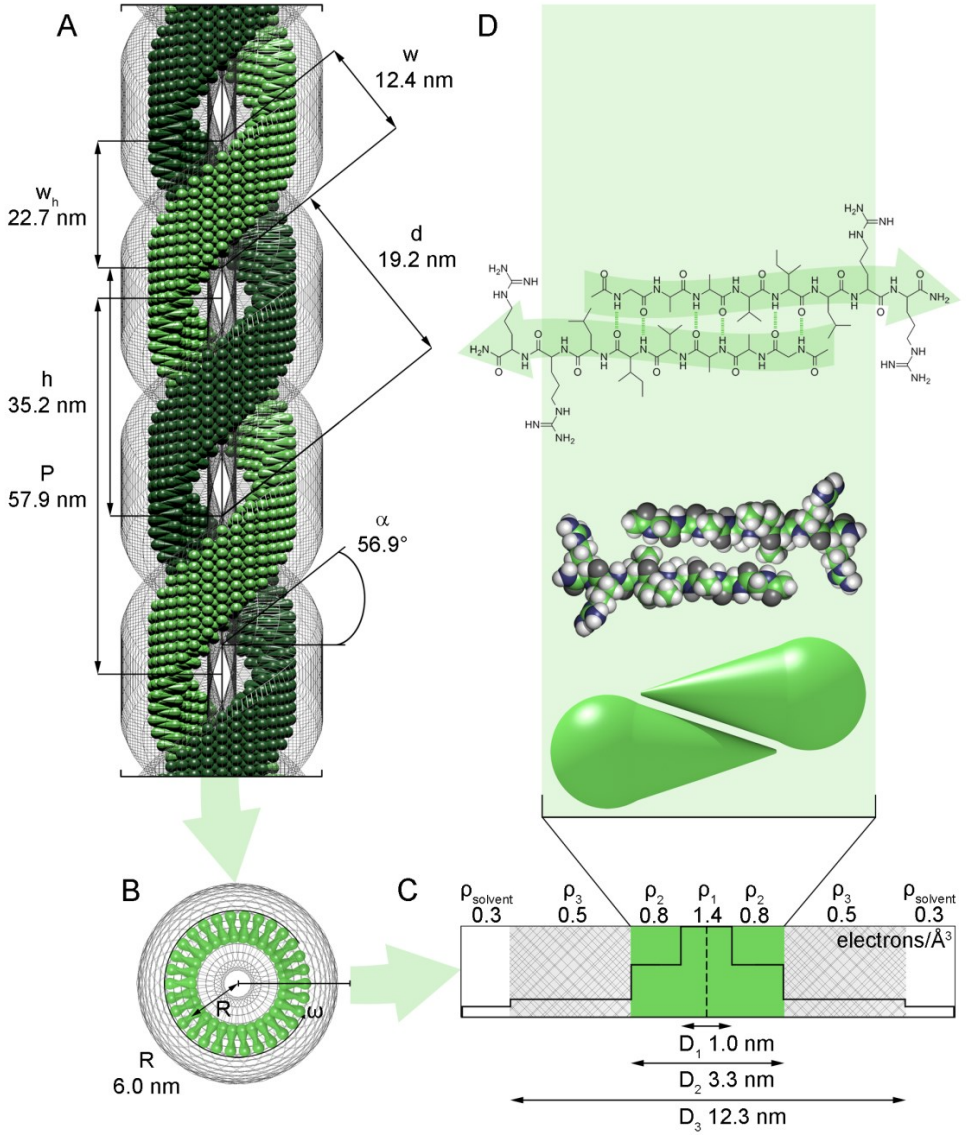

amenitsch@tugraz.at &
amenitsch@elettra.trieste.it

The self-assembly process

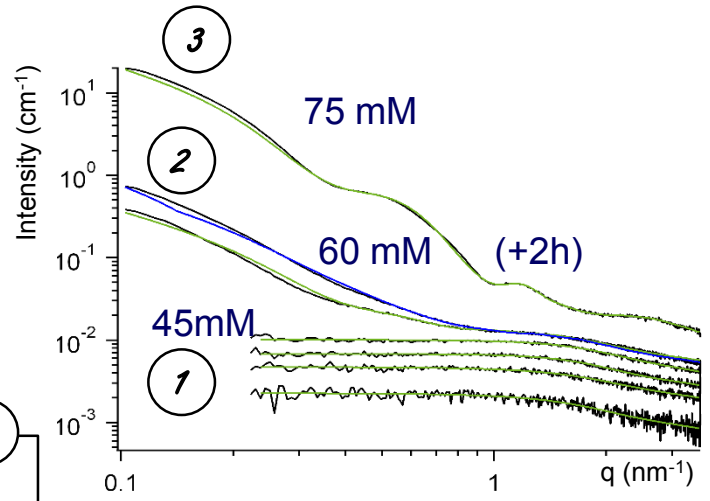

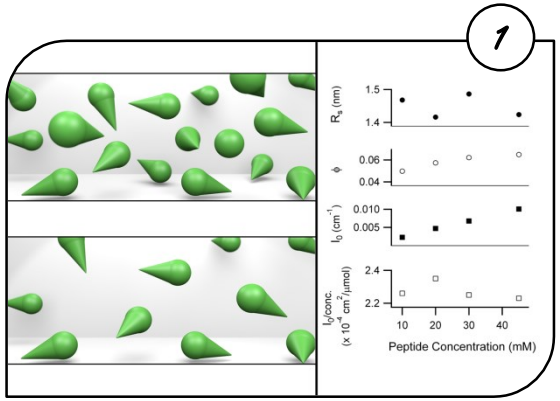

10-45 mM Monomers

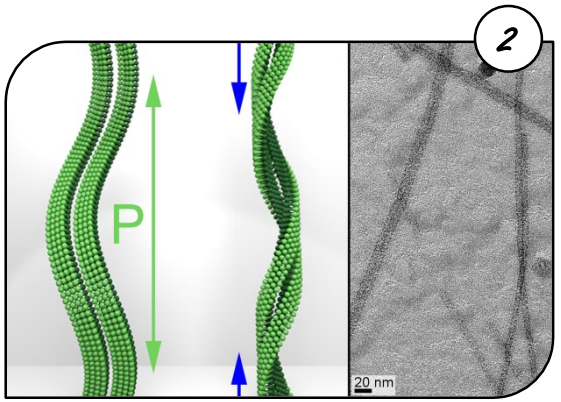

60m M 3-layered single helical tape

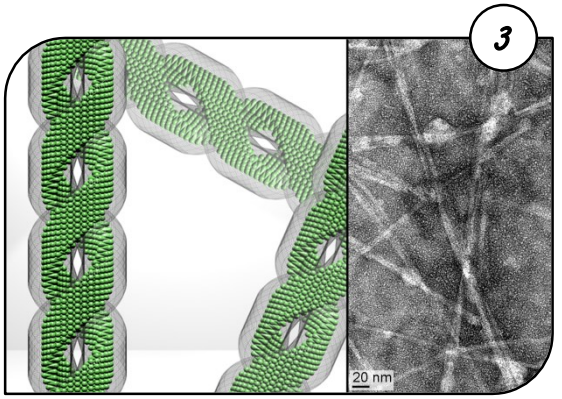

75 mM 3-layered double helical tape

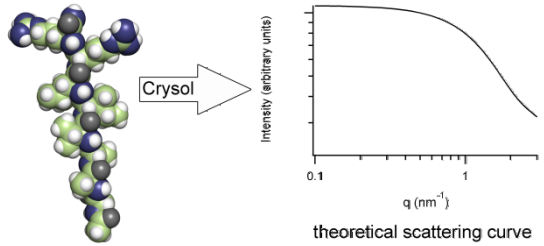

theoretical scattering curve

Pontoni D. et al., J. Chem, Phys, 2003
Svergun D.I. et al., J. Appl. Cryst., 1995

K.Kornmüller et al.
Nano Research (2015)

Self-assembly processes of Fibers/Helicals SASHel

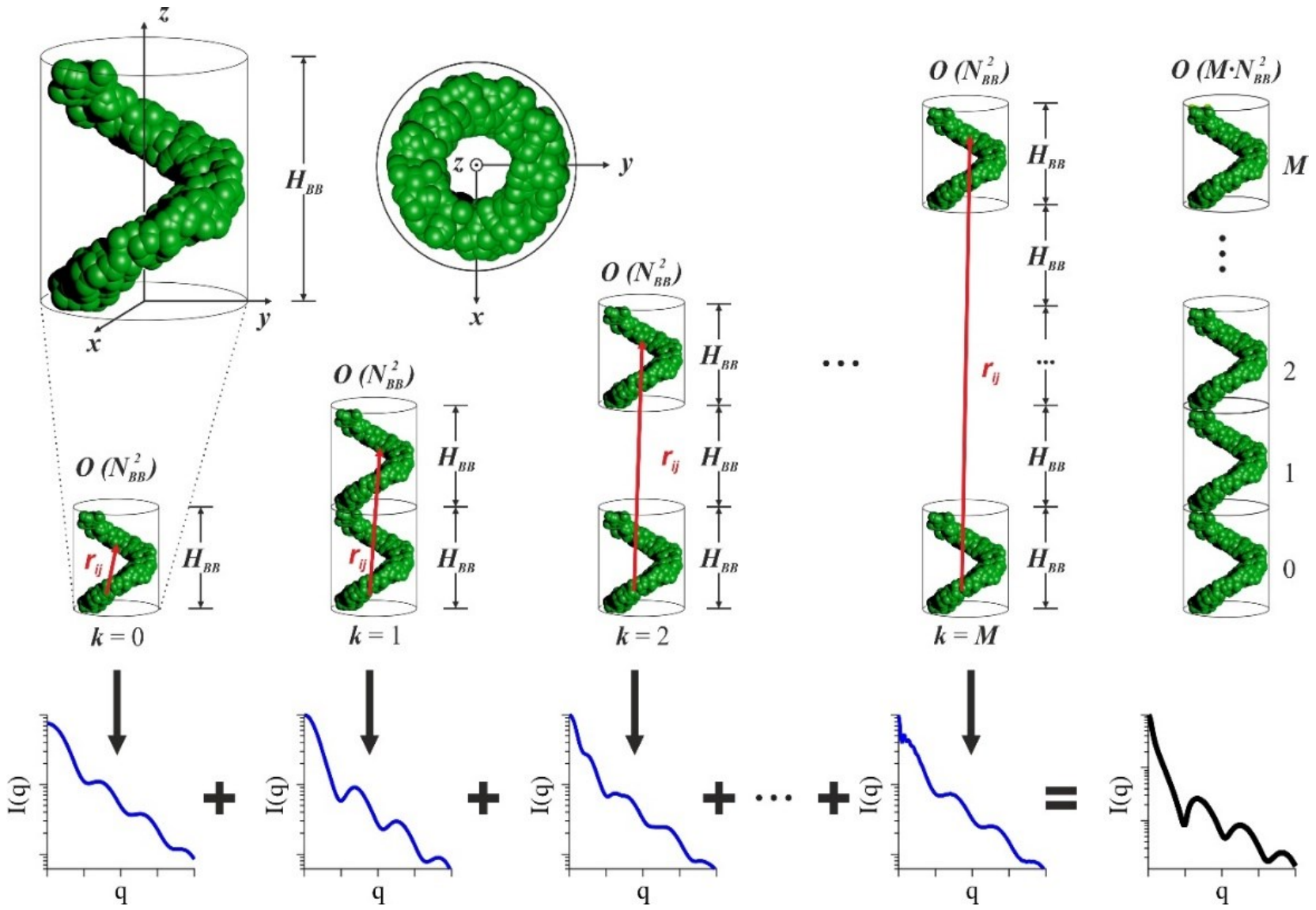

amenitsch@tugraz.at & amenitsch@elettra.trieste.it

Self-assembly processes of Fibers/Helicals SASHel

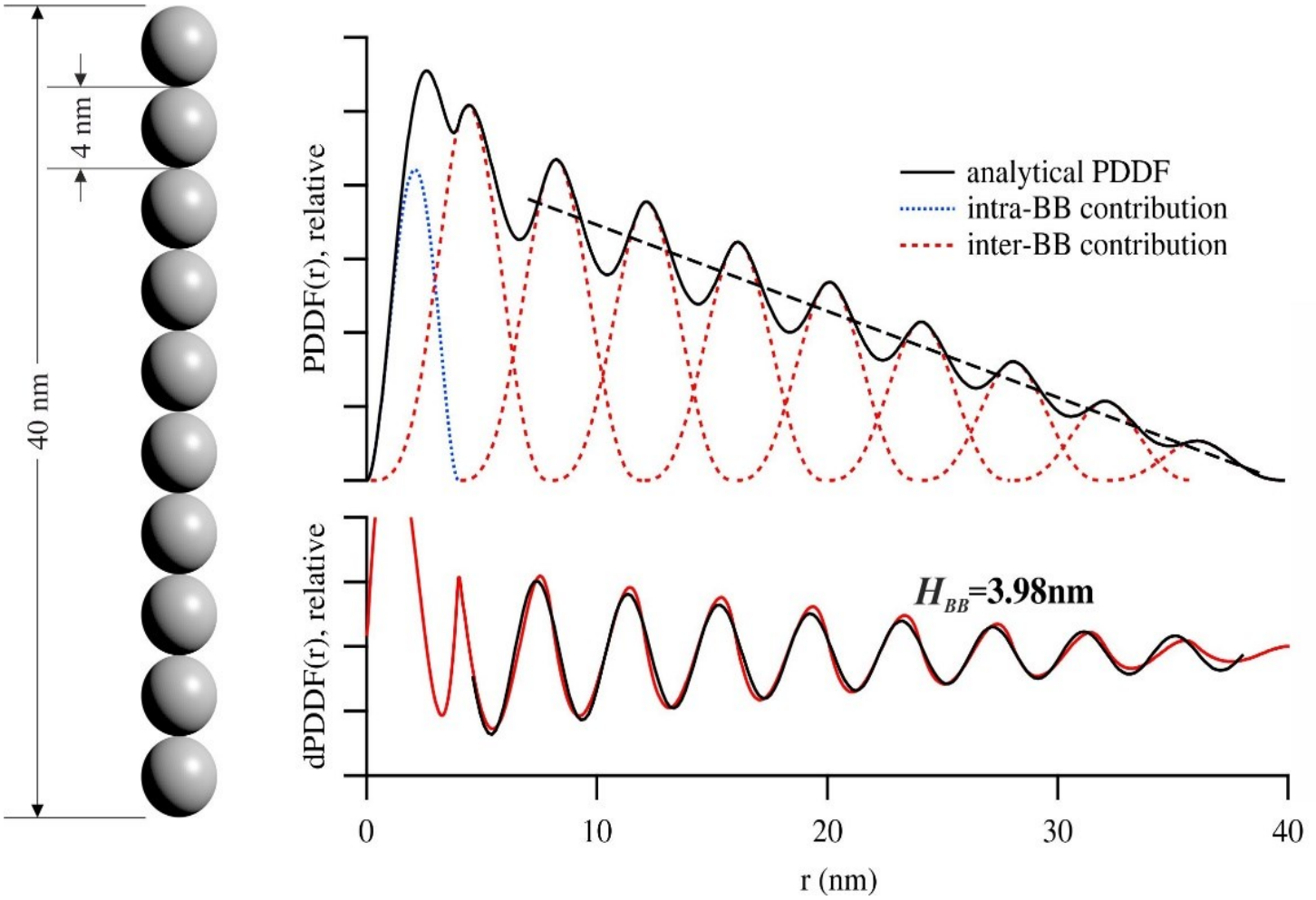

amenitsch@tugraz.at &
amenitsch@elettra.trieste.it

Self-assembly processes of Fibers/Helicals

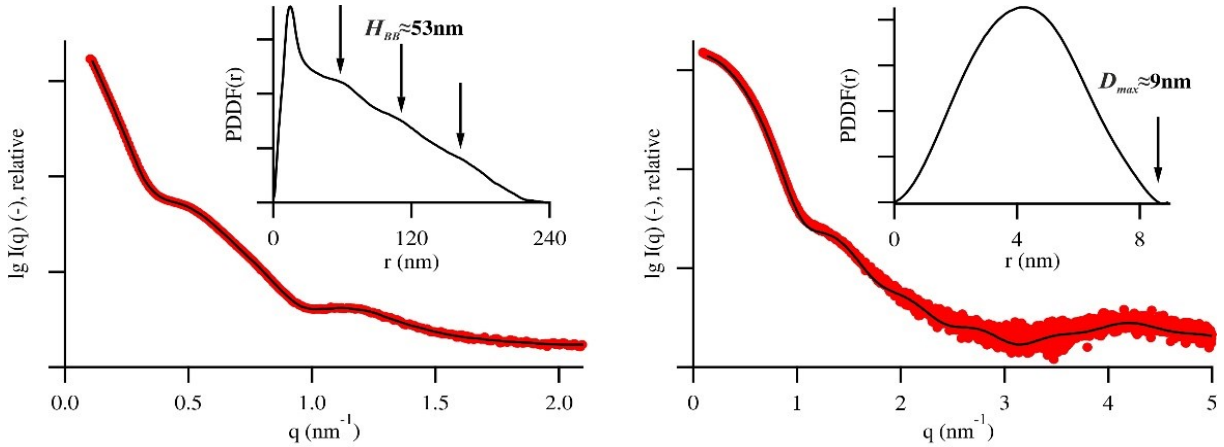

Alcohol Dehydrogenase 1
Valentini E et al., Nucleic Acids Res. **43** (2015)

Kornmueller,K, et al. NanoResearch (2018)

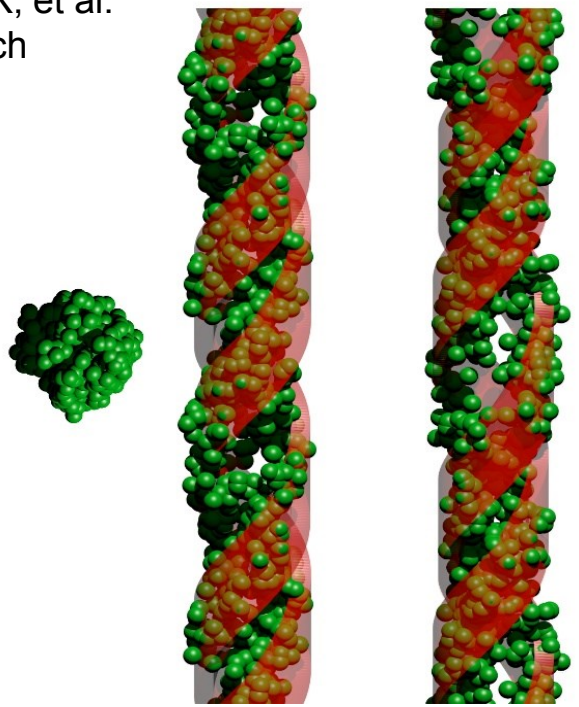

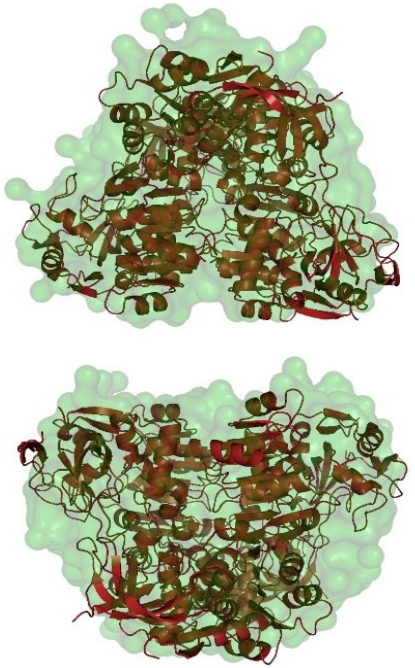

M.Burian, H.A. accepted IUCrJ (2018)

amenitsch@tugraz.at &
amenitsch@elettra.trieste.it

Biomechanics on Human Aorta: Motivation

Macroscopic response ⟷ **Model** ⟷ Micro- and nano-structure

Pathology, Clinics

Characterization of vascular disease
Effects of aging
Identification of therapeutic targets (Balloon Angioplasty)

Graft design

Biomimetic materials

Functional tissue engineering

Mechanobiology

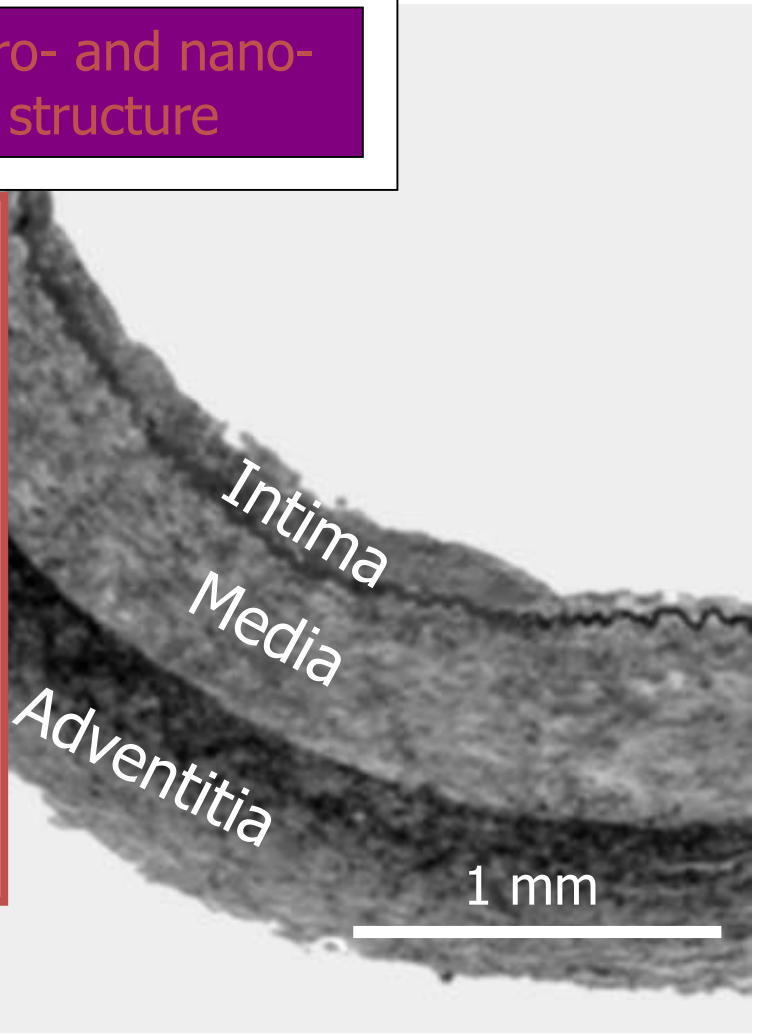

Cross section of a human artery

amenitsch@tugraz.at &
amenitsch@elettra.trieste.it

Human Aorta: Mechanical Parameters

Macroscopic

geometric deformation

stress

strain

Nanoscopic

fiber – matrix composite

fiber alignment

fiber strain

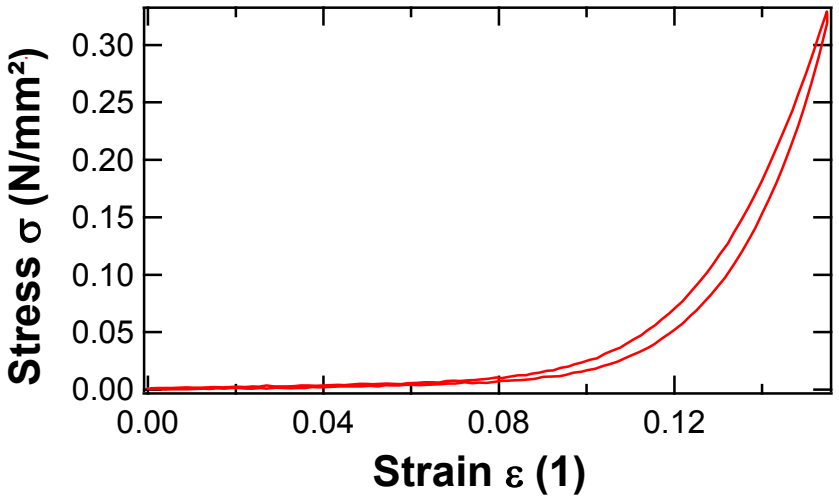

Collagen - The most abundant protein

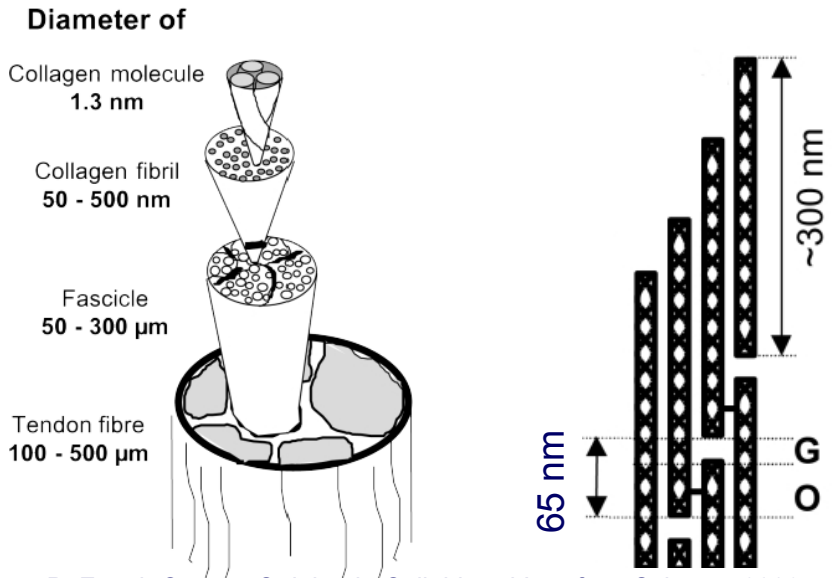

P. Fratzl, Current Opinion in Colloid and Interface Science, 2003

amenitsch@tugraz.at &
amenitsch@elettra.trieste.it

Human Aorta: Sample Preparation

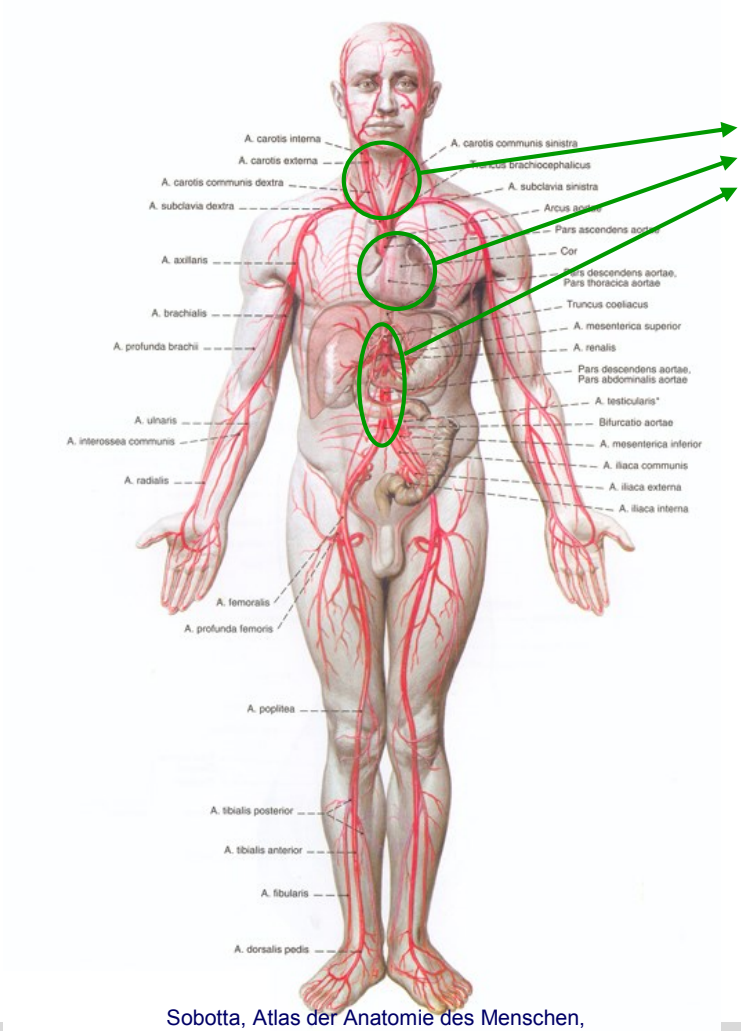

Sobotta, Atlas der Anatomie des Menschen, Band 2, 20. Auflage, S.14, Abb31

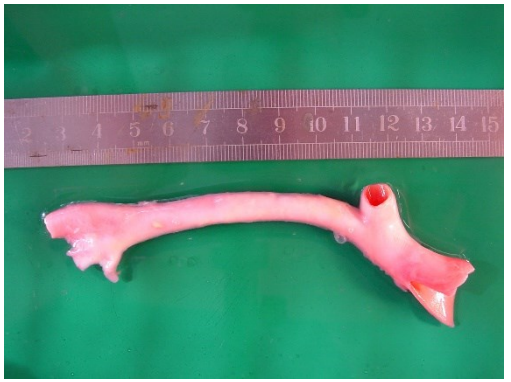

An artery, cleaned from surrounding tissue

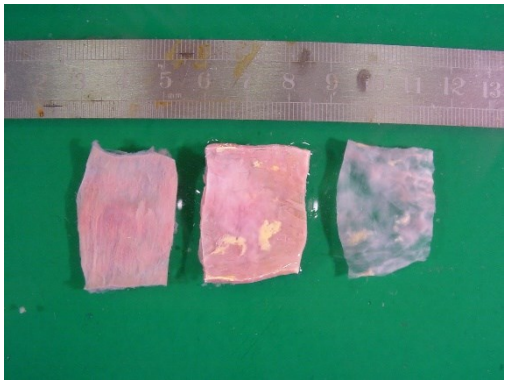

After dissection into its major layers

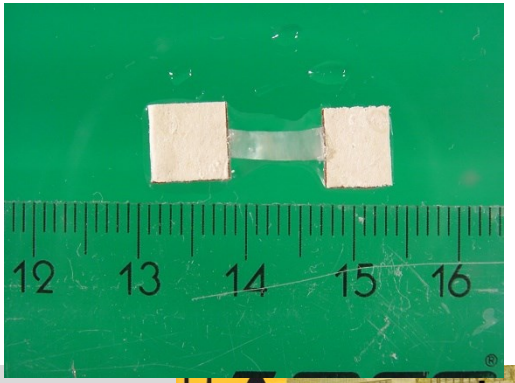

The final sample

amenitsch@tugraz.at &
amenitsch@elettra.trieste.it

Human Aorta: Collagen Fiber Orientation

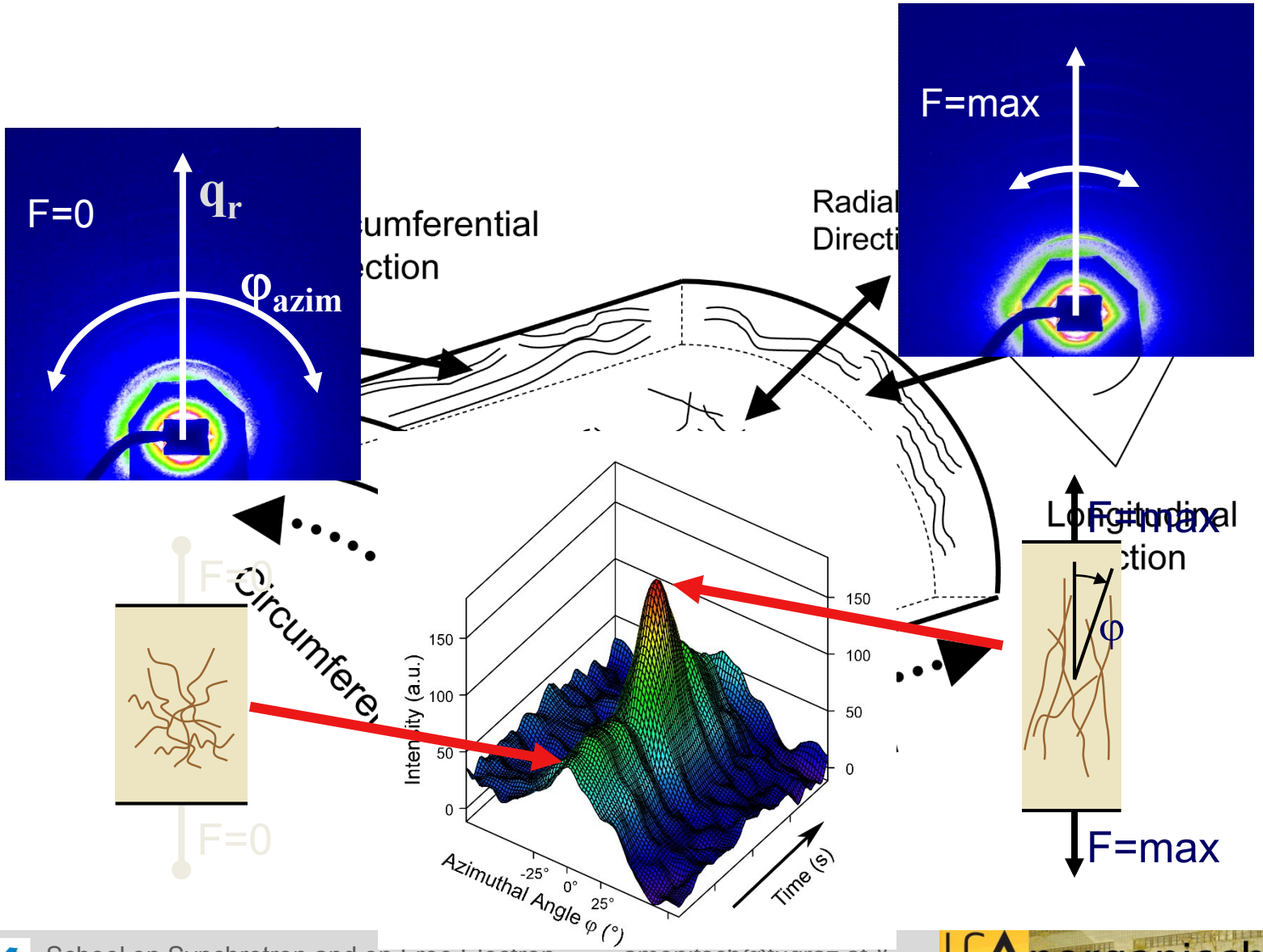

amenitsch@tugraz.at & amenitsch@elettra.trieste.it

Nano – Macro Coupling

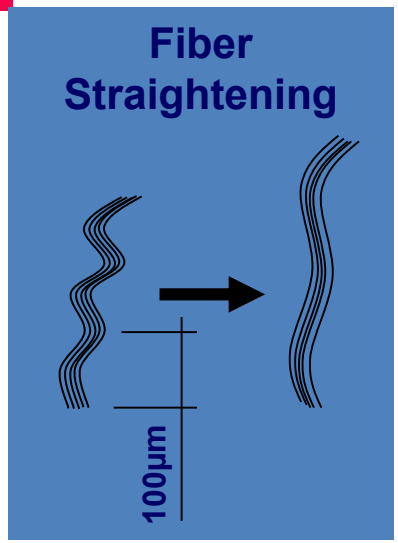

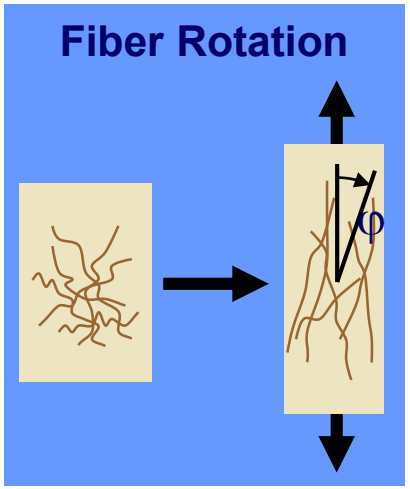

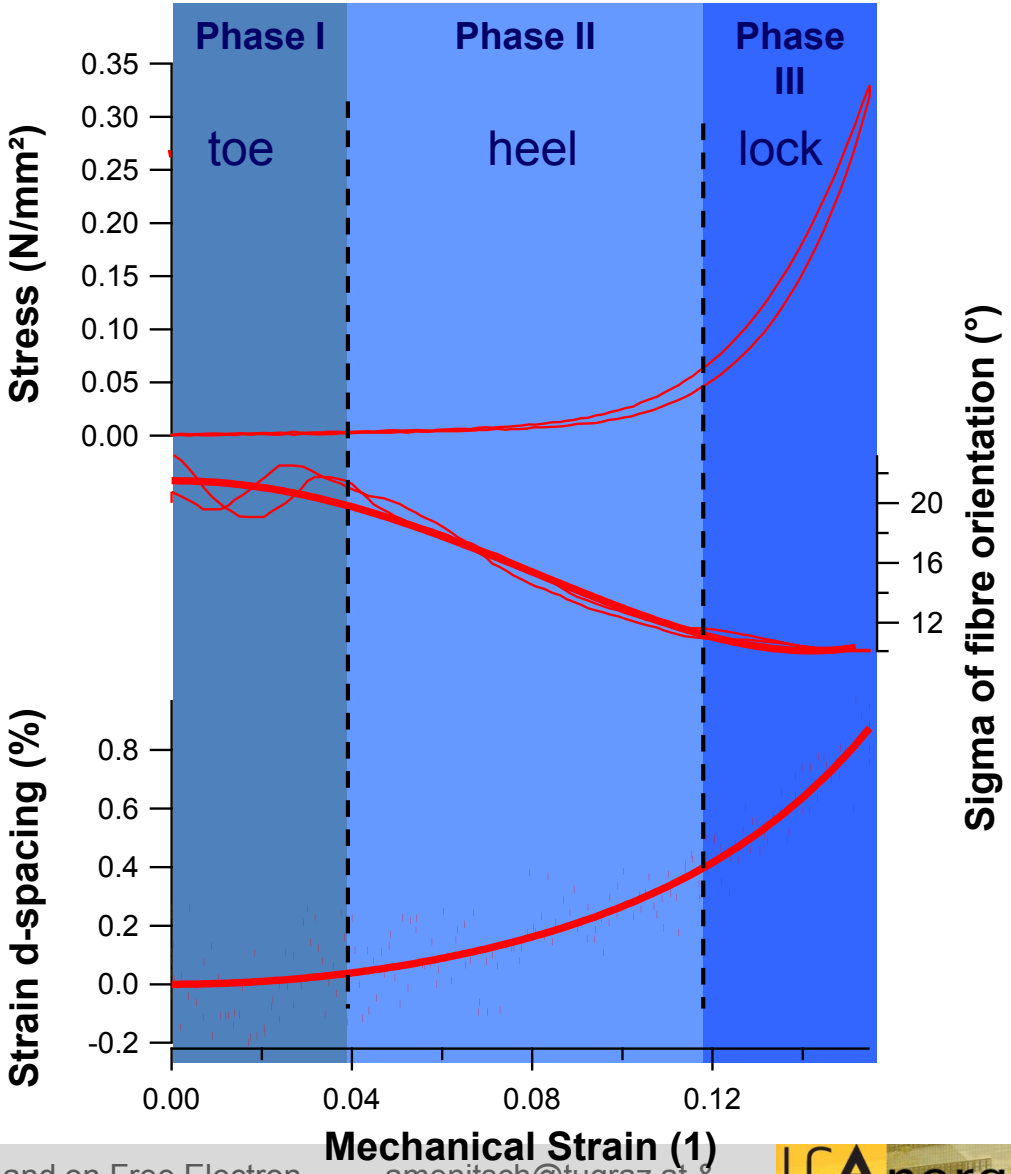

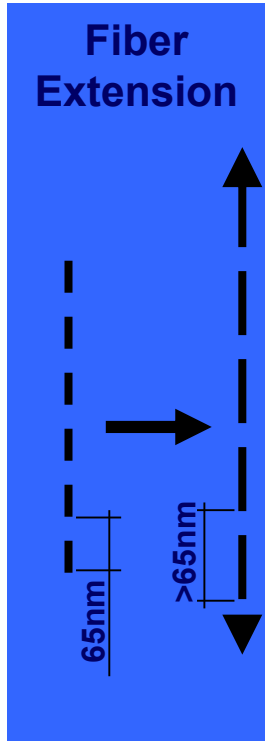

amenitsch@tugraz.at &
amenitsch@elettra.trieste.it
F. Schmid et al., J.Synchr.Rad., 2018, in press

Scanning SAXS - Biomaterials

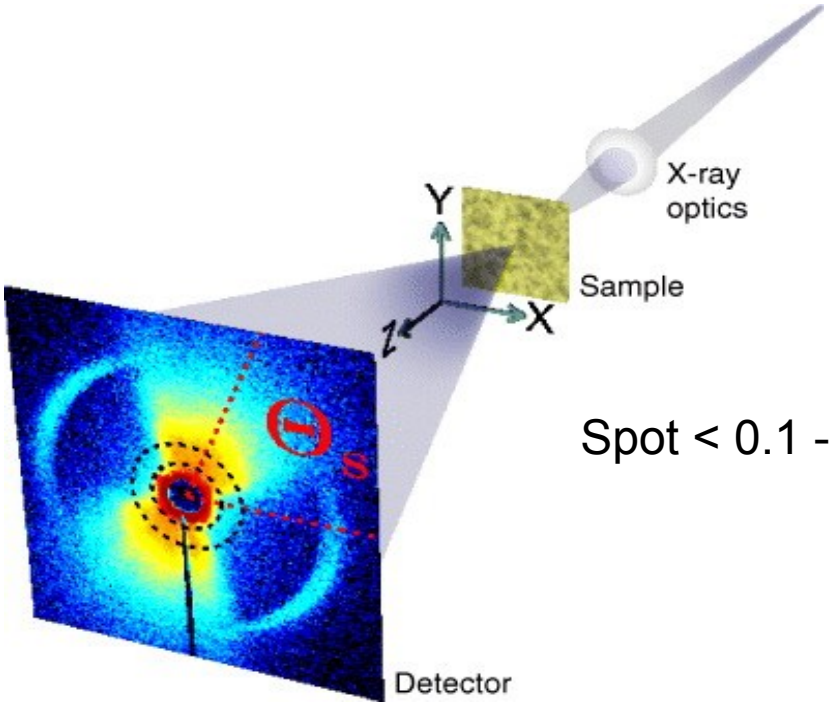

Spot < 0.1 -1 µm

Bone

P.Fratzl

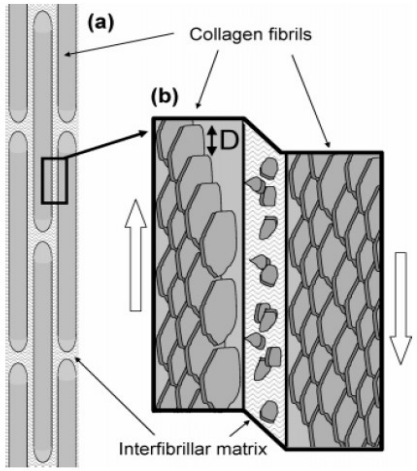

Wood P.Fratzl

Pic. O.Bunk, et al. New J. Phys. **11** (2009) 123016

Silica-Sponges, Shells,
Tooth, Lobster, Worms,
Starch, Eyes……,

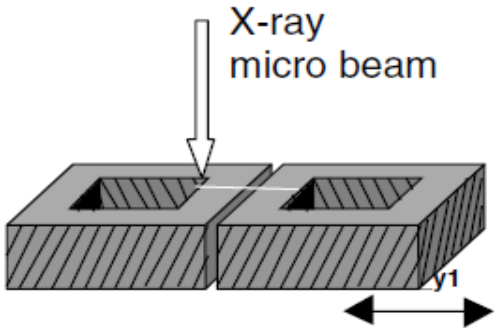

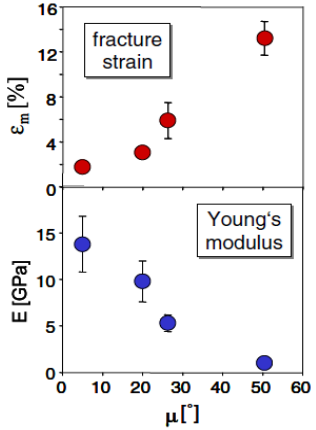

amenitsch@tugraz.at &
amenitsch@elettra.trieste.it

Scanning SAXS-Integral Parameters

Integrated Intensity

$$I = \int_{q\,\min}^{q\,\max} \int_{\chi_1}^{\chi_2} I(q, \chi) q^2 \, \mathrm{d}q \, \mathrm{d}\chi$$

Porod Invariant

$$\tilde{I} = \int I(\mathbf{q}) \, \mathrm{d}^3 q = \int_0^{\infty} q^2 \, \mathrm{d}q \int_0^{\pi} \sin\psi \, \mathrm{d}\psi \int_0^{2\pi} I(q, \psi, \chi) \, \mathrm{d}\chi$$

$$= 2\pi^2 \varphi_1 \varphi_2 (\Delta\rho)^2,$$

T-Parameter

$$T = \frac{4}{\pi P} \int_0^{\infty} I(q) q^2 \, \mathrm{d}q = 4 \frac{\varphi_1 \varphi_2}{\sigma}$$

Porod (1951,1952)

Scattered Intensity

$$\Sigma \cdot \mathrm{D_s} \propto \int \mathrm{I(q)} \cdot q \cdot \mathrm{dq} \propto \mathrm{p} \cdot \Delta\rho^2 \cdot l_c$$

Σ Macroscopic Cross Section $\quad D_s$ Sample Thickness

p Volume Fraction
Δρ Electron Density Contrast
l_c Correlation Length
R Radius

amenitsch@tugraz.at & amenitsch@elettra.trieste.it

Scanning SAXS - Orientation

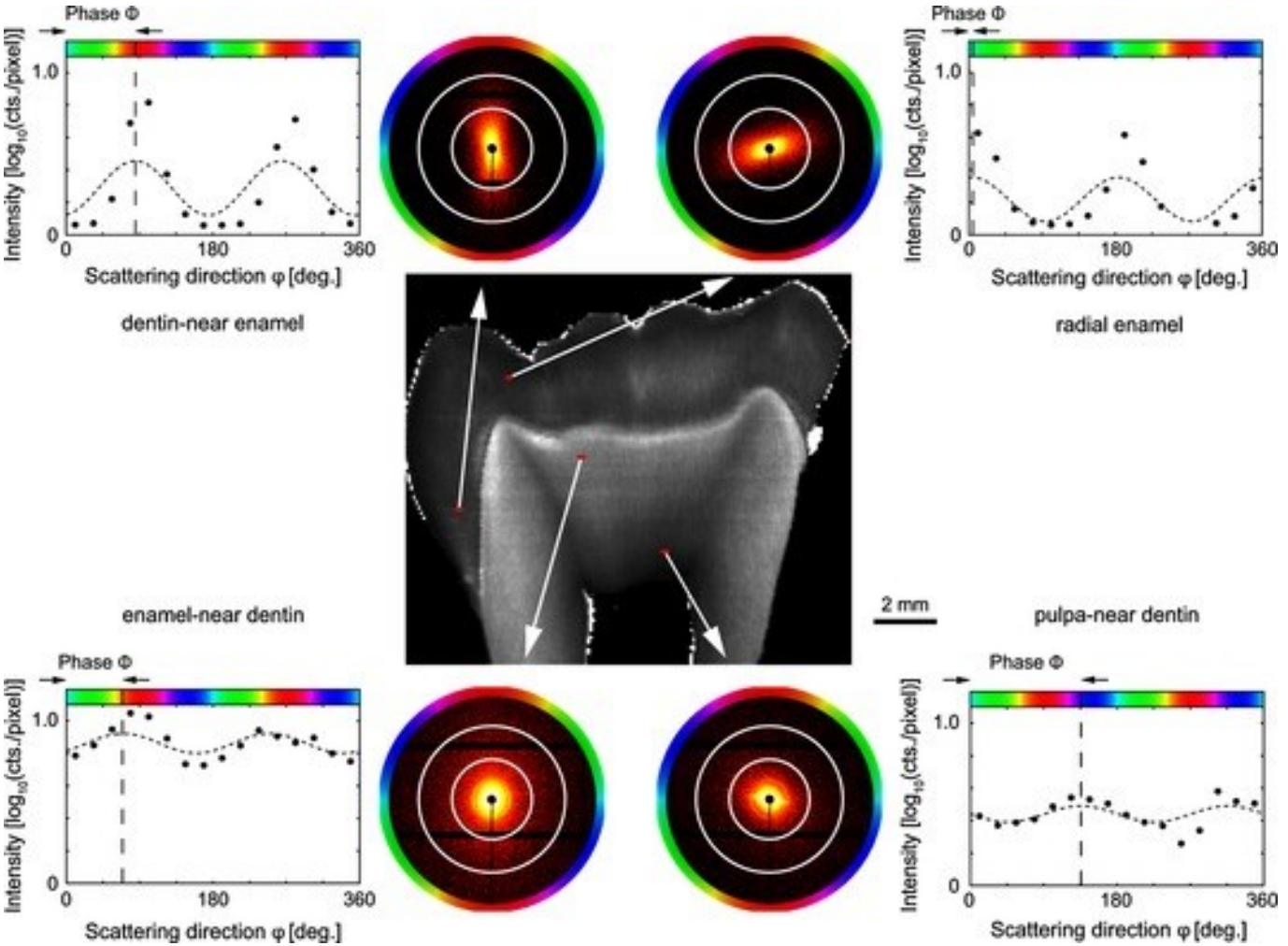

Geiser S. et al., Biointerphases
Journal for the Quantitative Biological Interface Data, 2012

amenitsch@tugraz.at &
amenitsch@elettra.trieste.it

Scanning SAXS - Tooth

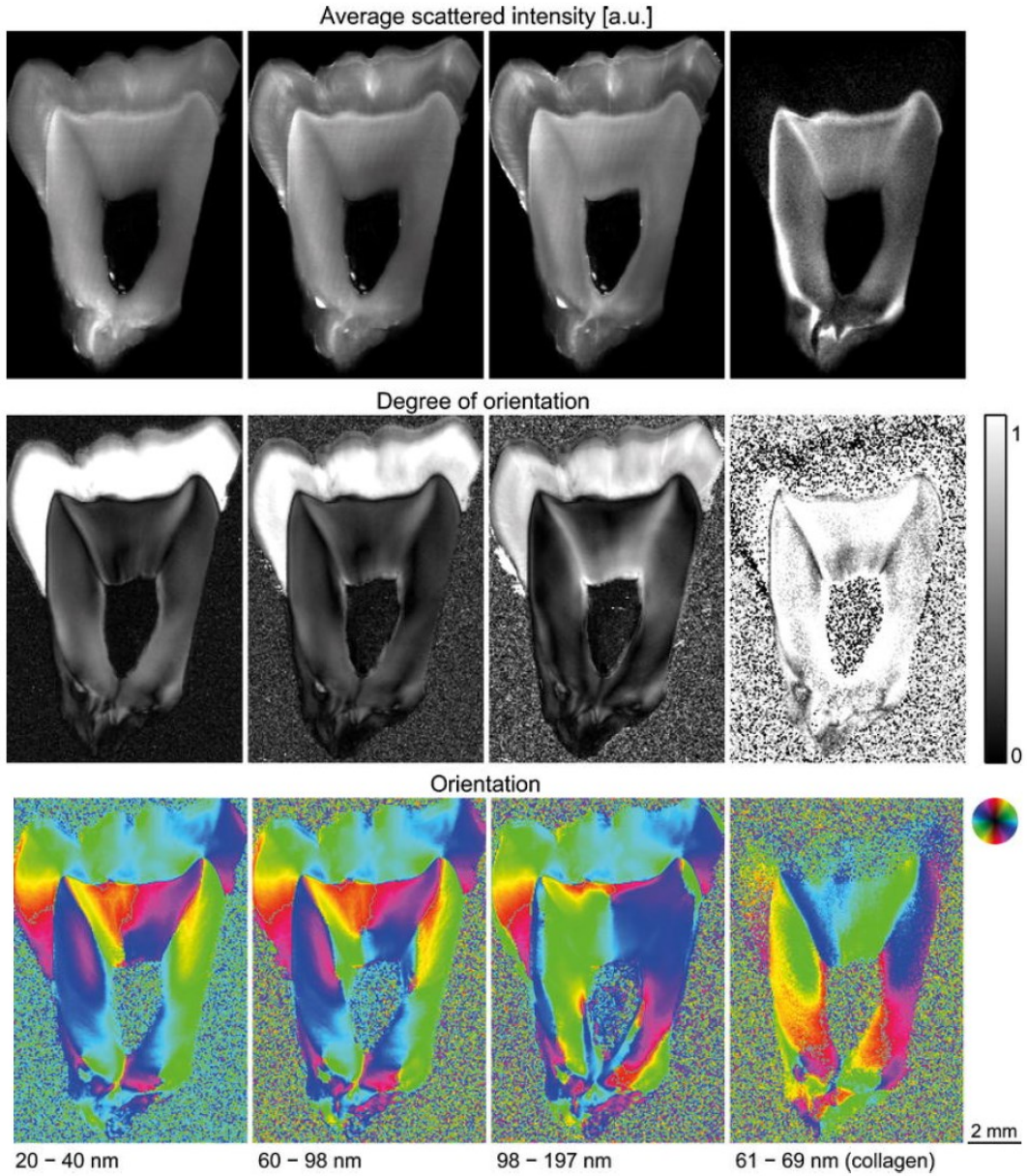

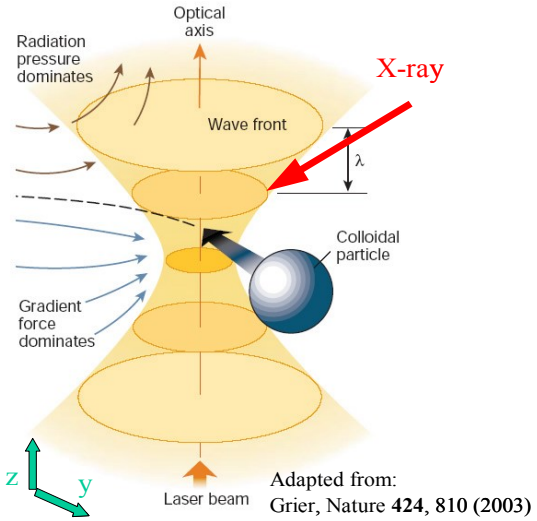

Adapted from:
Grier, Nature **424**, 810 (2003)

Bulk: time and assemble averaged properties

Single Particle: local fluctuations
μ-shape nanostructure corr.
single particle chemistry

Multiple Particle Trapping: local information on interactions
single shot experiments

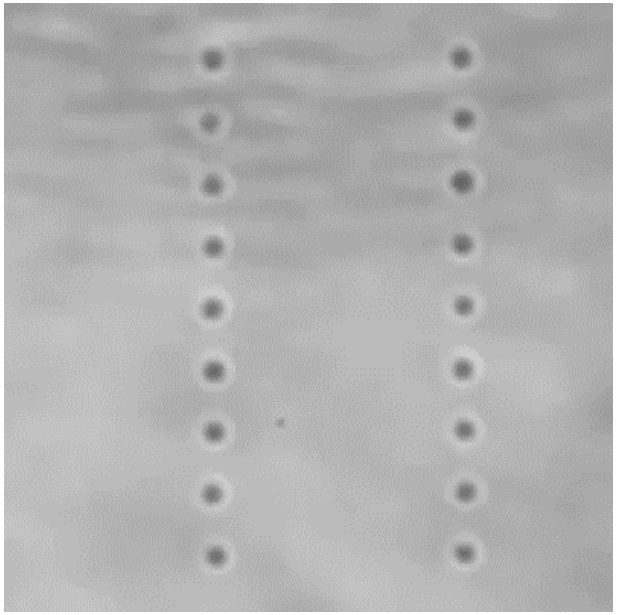

18 silica micro-beads trapped and manipulated to form the vortices of a Diamond cell.

(M. Padgett group @ Univ. St. Andrews UK)

amenitsch@tugraz.at &
amenitsch@elettra.trieste.it

Schematic of the optical manipulation for SAXS

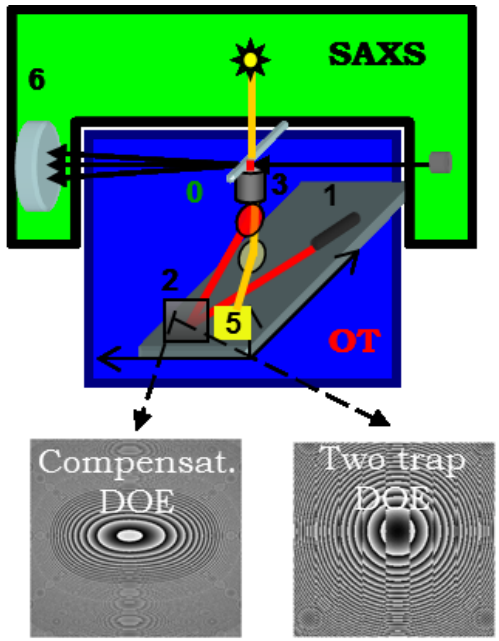

DOE = Diffractive Optic Element

paths

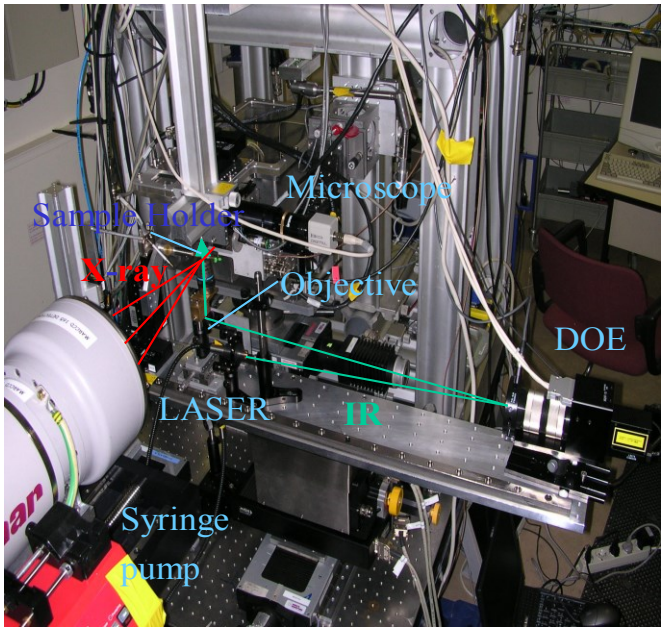

ESRF: ID13
@46 m & @100 m
KB Mirror
Ref. Lenses
Beam size: ~1 µm
X-rays: ~13.0 keV
(λ = ~0.94 Å)
Detectors:
Mar165
Frelon

0 – sample cell (capillary connected to µfluidics)
1 - IR laser @ 1064 nm
2 - Phase Programmable Modulator (PPM) Hamamatsu
3,4 - microscope objectives, Nikon, Olympus
5,6 - CCDs

D. Cojoc *et al.*, *Proc. SPIE* 6326, 63261M (2006)
H. Amenitsch, *et al.*, CP879, *SRI:Ninth International Conference, AIP*, 1287 (2007)

D. Cojoc et al., *APL, 91, 234107, (2007)*

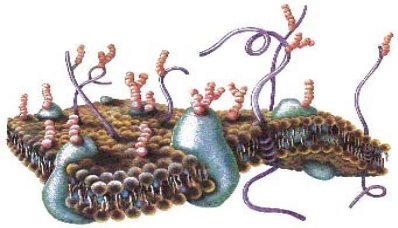

The boundaries of cells are formed by biological membranes, the barriers that define the inside and the outside of a cell.

Phospholipids are the major components of biological membranes that form the structural matrix into which proteins are imbedded.

In aqueous solution:
self assembly into, e.g.,
unilamellar vesicles

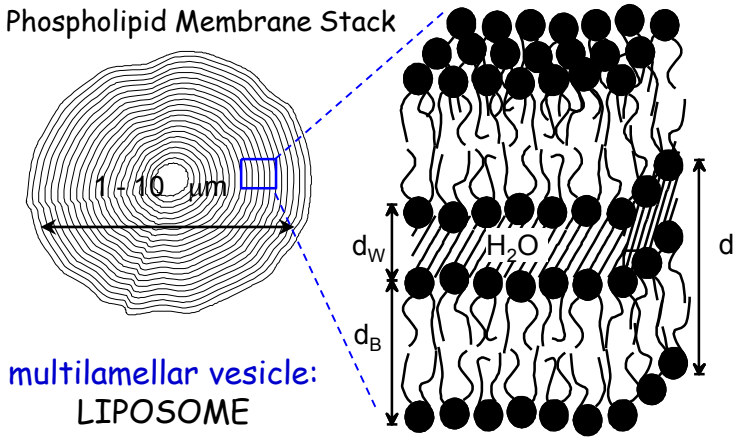

multilamellar vesicle:
LIPOSOME

Lyotropic Phases

Bilayer

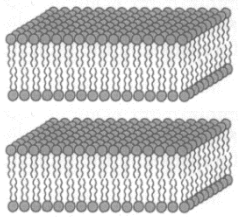

Micelle

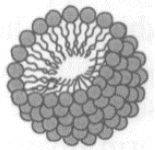

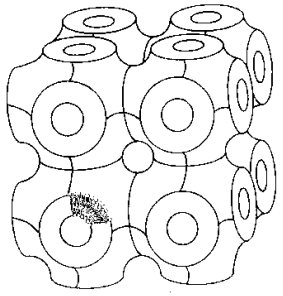

Cubic Phase

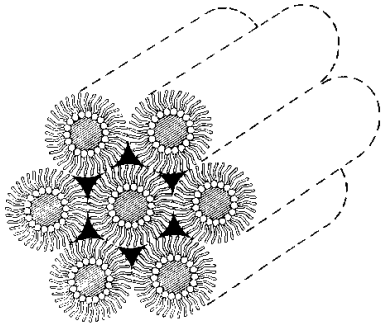

Hexagonal Phase

amenitsch@tugraz.at &
amenitsch@elettra.trieste.it

Diffraction from single cluster (10 µm)

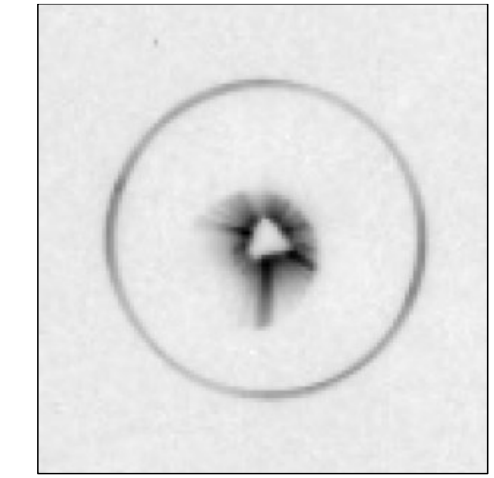

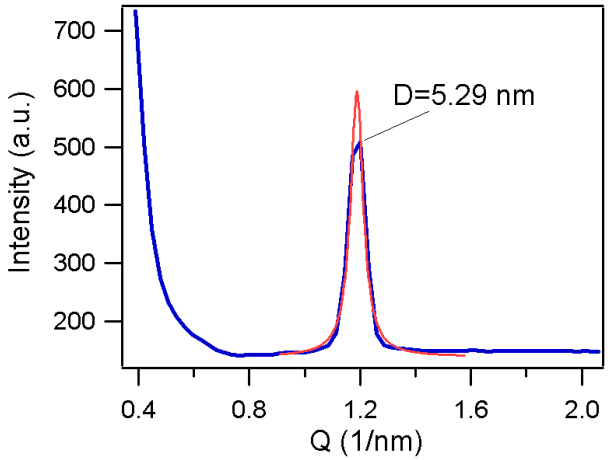

Diffraction pattern and azimuthally integrated diffraction pattern

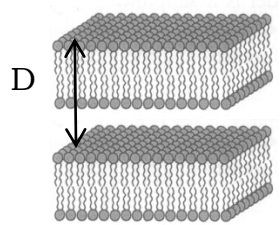

Diffraction image: exposure time 5 s

POPE (Palmitoyl-Oleoyl-Phosphatidyl-Ethanolamine) multilamellar vesicle (1 wt%) in 1 mol $CaCl_2$, Cluster size: 8-10 µm

Liposome size: 1-2 µm, Phase: Liquid crystalline L_α

amenitsch@tugraz.at &
amenitsch@elettra.trieste.it

SAXD of optically trapped liposomes

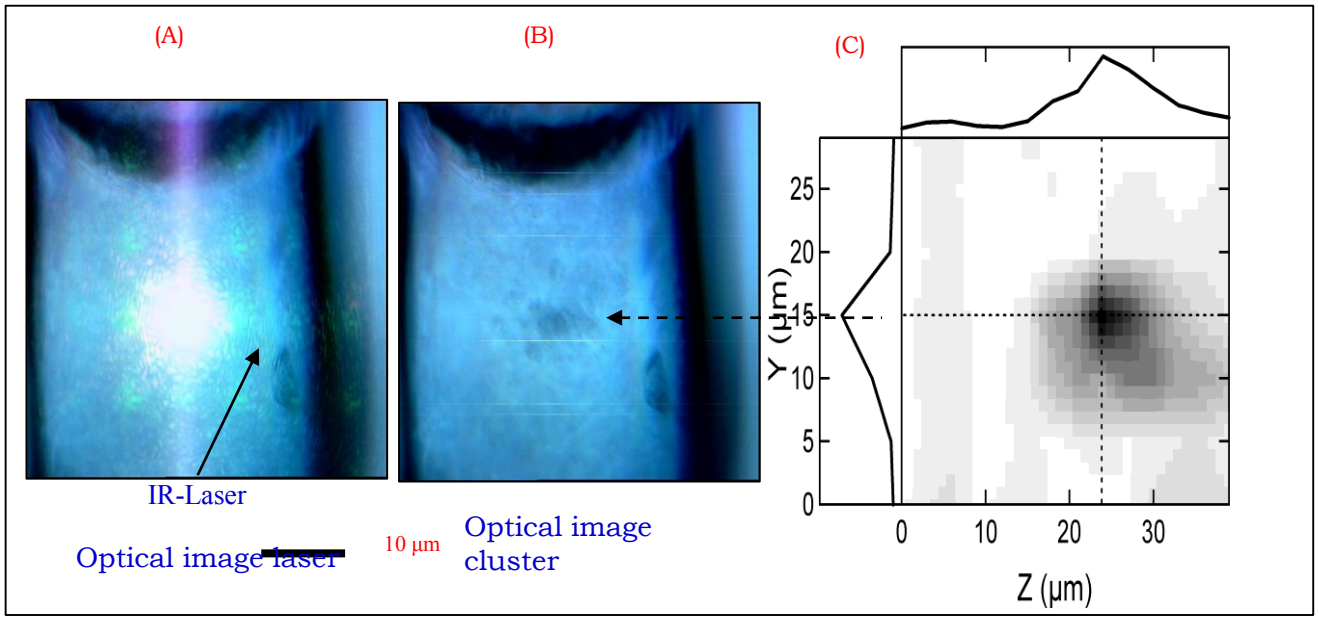

Diffraction from single clusters (8-10 µm)

Step: 2.5 x 5 µm²

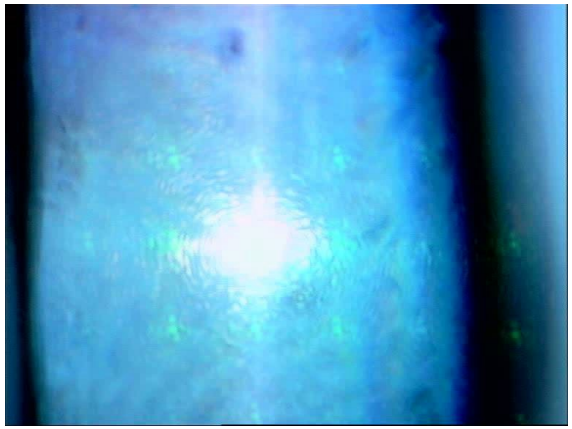

‚Diffraction image' (1st order reflection) of the cluster

amenitsch@tugraz.at &
amenitsch@elettra.trieste.it

Scanning Diffraction from two clusters multiple trapping

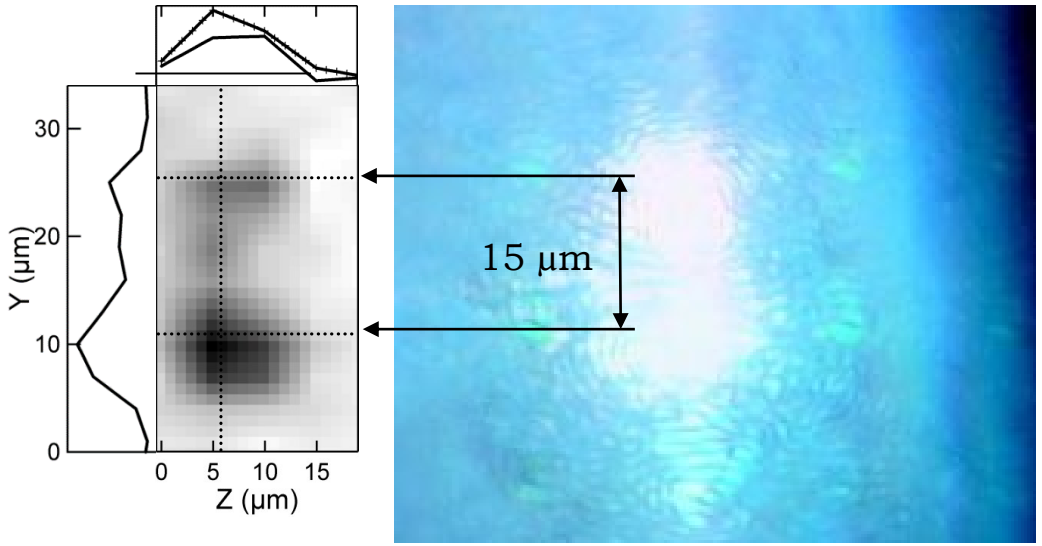

**‚diffraction image'
of two clusters**

**Optical image
of the clusters +
laser**

Step: 3x5 µm²

DOPE (hexagonal structure)

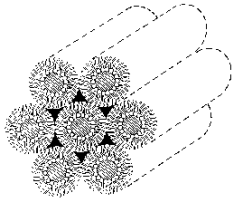

amenitsch@tugraz.at &
amenitsch@elettra.trieste.it

New LT set-up

Improved Sample container

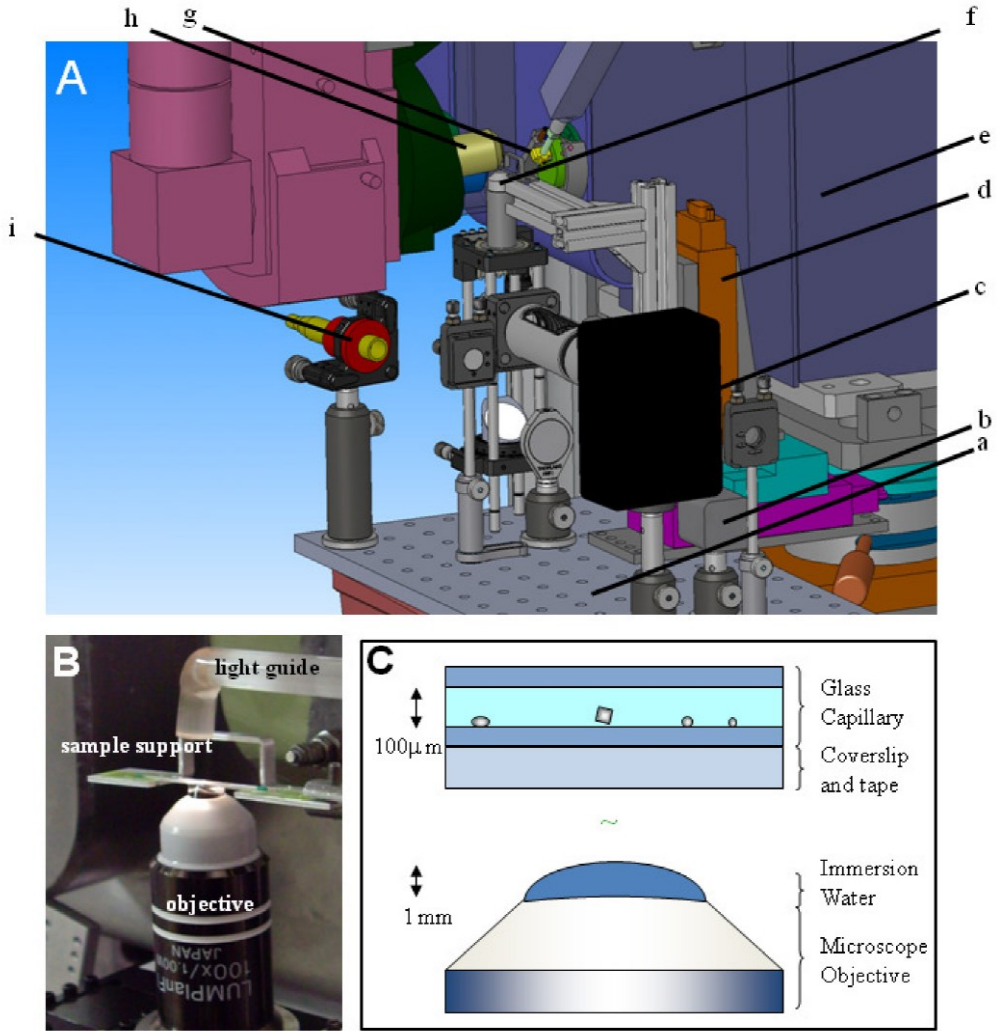

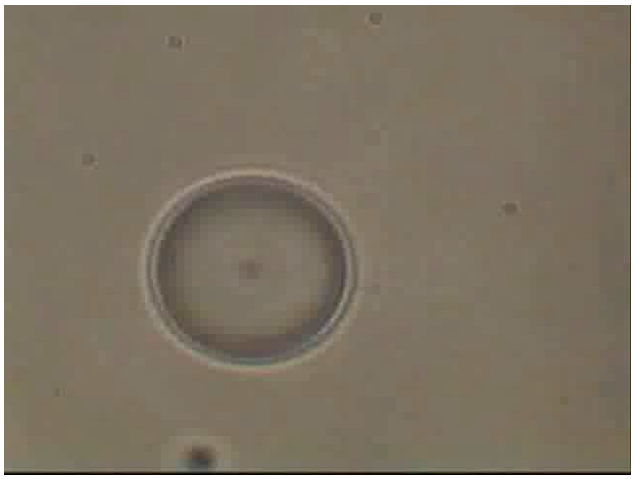

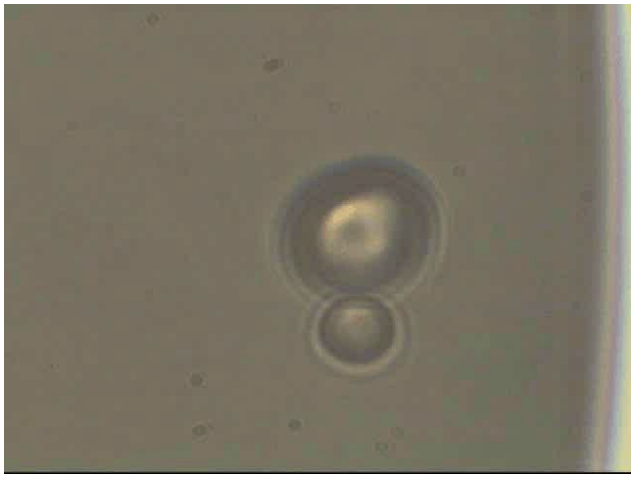

S.Santucci, et al. Biochemistry 2011

Heinz Amenitsch (amenitsch@tugraz.at)
amenitsch@tugraz.at &
amenitsch@elettra.trieste.it

X-ray Diffraction from Starch

Phase Contrast Image of Potato Starch Granules

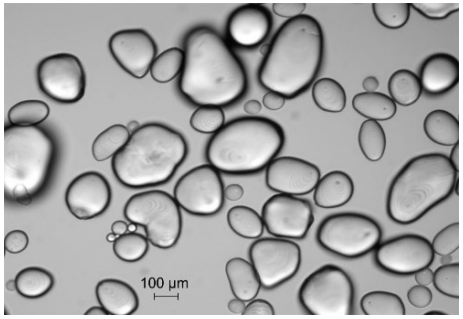

Cartoon Amylopectin Structure

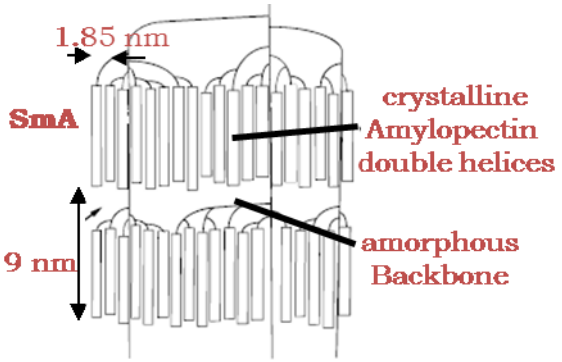

WAXD d(100) = 1.5 nm

SAXD d = 9 nm

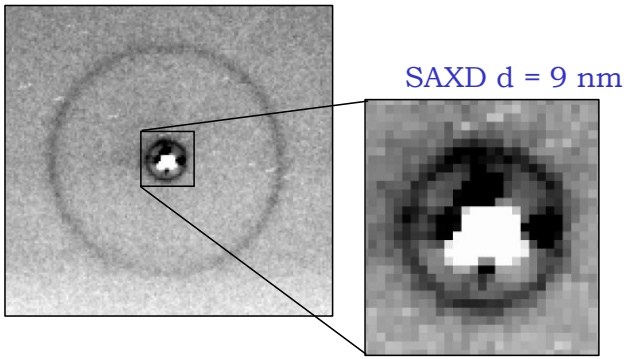

Waigh T et al., *Macromolecules, 1997*

Cartoon Starch Ganule

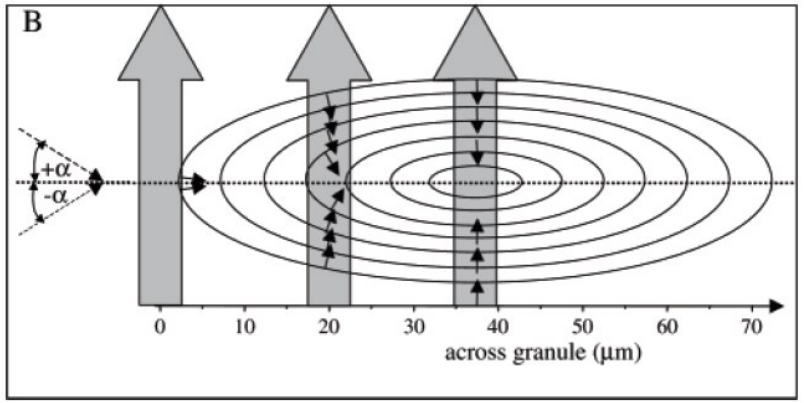

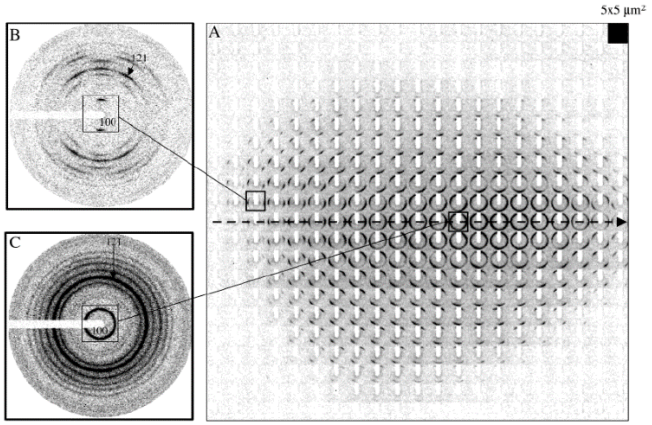

H. Lemke et al., Biomacromolecules **2004, 5**, *1316-1324*

amenitsch@tugraz.at &
amenitsch@elettra.trieste.it

Scanning diffraction experiment

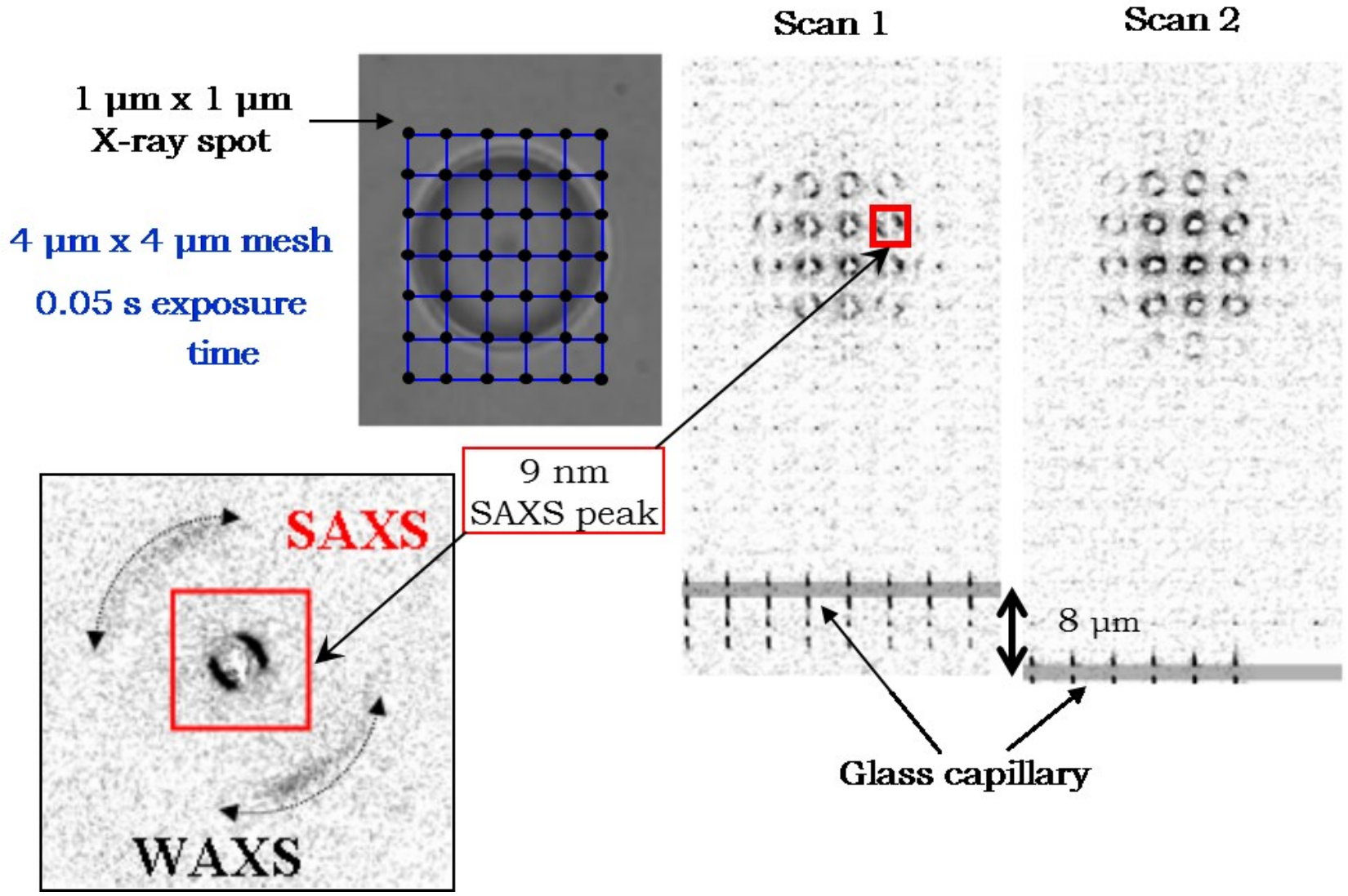

amenitsch@tugraz.at &
amenitsch@elettra.trieste.it

SAXS of optically trapped starch granules (from potato)

Integrated Intensity & I(100) Reflection

Max. exp.
Time: 200 ms!!!

Time: 1.5 s !!!

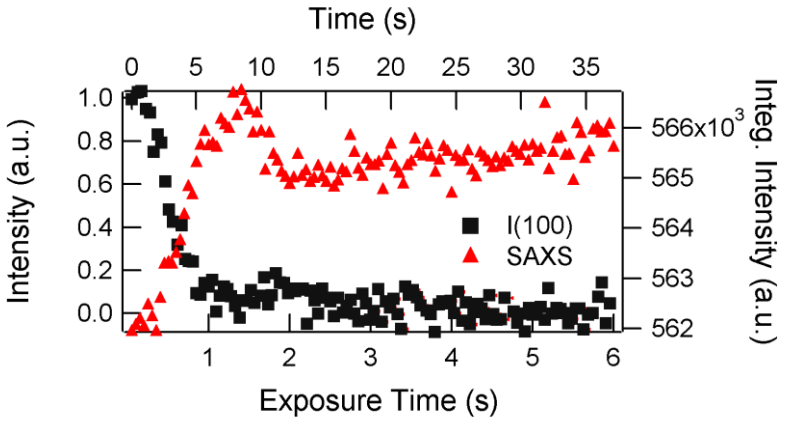

FoV 40 x 30 µm

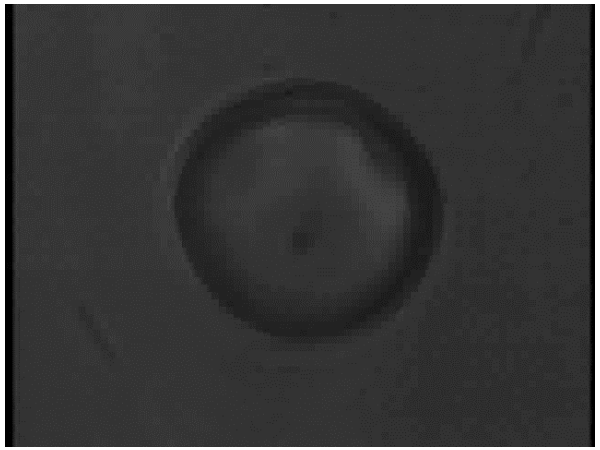

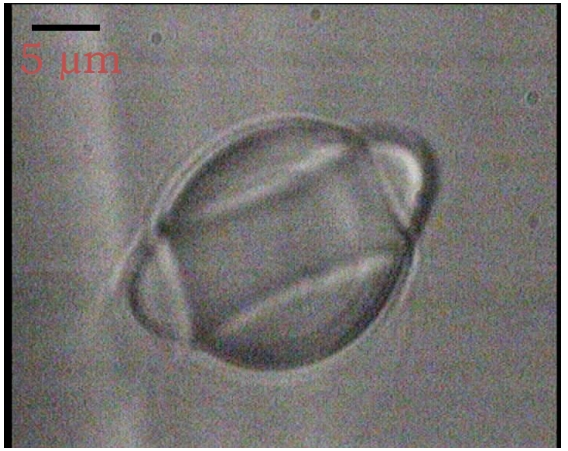

2.12 min x 4 accel.

amenitsch@tugraz.at &
amenitsch@elettra.trieste.it

Radiation Damage

Simultaneous Fitting SAXS and WAXS
Porod & Lorentzian Peak

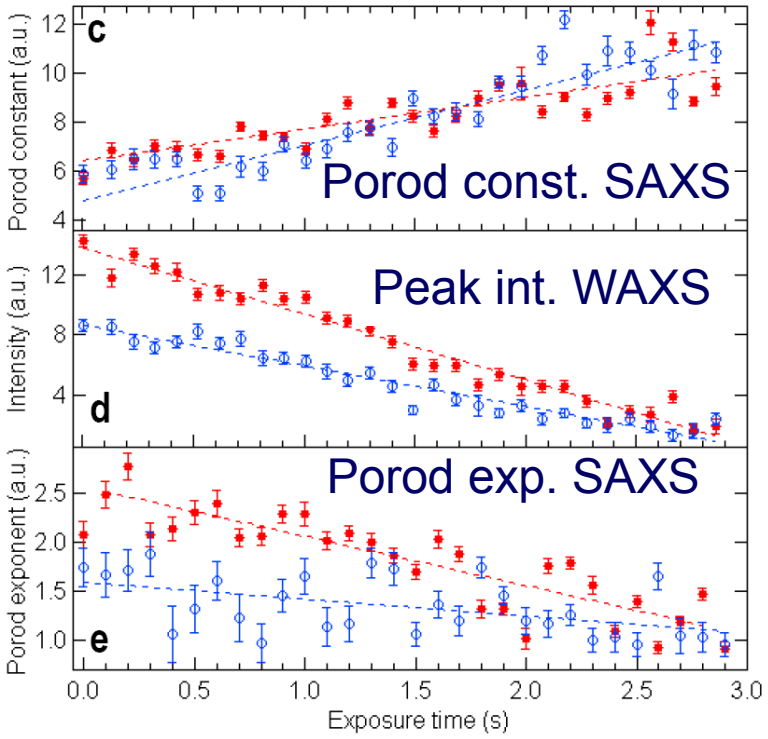

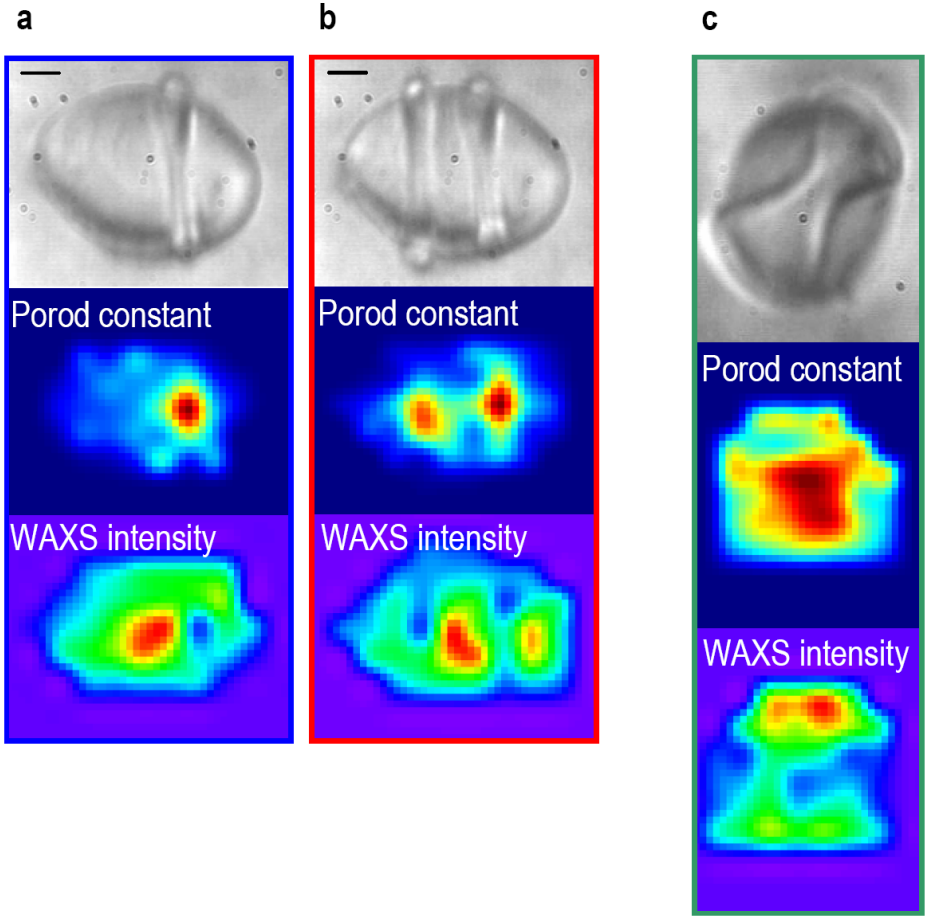

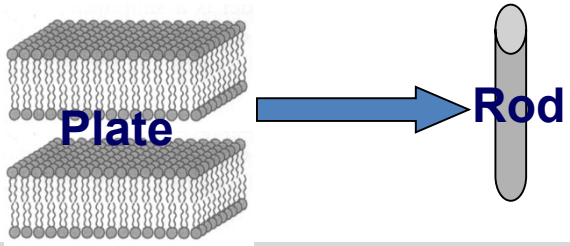

D.Cojoc, H. Amenitsch et al., APL, 2010

Laser Tweezers Protein Crystals

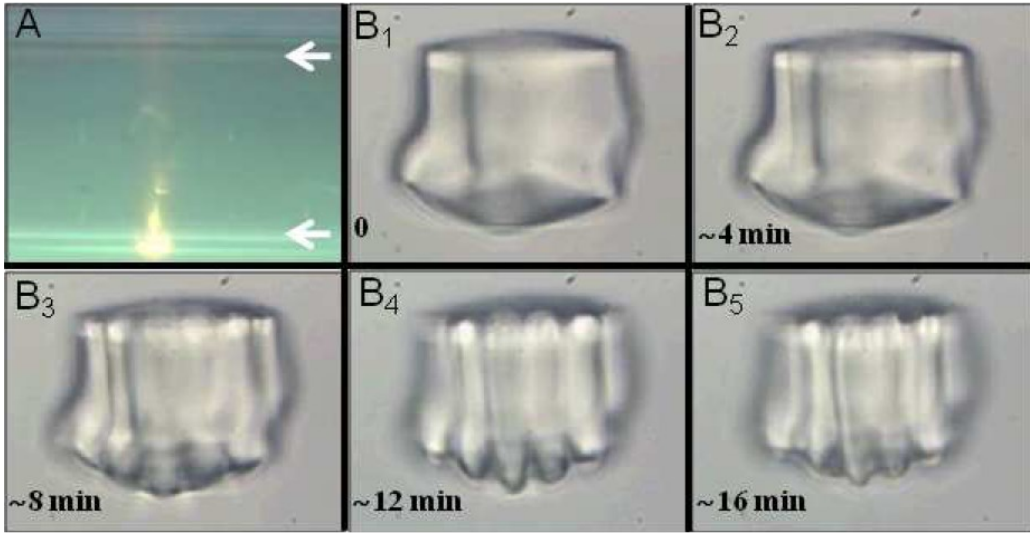

Insulin Crystal

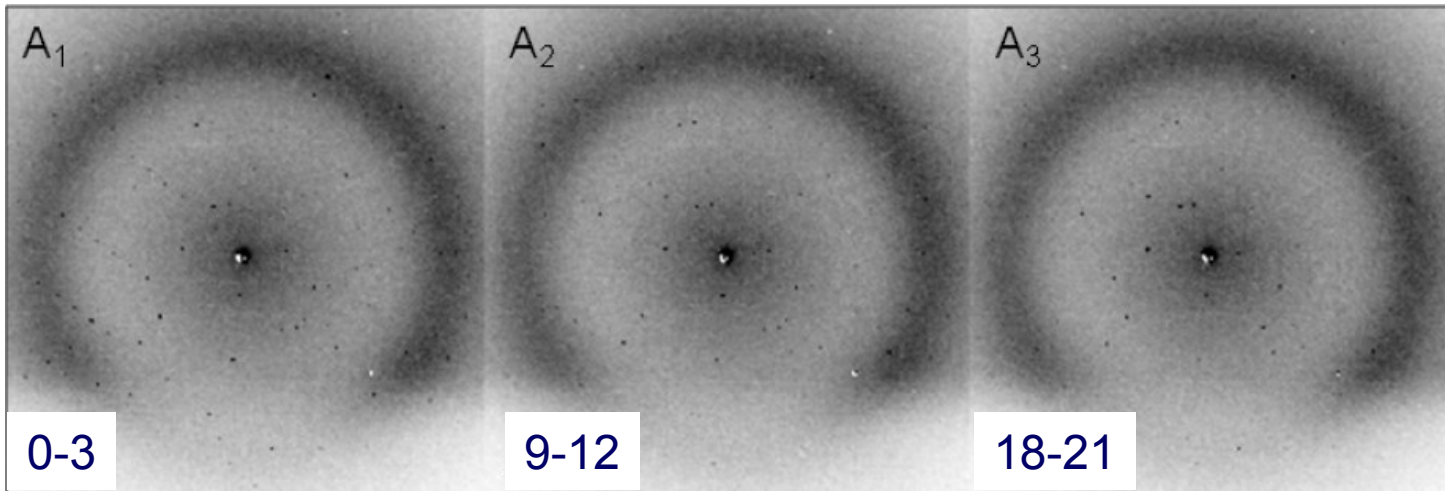

S.Santucci, C.Riekel et al. Biochemistry 2011

Liposomes and SAXS

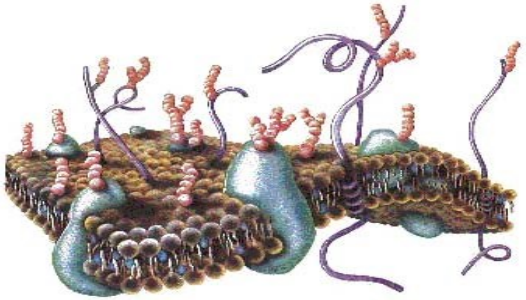

The boundaries of cells are formed by biological membranes, the barriers that define the inside and the outside of a cell.

Phospholipids are the major components of biological membranes that form the structural matrix into which proteins are imbedded.

In aqueous solution:
self assembly into, e.g.,
unilamellar vesicles

Phospholipid Membrane Stack

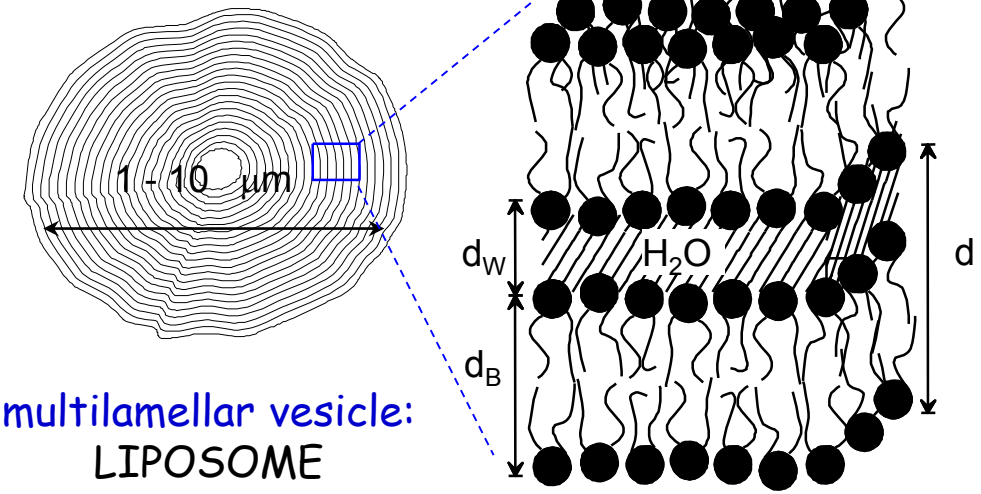

multilamellar vesicle:
LIPOSOME

Lyotropic Phases

Bilayer

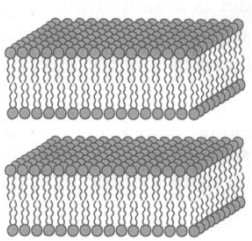

Micelle

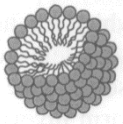

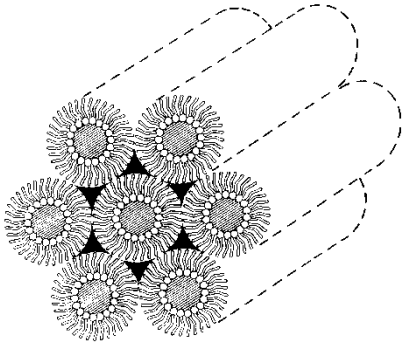

Hexagonal Phase

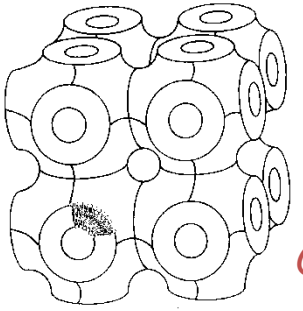

Cubic Phase

amenitsch@tugraz.at &
amenitsch@elettra.trieste.it

Small Angle Scattering - Surface Diffraction

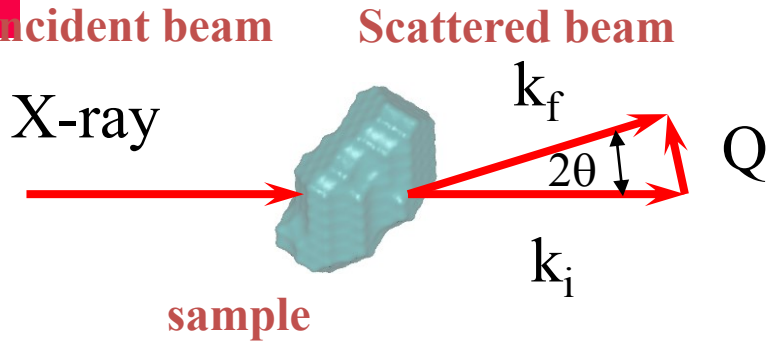

Small-Angle Scattering (Diffraction)

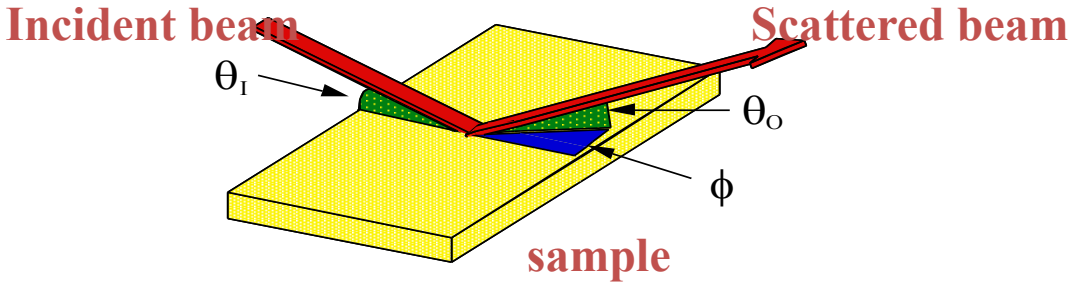

Grazing Incidence Small-Angle Scattering (GISAS) + Reflectometry

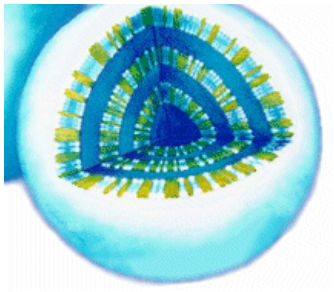

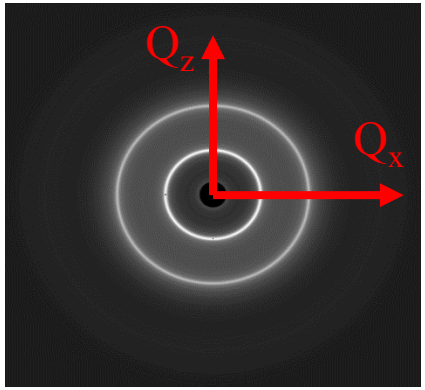

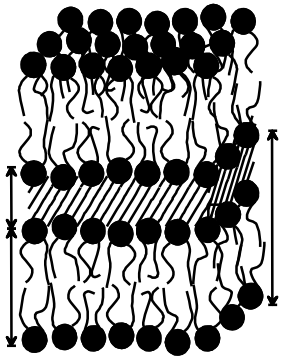

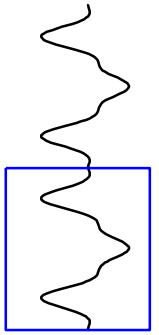

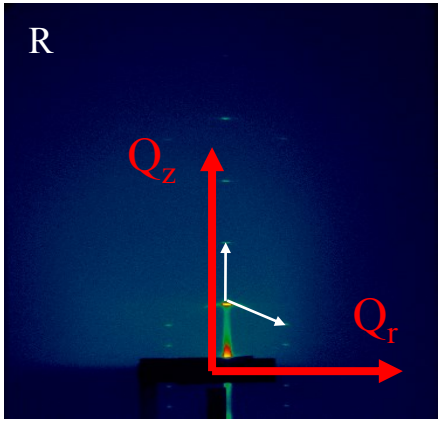

$$I(Q) = \left\langle \left| \int_V d^3r \cdot \rho(\vec{r}) \cdot \exp(-i \cdot \vec{Q} \cdot \vec{r}) \right|^2 \right\rangle_r \qquad I(Q_z, Q_r) = \left\langle \left| \int_V d^3r \cdot \rho(\vec{r}) \cdot \exp(-i \cdot \vec{Q} \cdot \vec{r}) \right|^2 \right\rangle_r$$

amenitsch@tugraz.at &
amenitsch@elettra.trieste.it

Distorted Wave Born Approximation

Vineyard (1982), Shinha et.al. (1988)

$$I(Q_z, Q_r) = |T_i(\alpha_i)|^2 \left\langle \left| \int_V d^3r \cdot \rho(\vec{r}) \cdot \exp(-i \cdot \vec{Q} \cdot \vec{r}) \right|^2 \right\rangle_r |T_f(\alpha_f)|^2$$

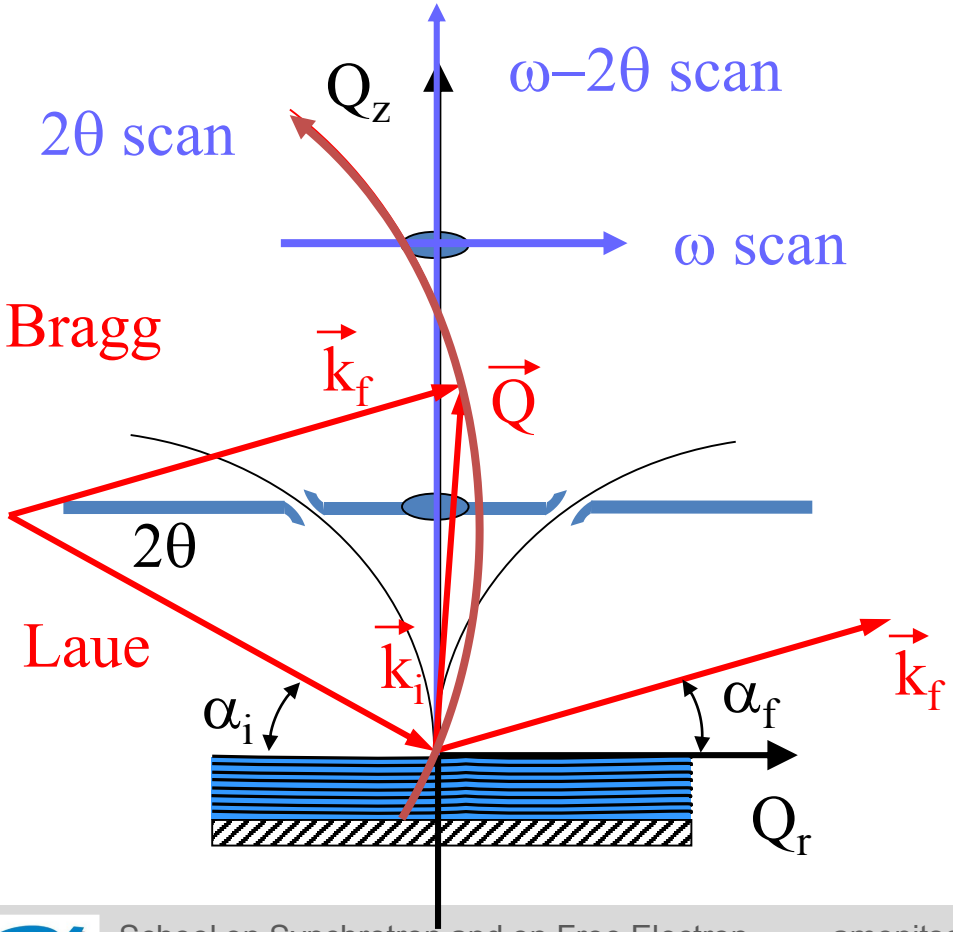

Refraction Effects

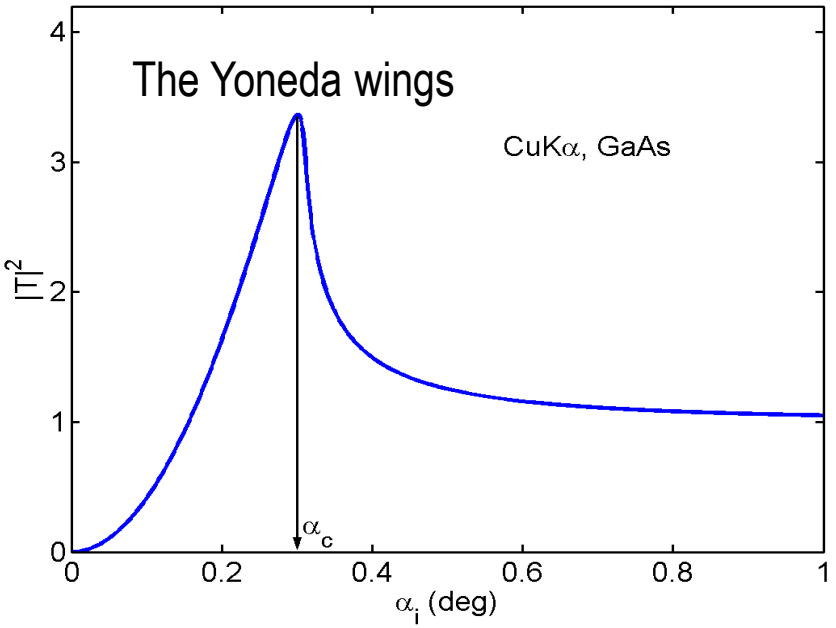

amenitsch@tugraz.at & amenitsch@elettra.trieste.it

„Higher Orders“ of DWBA

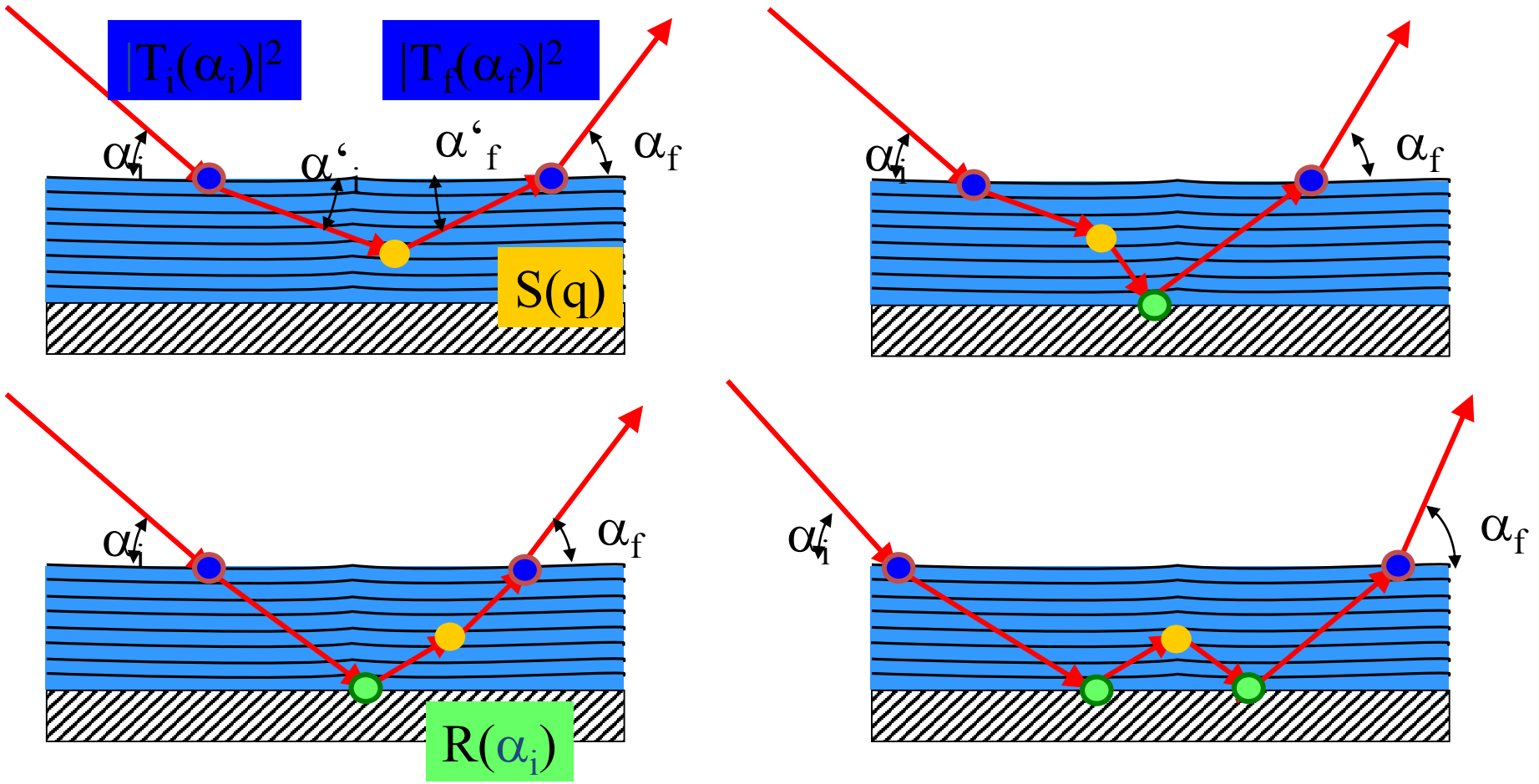

Lazzari R, ISGISAXS: program, J APPL CRYSTALLOGR 35: 406, (2002)
http://www.esrf.fr/computing/scientific/joint_projects/IsGISAXS/isgisaxs.htm

M.P.Tate et al., J.Phys.Chem, 2006

amenitsch@tugraz.at & amenitsch@elettra.trieste.it

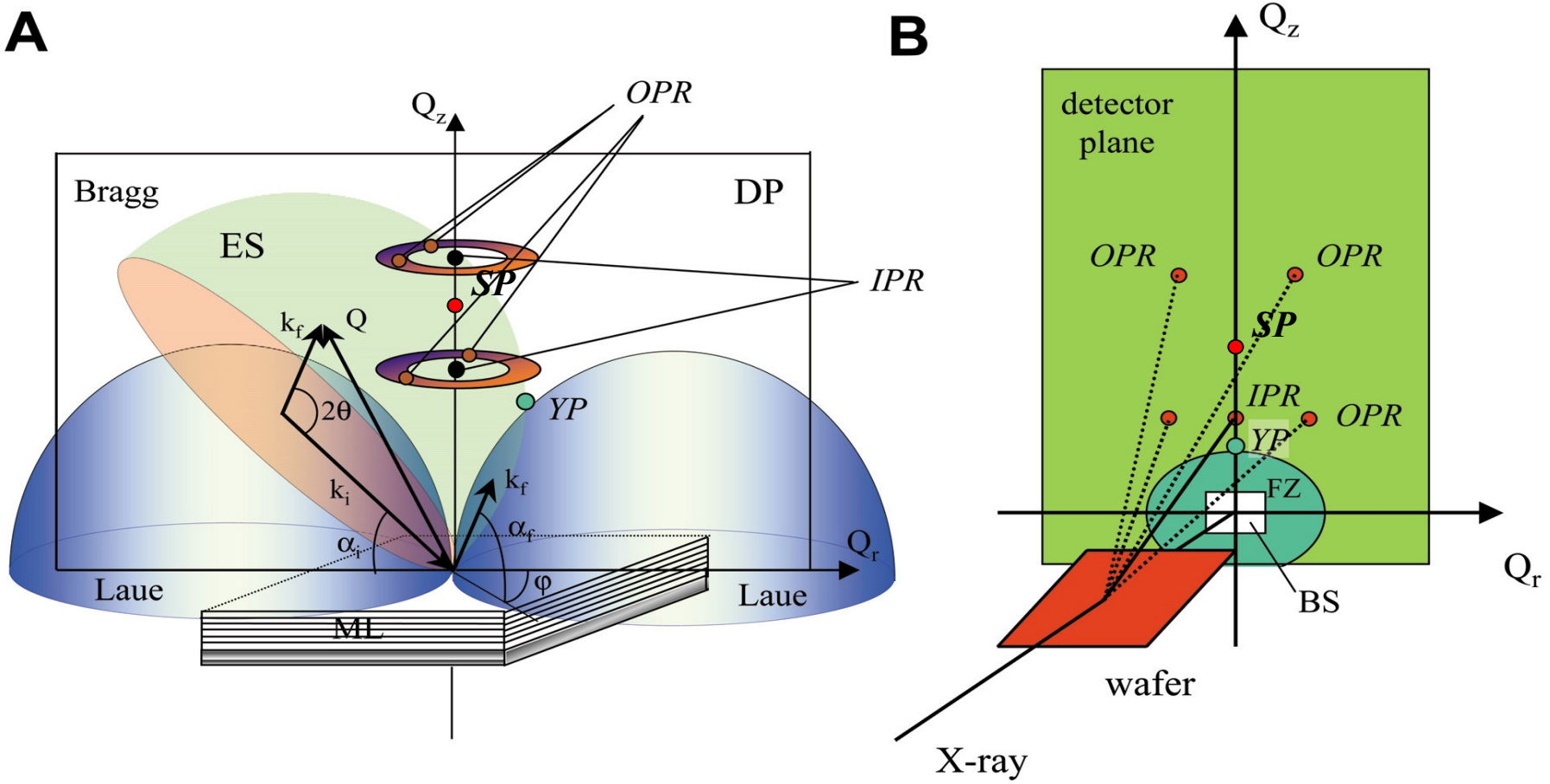

Fig. (A) the scattering geometry in reciprocal space. (B) Scattering geometry in real space. The abbreviations are: (ES) Ewald sphere, (DP) diffraction plane, (OPR) out-of plane reflections, (IPR) in-plane reflections, (ML) multi-layer, (FZ) forbidden zone, (BS) beam stop.

amenitsch@tugraz.at &
amenitsch@elettra.trieste.it

Surface Diffraction Lipids – Rhombohedral Phase

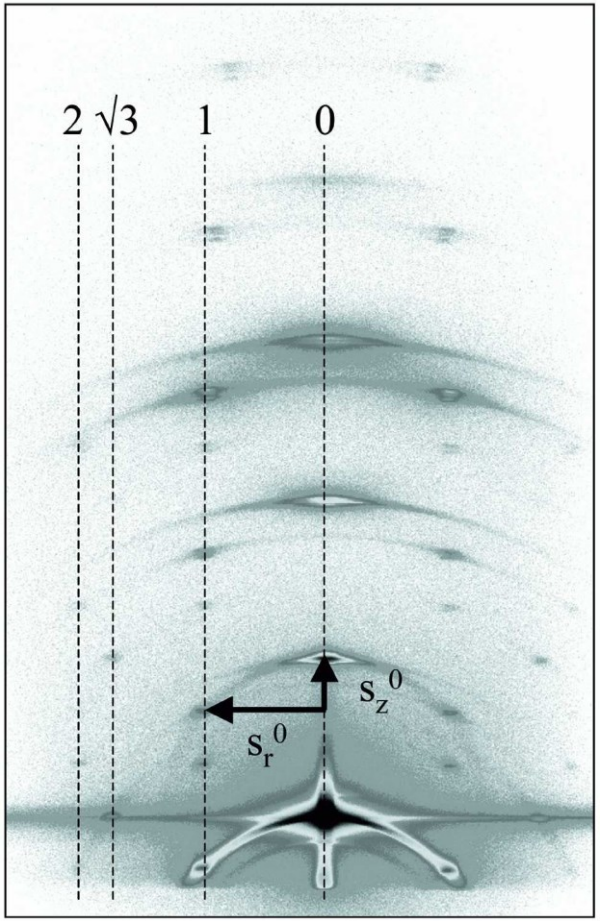

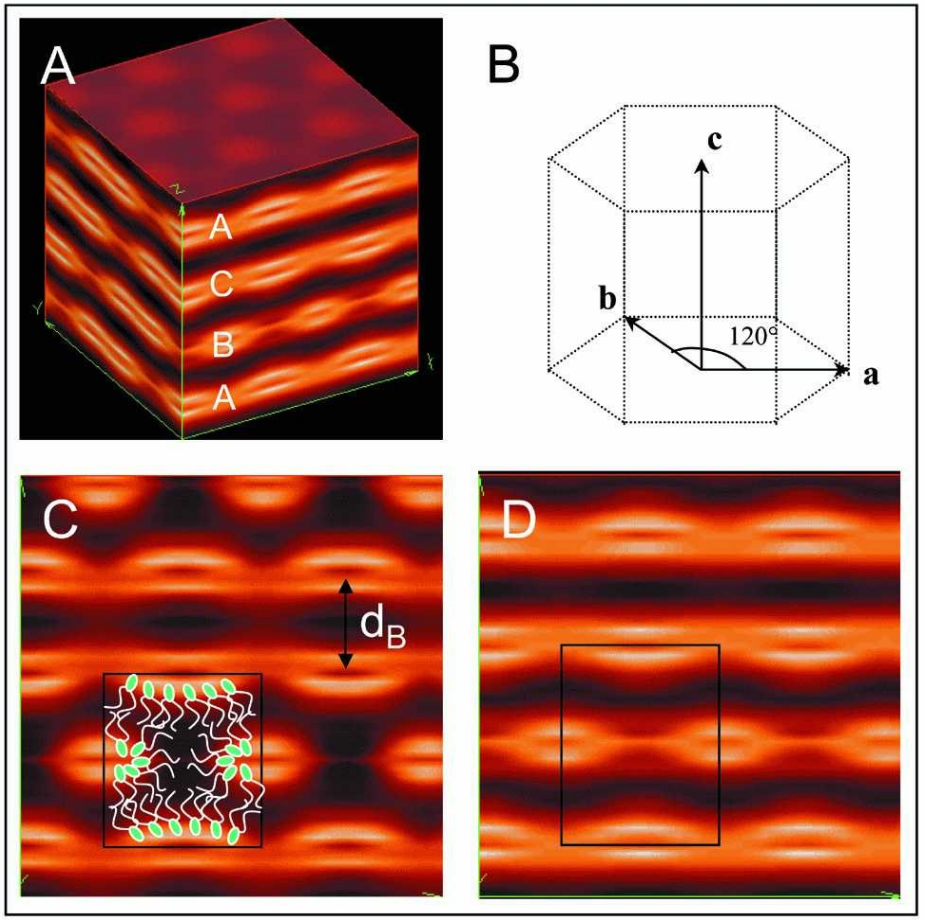

Diffraction Pattern DOPC @ 25° C, 35% rel. humidity

Electron Density Reconstruction: -C DPhPC (d_B= 44.3 Å) -D DOPC (d_B= 48.7 Å), but a= 67 Å / 68 Å

Rappolt,M, et.al., Adv. Coll. and Interf. Science, 111 (2004)

L. Yang, H.W. Huang, Biophys. J. 84 (2003)

amenitsch@tugraz.at & amenitsch@elettra.trieste.it

What do we learn? Membrane Fusion

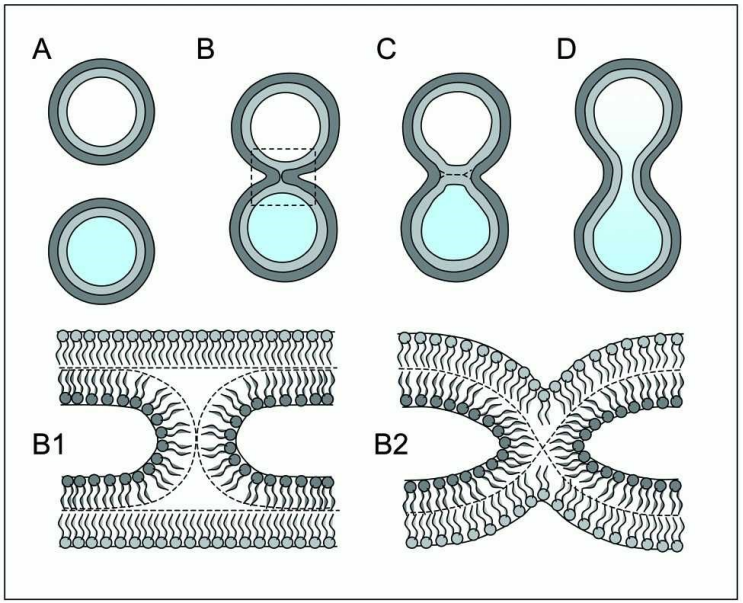

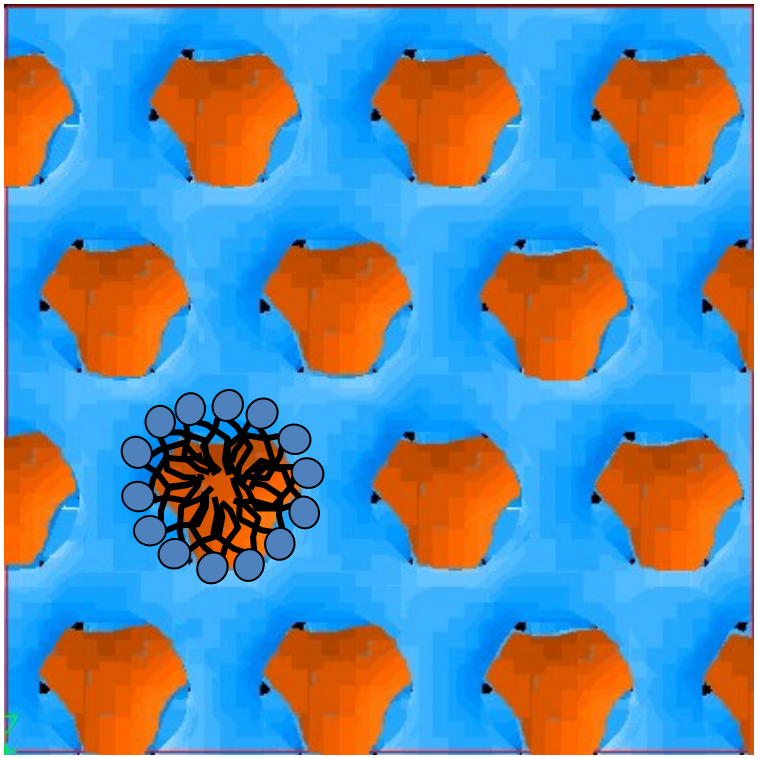

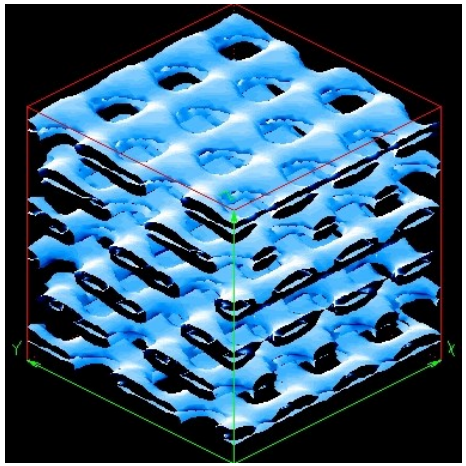

The radius of the torus seems to be confined by the head-group size…

amenitsch@tugraz.at &
amenitsch@elettra.trieste.it

Surface diffraction: Formation of aligned mesoporous thin films

Sol-gel chemistry + surfactant mesophase

Self-assembly

Mesostructured hybrids

Treatment

Mesoporous materials with organised porosity

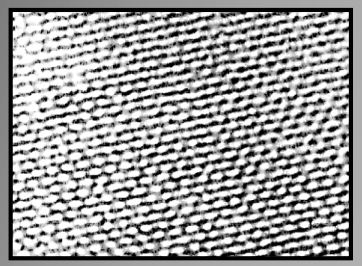

C. J. Brinker et al. Adv. Mater., 1999, 11, 579.

Particles made by aerosols

Films and **fibres** made by liquid deposition

Monoliths made by controlled evaporation

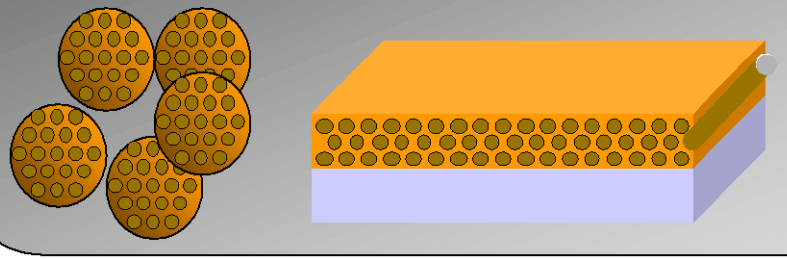

Triblocks POE-POP-POE

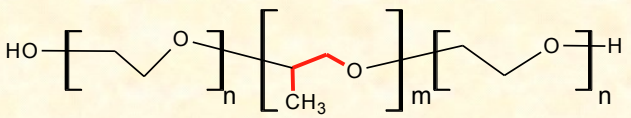

Diblocks C_iE_j

CTAB

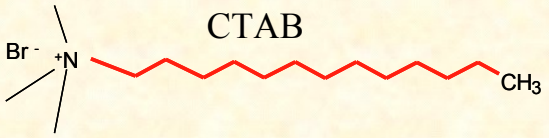

SiO_2 : $Si(OR)_4$

TiO_2 : $TiCl_4$ - $Ti(OR)_4$

ZrO_2 : $ZrCl_4$ - $Zr(OR)_4$

Al_2O_3 : $AlCl_3$

VO_{2-x} : $VOCl_3$

Y_2O_3 : YCl_3

Nb_2O_5 : $NbCl_5$

And binaries systems

amenitsch@tugraz.at & amenitsch@elettra.trieste.it

The Self-Assembly of thin films as seen by In- Situ SAXS and interferometry

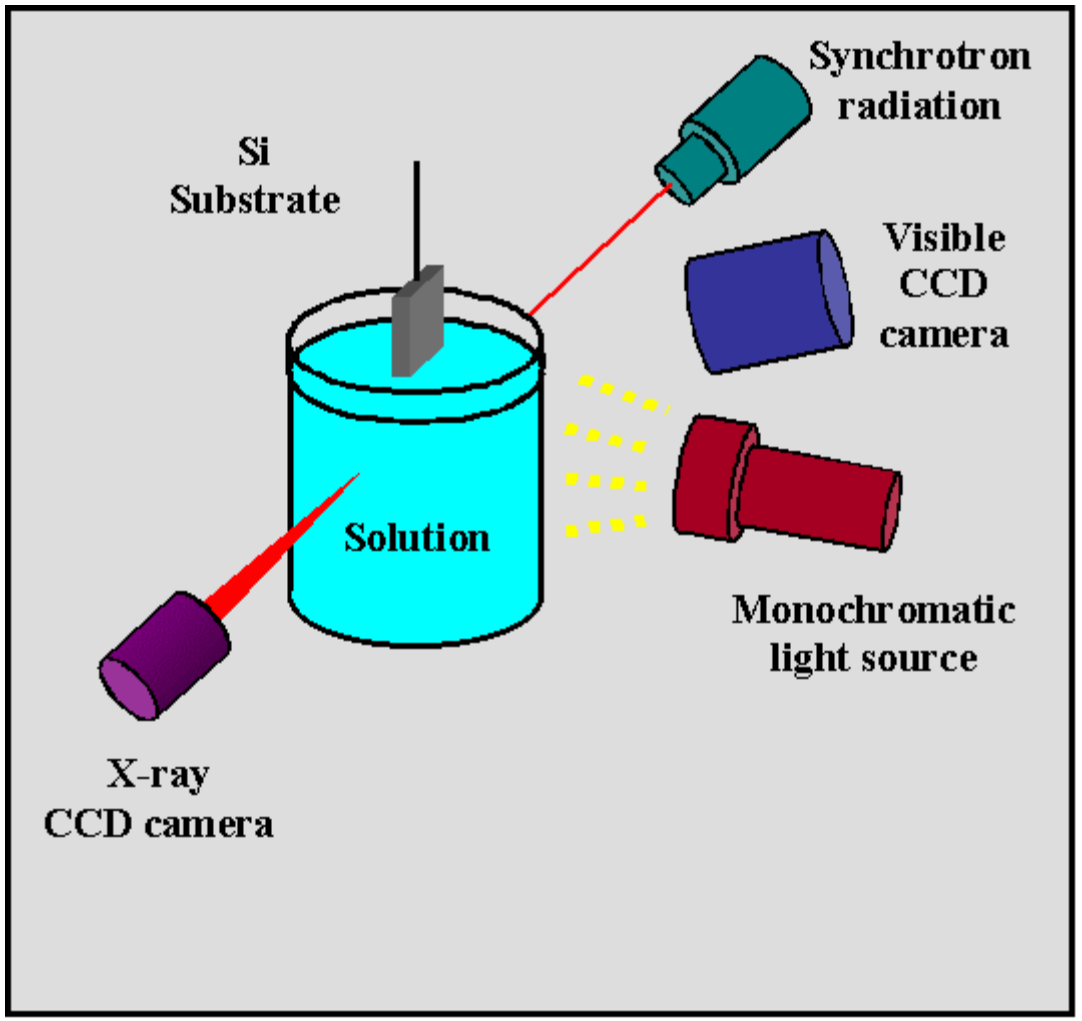

Film mesostructure

Film thickness profile

amenitsch@tugraz.at &
amenitsch@elettra.trieste.it

Surface diffraction: Formation of aligned mesoporous thin films

CTAB / Si = 0,18
H_2O / Si = 5
HCl / Si = 0.15
Ageing time
Relative Humidity

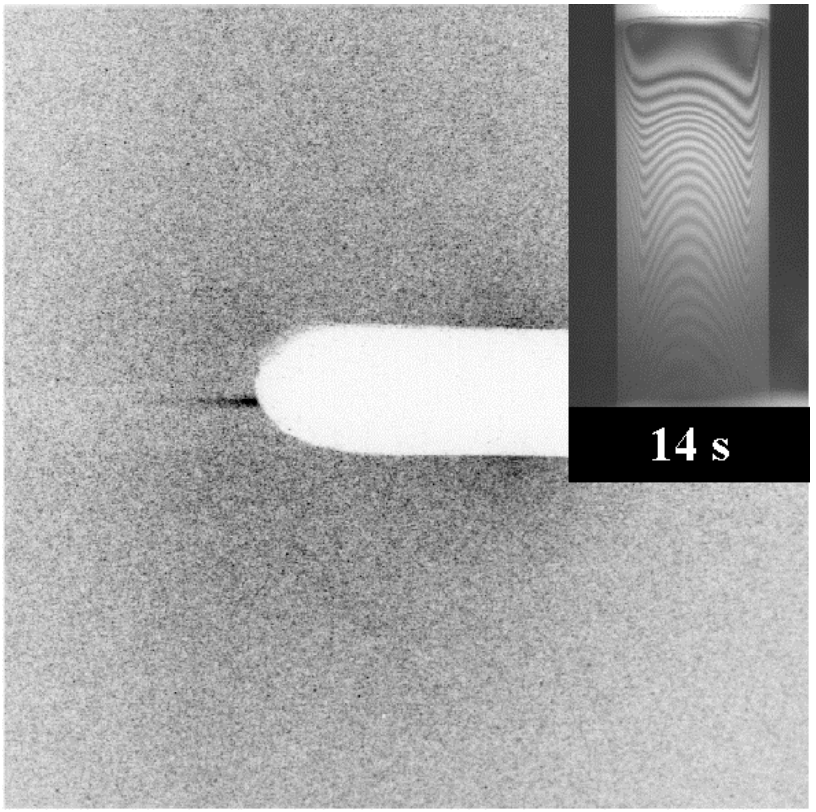

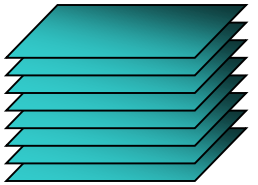

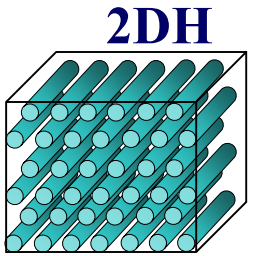

P6m

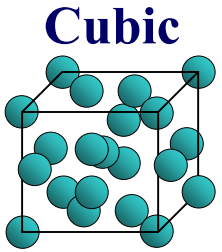

Pm3n
Im3m

Grosso D, et.al., CHEMISTRY OF MATERIALS *14*, 931,(2002)

amenitsch@tugraz.at &
amenitsch@elettra.trieste.it

The Modulable Steady State

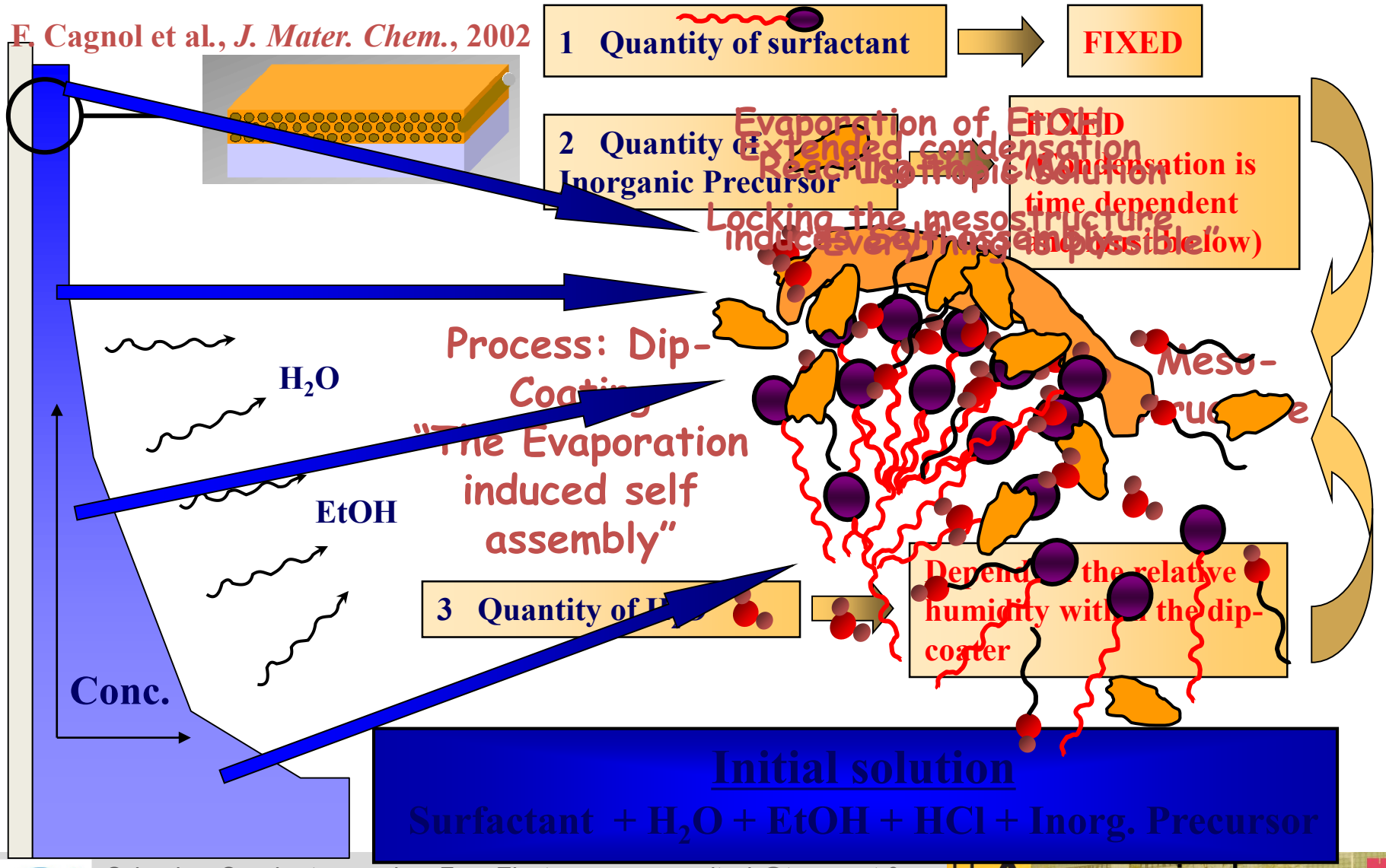

Nanoimprinting and Hybrid Solar Cells

ACS APPLIED MATERIALS & INTERFACES

Research Article

www.acsami.org

(2014)

Nanoimprinted Comb Structures in a Low Bandgap Polymer: Thermal Processing and Their Application in Hybrid Solar Cells

Sebastian Dunst,[†,‡] Thomas Rath,[*,†] Andrea Radivo,[§] Enrico Sovernigo,[§,∥] Massimo Tormen,[§,∥] Heinz Amenitsch,[⊥] Benedetta Marmiroli,[⊥] Barbara Sartori,[⊥] Angelika Reichmann,[#] Astrid-Caroline Knall,[†] and Gregor Trimmel[*,†]

[†]Institute for Chemistry and Technology of Materials, Graz University of Technology, Stremayrgasse 9, 8010 Graz, Austria

[‡]Polymer Competence Center Leoben GmbH, Roseggerstraße 12, 8700 Leoben, Austria

[§]IOM CNR, Laboratorio TASC Area Science Park—Basovizza, S.S. 14 Km 163.5, 34149 Trieste, Italy

[∥]ThunderNIL srl, via Ugo Foscolo 8, 35131 Padova, Italy

[⊥]Institute of Inorganic Chemistry, Graz University of Technology, Stremayrgasse 9, 8010 Graz, Austria

[#]Institute for Electron Microscopy and Nanoanalysis, Graz University of Technology & Centre for Electron Microscopy Graz, Steyrergasse 17, 8010 Graz, Austria

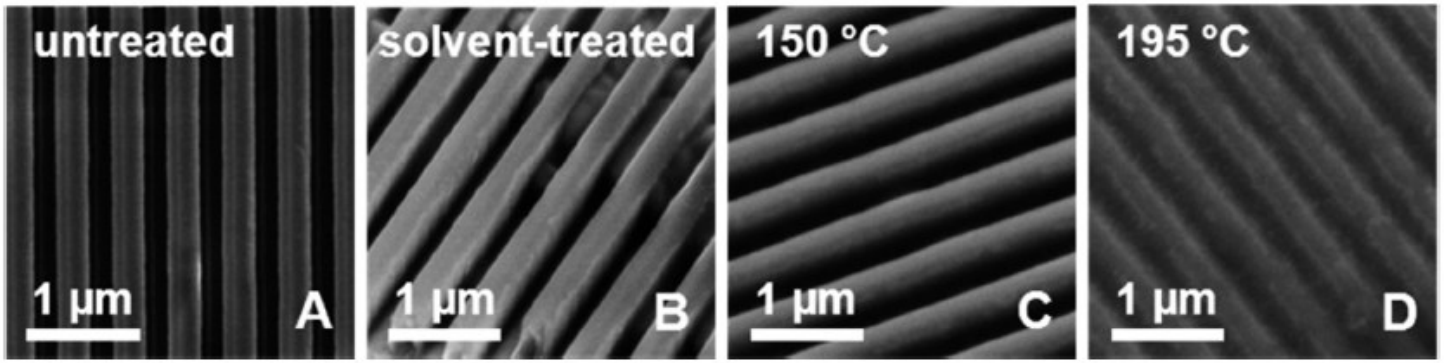

Nanoimprinting and Stability

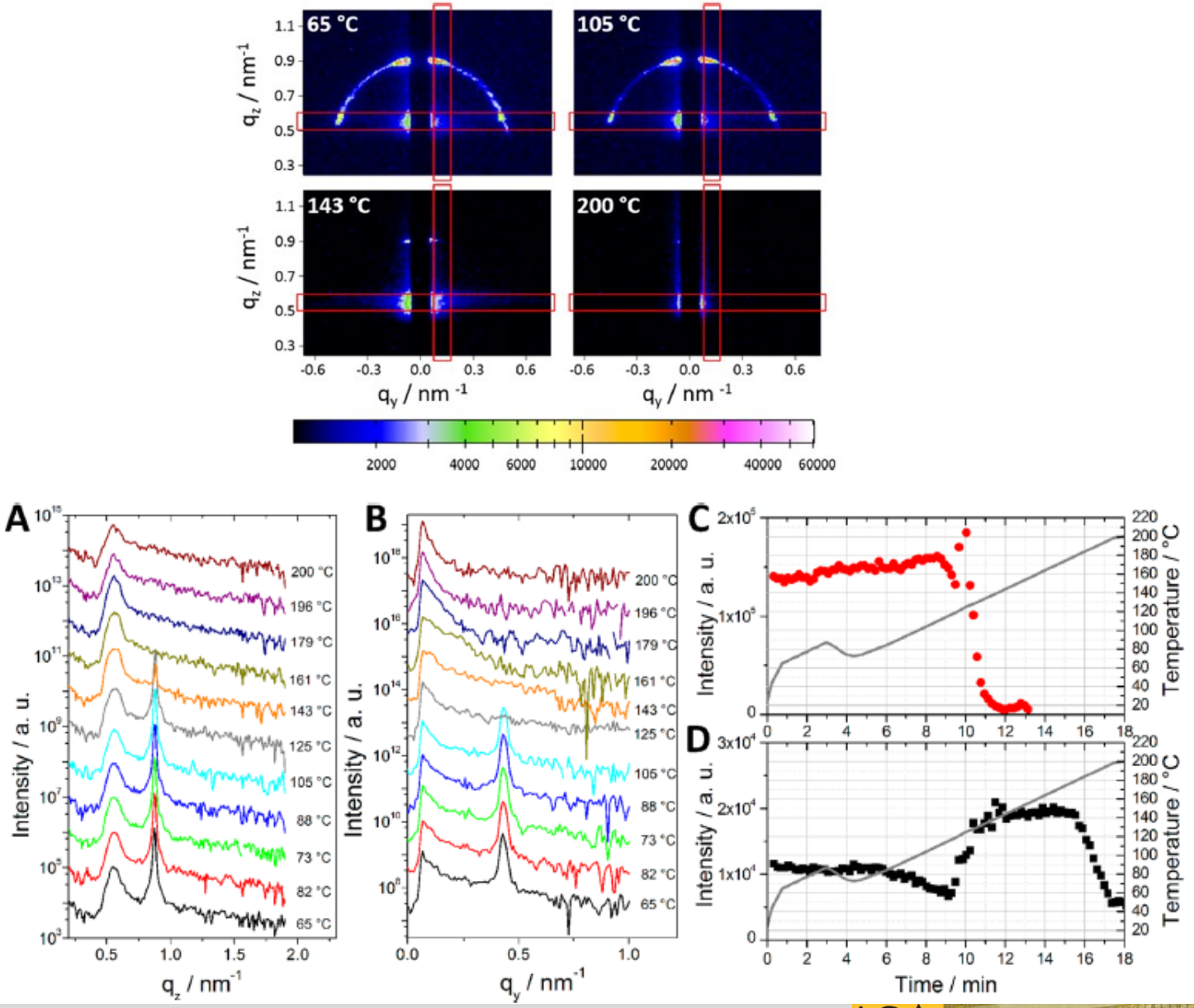

amenitsch@tugraz.at &
amenitsch@elettra.trieste.it

Making of Hybrid Solar Cells

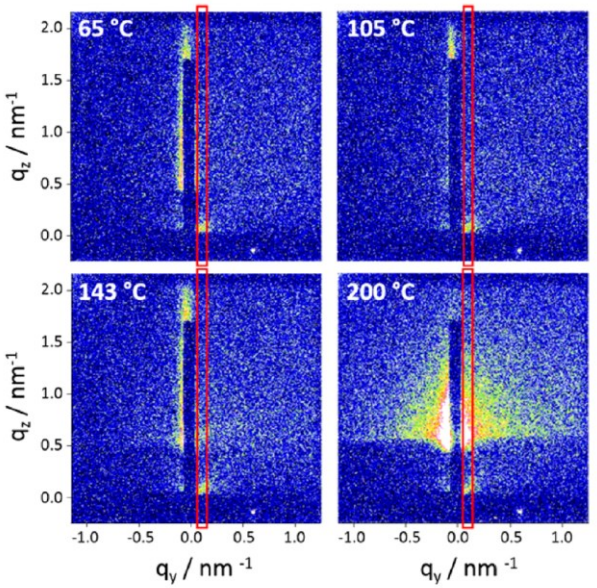

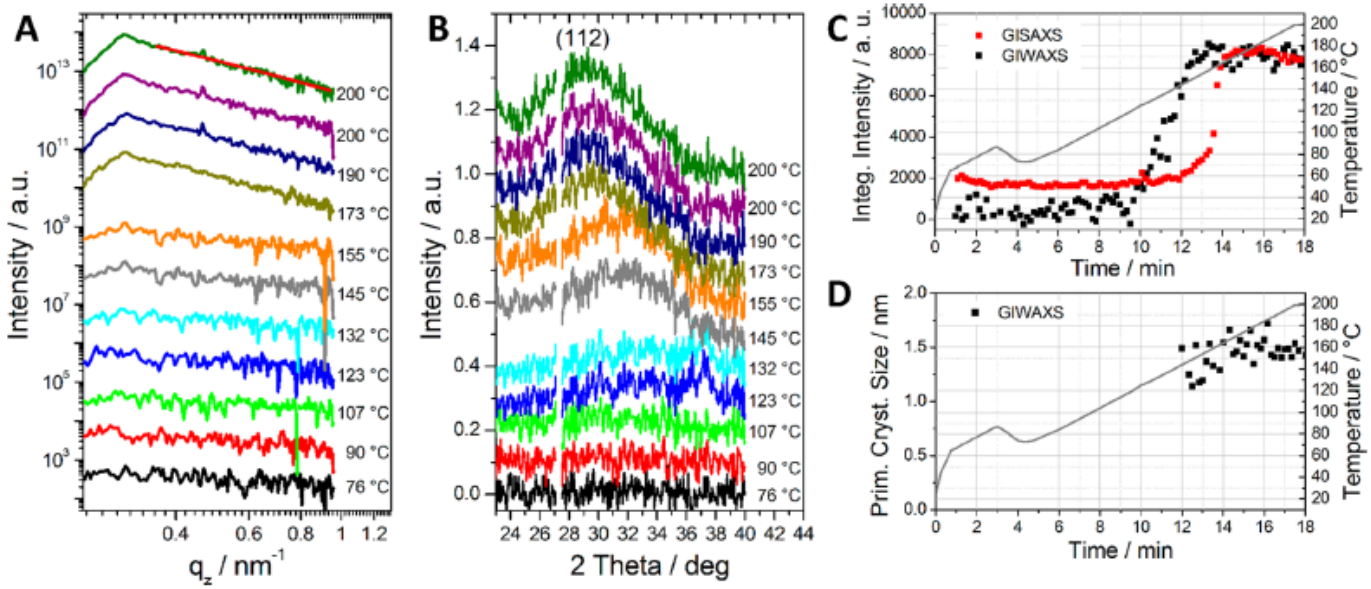

amenitsch@tugraz.at &
amenitsch@elettra.trieste.it

NIL Hyprid Solar Cells: Power conversion

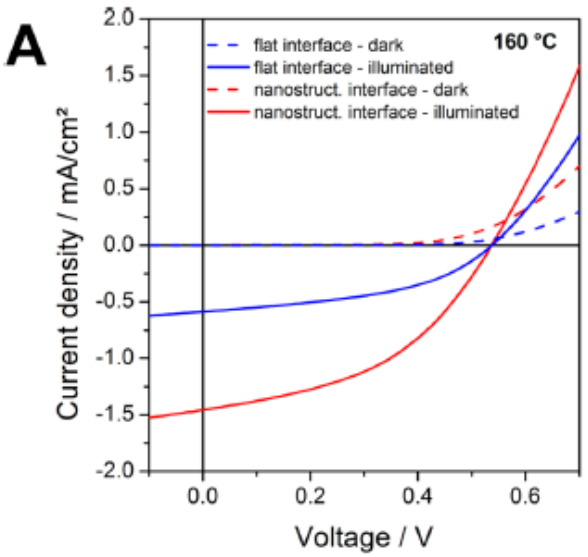

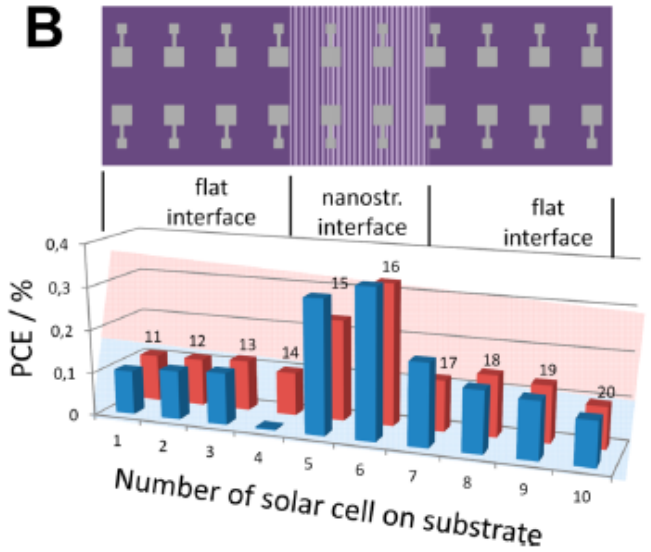

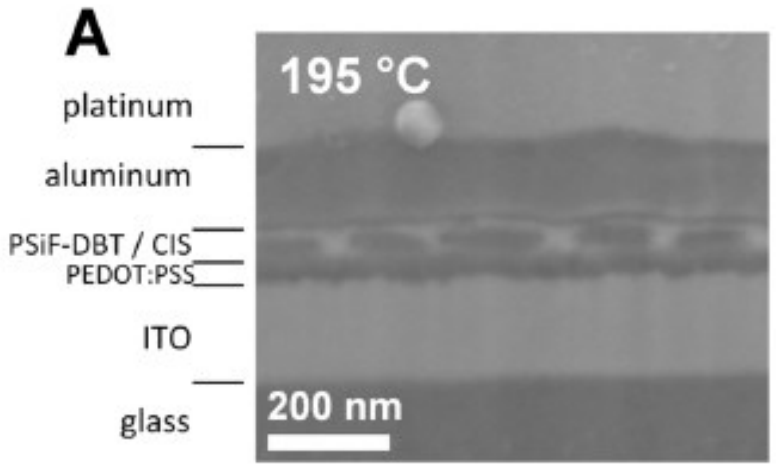

Out come:

(i) Improvement up 3 times in PCE

(ii) Lower annealing temperatures better
3 at 160° C to 1.5 at 195° C
Absolute higher T better

amenitsch@tugraz.at &
amenitsch@elettra.trie

Conclusion

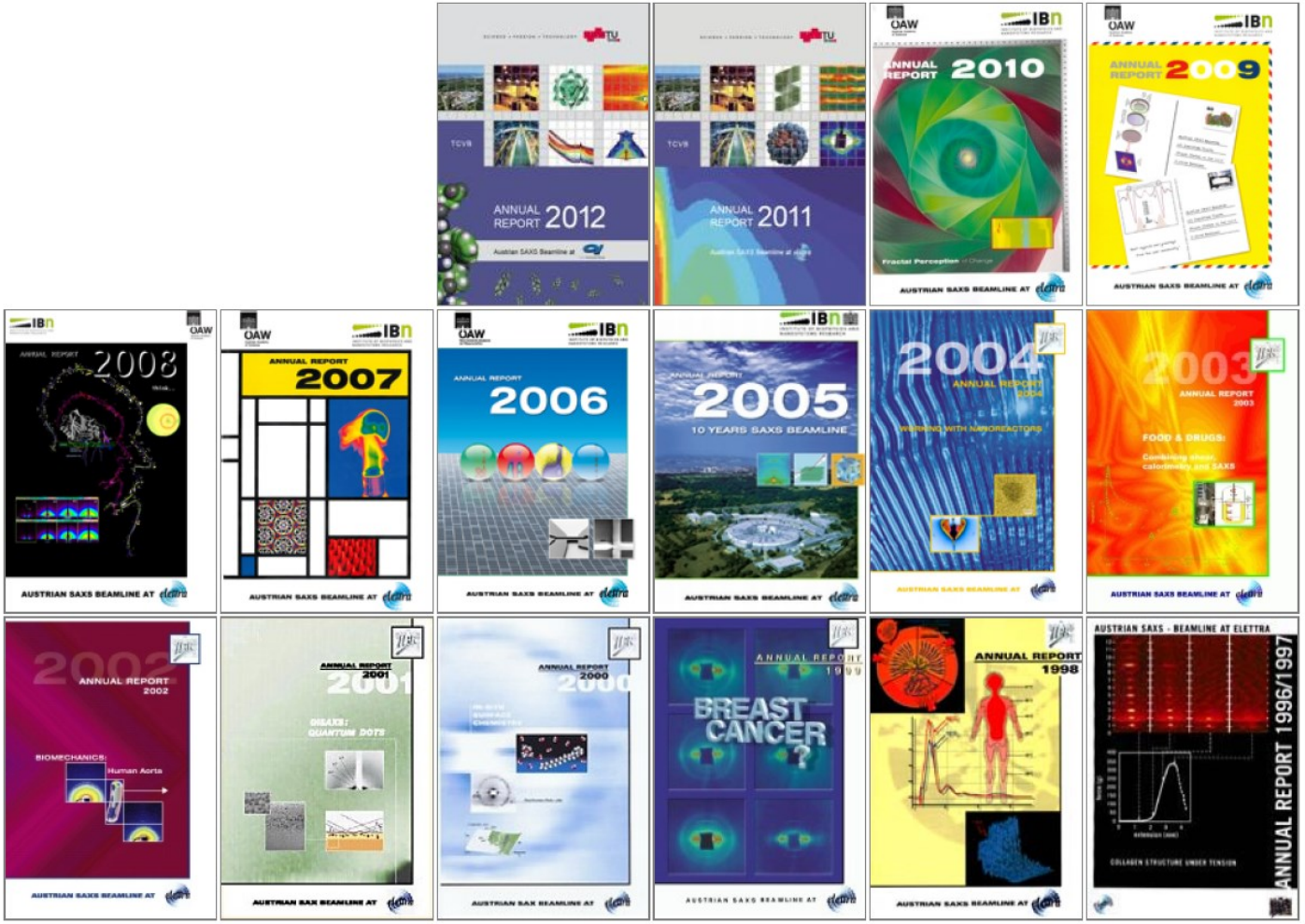

www.elettra.eu

amenitsch@tugraz.at &
amenitsch@elettra.trieste.it

SAXS on the beach

ch@tugraz.at &
amenitsch@elettra.trieste.it